Title
Molecular Synthetic Techniques for the Study of Nanoporous Materials

Author
Stevens, Caitlin

Publication Date
2019

Peer reviewed|Thesis/dissertation

Molecular Synthetic Techniques for the Study of Nanoporous Materials

By

Caitlin J. Stevens

A dissertation submitted in partial satisfaction of the

requirements for the degree of

Doctor of Philosophy

in

Chemistry

in the

Graduate Division

of the

University of California, Berkeley

Committee in Charge:

Professor David E. Wemmer, Chair
Professor F. Dean Toste
Professor Jeffrey A. Reimer

Fall 2019

Abstract

Molecular Synthetic Techniques for the Study of Nanoporous Materials

by

Caitlin J. Stevens

Doctor of Philosophy in Chemistry

University of California, Berkeley

Professor David E. Wemmer, Chair

This dissertation documents the development of molecular synthetic techniques for the study of nanoporous materials. Chapter 1 is an introduction to nanoporous materials and reticular chemistry. The concepts to design and synthesize a wide variety of increasingly complex microporous materials for a range of potential applications are discussed. Chapter 2 introduces [12]dehydrobenzannulene ([12]DBA) as a trigonal planar molecule that is useful in approach the synthesis of graphyne materials. A new, efficient synthesis of this building block is presented. Chapter 3 presents the first synthesis of a metal-organic framework (MOF) constructed with a [12]DBA building blocks. The **srs** topology demonstrates how chiral frameworks can be constructed from achiral organic linkers. The double-walled framework demonstrates the ability to control the orientation of two face-to-face π-stacked macrocycles using the microporous framework as a scaffold in crystal engineering. Chapter 4 further investigates the ability to modify the [12]DBA building block in order to control the orientation of two eclipsed π-stacked macrocycles in a top-to-bottom fashion resulting in a novel double-walled framework with **apo** topology. Chapter 5 conclusively demonstrates the robustness of framework design using principles of reticular chemistry to produce a single-walled MOF by modifying the [12]DBA starting material to produce a paddlewheel secondary building unit (SBU) to yield the predicted **rht** topology. Chapter 6 moves into an organic class of nanoporous materials, covalent organic frameworks (COFs) to extended to other classes of nanoporous materials an alternative form of synthesis, mechanochemical synthesis, to produce the materials predicted by reticular chemisty.

This dissertation is dedicated to all that made it possible.

Table of Contents

List of Figures

Chapter 2

Chapter 3

Chapter 4

Chapter 5

Chapter 6

List of Schemes

Chapter 2

Chapter 6

List of Tables

Chapter 3

Chapter 4

Chapter 5

List of Photographs

Chapter 3

Chapter 4

Chapter 5

List of Abbreviations and Acronyms

Å	angstroms
A	amp(s)
ABCN	1,1'-azobis(cyclohexanecarbonitrile)
Ac	acetyl, acetate
aq	aqueous
atm	atmosphere
BET	Brunauer-Emmet-Teller
Bn	benzyl
BPDC	biphenyl-4,4'-dicarboxylate
BTE	4,4',4''-[benzene-1,3,5-triyl-tris(ethyne-2,1-diyl)tribenzoate
BTEA	benzyltriethylammonium
Bu	butyl
°C	degrees Celsius
calcd	calculated
cm	centimeter(s)
cm^{-1}	wavenumber(s)
COF	covalent organic framework
d	doublet (spectral)
DBA	dehydrobenzannulene
DEF	*N,N*-diethylformamide
DI	deionized
DKP	diketopiperidine
DMF	*N,N*-dimethylformamide
DMSO	dimethyl sulfoxide
equiv	equivalents
Et	ethyl
eV	electron volt(s)
FCC	flash column chromatography
FT	Fourier transform
g	gram(s)
h	hour(s)
Hz	hertz
IR	infrared (spectroscopy)
J	coupling constant
k	kilo

K	kelvin(s)
λ	wavelength
L	liter(s)
lit.	literature value
μ	micro
m	multiplet (spectral); meter(s); milli
Me	methyl
MHz	megahertz
min	minute(s)
MOF	metal organic framework
mol	mole(s)
mp	melting point
MS	molecular sieves
NBS	*N*-bromosuccinimide
NMO	*N*-methylmorpholine-*N*-oxide
NMP	*N*-methyl-2-pyrrolidone
NMR	nuclear magnetic resonance
P	para
PAF	porous aromatic framework
Ph	phenyl
pin	pinacol
ppm	part(s) per million
Pr	propyl
PXRD	powder X-ray diffraction
q	quartet (spectral)
rt	room temperature
R_f	retention factor (in chromatography)
s	seconds; singlet (spectral)
SBU	secondary building unit
SCXRD	single crystal X-ray diffraction
SPS	solvent purification system
t	triplet (spectral)
t	time; temperature in units of degrees Celsius (°C)
T	absolute temperature in units of kelvins (K)
TBAF	tetra-*n*-butylammonium fluoride
temp	temperature
TFA	trifluoroacetic acid
THF	tetrahydrofuran
TLC	thin-layer chromatography

TMSA	trimethylsilylacetylene
TTCA	triphenylene-2,6,10-tricarboxylate
UV	ultraviolet
V	volt(s)
vol	volume
v/v	volume per unit volume (volume-to-volume ratio)
W	watt(s)
wt	weight
w/w	weight per unit weight (weight-to-weight ratio)
ZIF	zeolitic imidazolate framework
2D	two-dimensional
3D	three-dimensional

Acknowledgements

I would first like to acknowledge my teachers who have I learned so much from throughout my degree: Professor Omar Yaghi (UC Berkeley), Professor Yves Rubin (UCLA), Professor David Wemmer (UC Berkeley), Professor Heather Maynard (UCLA), and Professor Peter Iovine (University of San Diego).

I would also like to acknowledge my family who has been supportive throughout this whole process, especially my parents, James and Elaine, and sisters, Hilary and Melissa. I would also like to thank my extended family: Aunt Sue, Uncle John and Aunt Salli, Uncle Tom and Aunt Linda, Uncle Charlie and Aunt Janice and cousins Simon, Charis, and Devon for keeping my spirits high over the years.

I am really grateful for my mentors at the University of California, Los Angeles, especially Professor Yves Rubin for mentorship in synthetic organic chemistry and Dr. Carolyn Knobler and Dr. Dulio Cascio for their expertise and knowledge in crystallography. I would like to give a special thank you to Dr. Dulio Cascio in the Molecular Biology Institute at UCLA with his help in acquiring single crystal X-ray diffraction data and the folks at the APS Beamline 24-ID-C and their DOE grants that made this data collection possible.

I've had the opportunity to work with so many talented scientists while in the Yaghi group and I'd especially like to thank my mentors Dr. Will Morris, Professor Mitsuharu Suzuki, and Professor Alejandro Fracaroli as well as the students that I had the opportunity to mentor: Derek Mull, Jenny Bae, Josh Ivy, and Dr. Christian Diercks.

A special thank you to my colleagues in the Liu Group at the Molecular Foundry at the Lawrence Berkeley National Laboratory who made me feel so welcome in my transition: Dr. Yi Liu, Liana Klivansky, Dr. Bo He, Vincent Hipwell, Matt Kolaczkowski, Hongxia Wang, Teresa Chen, Dr. Matt Jurrow, Chris Anderson.

I'd like to especially acknowledge the contributions of my collaborators at Osaka University in Osaka, Japan for their contributions on the [12]DBA macrocycle synthesis: Professor Ichiro Hisaki, Professor Mikiji Miyata, and students Hajime Shigemitsu, and Daisuke Yasumiya.I am so grateful for the opportunity to work on multidisciplinary research in an international collaboration.

Thank you to Derek Mull for help proofreading this dissertation and to everyone who has made the completion of my Ph.D. possible and kept supporting me through the process despite its many challenges. To those I have not explicitly mentioned, you know who you are and know that you have not been forgotten and my heart goes out to you.

Facility Acknowledgements

Department of Chemistry, University of California, Berkeley

Department of Chemistry & Biochemistry, University of California, Los Angeles, 607 Charles E. Young Drive East, Los Angeles, California 90095-1569, United States

Molecular Foundry, Materials Sciences Division,
Lawrence Berkeley National Laboratory, Berkeley, California

Advanced Light Source
Lawrence Berkeley National Laboratory, Berkeley, California

[‡]Department of Material and Life Science, Graduate School of Engineering, Osaka University, Yamadaoka, Suita, Osaka, 565-0871, Japan

CHAPTER 1

Introduction to Nanoporous Materials

1.1 Abstract

An introduction to nanoporous materials and a broad overview of current materials chemistry challenges are presented. In particular, design principles and traditional methods of construction are discussed as well as the opportunity to design and discover novel materials.

1.2 Current Challenges in the Synthesis of Carbon Nanomaterials

Carbon allotropes are of considerable interest to study due to their unique electronic and structural properties. The three hybridization states of carbon (sp^3, sp^2, and sp) lead to multiple topological possibilities due to their geometric difference. Naturally occurring pure forms of carbon include graphite, diamond, and fullerenes. Several Nobel prizes and other awards have been issued for carbon materials such as fullerenes,[1] graphene,[2] and carbon nanotubes;[3] however, the inability to reliably produce these materials in bulk prevent their applications from being fully realized. Several unique carbon allotropes have been proposed and studied by theoretical chemists.[4] So far, only small molecular fragments have been isolated and characterized due to their ability to be synthesized and studied using solution chemistry.[5] Current synthetic routes to these supramolecular materials result in amorphous polymers due to the irreversible nature of the bond forming reaction hindering the accessibility of well-defined materials.[6] Despite their amorphous structures, these materials have demonstrated impressive properties with useful applications.[7]

The preparation of synthetic carbon allotropes and carbon-based crystalline supramolecular architectures has proven difficult over the decades, chemists and materials scientists have had much greater success exploring inorganic-organic hybrid materials.[8] Several classes of crystalline porous materials have emerged in the last few decades and are intensely investigated for their wide applications in gas storage, separation, and catalysis. In contrast to irreversible polymer formation, reversibly driven bond-forming reactions as a supramolecular process mimic "crystallization" to produce highly ordered, crystalline frameworks. The reversible nature of the bond forming reaction allows for the construction of extended structures since defects created through incorrect bond formation are able to equilibrate to the thermodynamic product. These frameworks are advantageous over their amorphous polymer cousins due to their well-ordered structure that can be studied at the molecular level by x-ray crystallography.

1.3 Definition of Terms and Overview of Reticular Chemistry

Reticular chemistry defines principles of connecting molecular building blocks by strong bonds to yield ordered, periodic networks.[9] Secondary building units (SBUs) are coordinated molecular complexes that act as nodes bridged by ligands to form extended network topologies.[10] The Reticular Chemistry Structure Resource (RCSR) can be accessed online[11] and is a useful resource for studying the topology and nets of these materials.[12] Reticular chemistry can be especially useful for the design of materials with topologically dependent properties.[13] The underlying symmetry of SBUs and organic linkers directs the formation of network topology.

Furthermore, reticular chemistry has enabled the developed of controlled molecular networks with predicted topologies by designing the spatial arrangement of molecules. The isoreticular principle allows for the control of metrics and functionality while retaining same basic underlying structure.[14]

Reticular synthesis constructs predetermined networks from the combination of different building blocks. Materials of the future will include increasing structural complexity and hierarchically organized systems.[15] Many topological outcomes are possible but a few primary networks are predominantly formed allowing for the rational design of carbon-rich, 2D and 3D networks ideal for X-ray studies. The advantage here is to construct well-ordered networks whose structures can be clearly defined by precise atomic positions.

Advances in reticular chemistry have provided a useful scaffold for constructing these molecular networks by reducing the design down to the geometric combination of organic linkers and secondary building units to yield multiple classes of crystalline, porous materials including, but not limited to metal organic frameworks (MOFs), covalent organic frameworks (COFs), zeolitic imidazolate frameworks (ZIFs), and other amorphous materials such as polycyclic aromatic frameworks (PAFs). A few classes of nanoporous materials of particular interest are discussed below.

Metal Organic Frameworks (MOFs)

Metal-organic frameworks (MOFs) are composed of metal-oxide secondary building units (SBUs) joined by coordinating carboxylates on organic linkers. Many metal cations have demonstrated to be useful in linking structures as well as functionalized linkers demonstrating the versatility of building a large library of highly functionalized MOFs for a variety of potential applications.[16]

Covalent Organic Frameworks (COFs)

Introduced by Yaghi in 2005, covalent organic frameworks (COFs) represent a new class of crystalline, porous materials that are constructed exclusively of light, organic elements (C, H, N, O, B) linked by covalent bonds.[17] COFs are set apart from other covalently linked, porous organic materials due to their crystalline nature, adjustable pore structures, and permanent porosity. Linkages in COFs have expanded from boroxines to other functional groups including, but not limited to, imine, triazine, borazine, and hydrazone, linkages.[18] Among the new COF materials, the carbon-carbon bond based linkages remain elusive to synthesize. Structures composed exclusively of carbon and hydrogen lack facile synthetic methods, limiting researchers' ability to generate novel materials of this type, which has prevented their isolation and study. Current synthetic routes to covalently linked, supramolecular carbon materials such as porous aromatic frameworks (PAFs)[19] result in amorphous materials due to the irreversible nature of the C-C bond forming reaction leading to structural defects in the crystal lattice cannot be corrected. In contrast, reversibly driven bond forming reactions as a supramolecular process mimic "recrystallization" to produce well-ordered framework materials. Reactions with reversible bond formation allow for the correction of defects since bonds leading to local defects are able to be broken and corrected.

1.4 Conclusions and Outlook

Carbon materials have great potential; however, there is a current lack of synthetic methods to fabricate these organic networks due to the challenges associated with creating regular materials with strong bonds. The synthetic methods to access these materials are greatly sought after since in order to fully realize the potential applications of these materials, their industrial production must be cheap and reliable for large-scale production.[20] New classes of nanoporous materials hold promise for creating carbon-rich networks that are well-ordered and can be studied at the molecular level with crystallographic techniques. A carbon-based platform was chosen as the organic linker in the studies presented in this dissertation to expand the field by synthesizing non-commercially available organic linkers to incorporate carbon-carbon triple bond containing moieties into MOFs to study their resulting properties. The organic linkers were selected for their rigid structure and high thermal stability suitable for the traditional solvothermal synthesis of nanoporous frameworks. These organic linkers represent a subunit of larger carbon networks and can be built into 3D architectures using nanoporous frameworks as a building scaffold and the design principles of reticular chemistry to engineer structures with interesting topological structures and properties. The introduction of these large, organic-rich moieties into nanoporous materials have the potential to approach graphene-like materials. The resulting frameworks will be crystalline, porous, and robust, making them ideal candidates for study by crystallography.

1.5 References and Notes

(1) Kroto, H. W.; Heath, J. R.; O'Brien, S. C.; Curl, R. F.; Smalley, R. E. C_{60}: Buckminsterfullerene. *Nature* **1985**, *318*, 162–163.

(2) (a) Novoselov, K. S.; Geim, A. K.; Morozov, S. V.; Jiang, D.; Zhang, Y.; Dubonos, S. V.; Grigorieva, I. V.; Firsov, A. A. Electric Field Effect in Atomically Thin Carbon Films. *Science* **2004**, *306*(5696), 666–669. (b) Geim, A. K.; Novoselov, K. S. The rise of graphene. *Nat. Mater.* **2007**, *6*, 183–191.

(3) Rahman, G.; Najaf, Z.; Mehmood, A.; Bilal, S.; Shah, A.; Mian, S. A.; Ali, G. An Overview of the Recent Progress in the Synthesis and Applications of Carbon Nanotubes. *C* **2019**, *5*(1), 3.

(4) Sakamoto, J.; van Heijst, J.; Lukin, O.; Schluter, A. D. Two-Dimensional Polymers: Just a Dream of Synthetic Chemists? *Angew. Chem., Int. Ed.* **2009**, *48*(6), 1030–1069.

(5) For example, see: Haley, M. M. Synthesis and properties of annulenic subunits of graphyne and graphdiyne nanoarchitectures. *Pure Appl. Chem.* **2008**, *80*(3), 519–532.

(6) Diederich, F.; Kivala, M. All-Carbon Scaffolds by Rational Design. *Adv. Mater.* **2010**, *22*(7), 803–812.

(7) Thomas, A. Functional Materials: From Hard to Soft Porous Frameworks. *Angew. Chem., Int. Ed.* **2010**, *49*(45), 8328–8344.

(8) (a) Saveleva, M. S.; Eftekhari, K.; Abalymov, A.; Douglas, T. E. L.; Volodkin, D.; Parakhonskiy, B. V.; Skirtach, A. G. Hierarchy of Hybrid Materials–The Place of Inorganics-*in*-Organics in it, Their Composition and Applications. *Front. Chem.* **2019**, *7*, 179. (b) Organic-Inorganic Hybrid Nanomaterials. *Nanomaterials* **2019**, *9*(19), 1197.

(9) Yaghi, O. M. Reticular Chemistry–Construction, Properties, and Precision Reactions of Frameworks. *J. Am. Chem. Soc.* **2016**, *138*(48), 15507–15509.

(10) Eddaoudi, M.; Moler, D. B.; Li, H.; Chen, B.; Reineke, T. M.; O'Keeffe, R.; Yaghi, O. M. Modular Chemistry: Secondary Building Units as a Basis for the Design of Highly Porous and Robust Metal-Organic Carboxylate Frameworks. *Acc. Chem. Res.* **2001**, *34*(4), 319–330.

(11) http://rcsr.anu.edu.au/

(12) O'Keeffe, M.; Peskov, M. A.; Ramsden, S. J.; Yaghi, O. M. The Reticular Chemistry Structure Resource (RCSR) Database of, and Symbols for, Crystal Nets. *Accts. Chem. Res.* **2008**, *41*(12), 1782–1789.

(13) For example, see: Wang, J.; Deng, S.; Liu, Z.; Liu, Z. The Rare Two-Dimensional Materials with Dirac Cones. *Natl. Sci. Rev.* **2015**, *2*(1), 22–39.

(14) Furukawa, H.; Go, Y. B.; Ko, N.; Park, Y. K.; Uribe-Romo, F. J.; Kim, J.; O'Keeffe, M.; Yaghi, O. M. Isoreticular Expansion of Metal-Organic Frameworks with Triangular and Square Building Units and the Lowest Calculated Density for Porous Crystals. *Inorg. Chem.* **2011**, *50(*18), 9147–9152.

(15) Müllen, K. Chemistry in a Materials World. *Angew. Chem., Int. Ed.* **2015**, *54*(35), 10040–10042.

(16) Hiroyasu, F.; Cordova, K. E.; O'Keeffe, M.; Yaghi, O. M. The Chemistry and Applications of Metal-Organic Frameworks. *Science* **2013**, *341*(6149).

(17) Côté, A. P.; Benin, A. L.; Ockwig, N. W.; O'Keeffe, M.; Matzger, A. J.; Yaghi, O. M. Porous, crystalline, covalent organic frameworks. *Science* **2005**, *310*, 1166–1170.

(18) Waller, P. J.; Gándara, F.; Yaghi, O. M. Chemistry of Covalent Organic Frameworks. *Acc. Chem. Res.* **2015**, *48*(12), 3053–3063.
(19) Ben, T.; Ren, H.; Ma, S.; Cao, D.; Lan, J.; Jing, X.; Wang, W.; Xu, J.; Deng, F.; Simmons, J. M.; Qiu, S.; Zhu, G. Targeted Synthesis of a Porous Aromatic Framework with High Stability and Exceptionally High Surface Area. *Angew, Chem., Int. Ed.* **2009**, *48*(50), 9457–9460.
(20) Peh, S. B.; Wang, Y.; Zhao, D. Scalable and Sustainable Synthesis of Advanced Porous Materials. *ACS Sustainable Chem. Eng.* **2019**, *7*(4), 3647–3670.

CHAPTER 2

Syntheses of a [12]Dehydrobenzannulene Building Block as a Subunit of Graphyne for the Construction of Metal-Organic Frameworks

2.1 Abstract

Two new syntheses of a tricarboxylic acid functionalized [12]dehydrobenzannulene linker for the construction of MOFs are presented. The first features optimizations and improvements to an established route while the second presents an abbreviated synthesis of the macrocyclization precursor intermediate.

2.2 Introduction

2.2.1 Design of a Thermally Stable, Shape Persistent Macrocyclic Ligand

The tricarboxylic acid modified triangular shape-persistent macrocycle [12]dehydrobenzannulene ([12]DBA) **2.1** was chosen as the initial target for this study (Figure 2.1). This organic linker was selected due to its rigid structure and high thermal stability suitable for the solvothermal synthesis of MOFs. Conjugated acetylene dicarboxylic acids are known to decarboxylate at temperatures from 80-160 °C, making these functional groups unsuitable for the solvothermal synthesis of MOFs.[1] Phenyl rings can be used as a design element to break the direct conjugation of the alkyne carboxylic acid by placing the two functionalities *meta* or *para* to one another on the aromatic ring. In addition, macrocyclic phenyl acetylene derivatives are known to be more thermally stable compared to their linear form. The [12]DBA structure can be further diversified in topicity by using one or two carboxylic acids at each vertex.

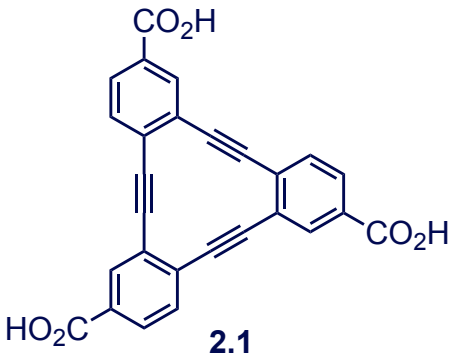

2.1

Figure 2.1. The tricarboxylic acid modified triangular shape-persistent macrocycle [12]DBA **2.1**.

In contrast to sp^2-hybridized alkenes, alkynes as a design element do not suffer from geometry changes arising from the *cis*/*trans* isomerization. Additionally, the structural linearity of the *sp*-hybridized carbon-carbon triple bond is convenient in connecting small building units into larger structures. Some studies suggest that in addition to unique structural and electronic

properties the alkyne bond may have valuable gas uptake properties. Of particular interest, the third order non-linear optic harmonics suggest the hyperpolarizabilty of the alkyne bond may lead to favorable hydrogen storage properties and will be further discussed in Chapter 3.[2]

2.2.2 12]Dehydrobenzannules

The [12]DBA macrocycle **2.2** is an interesting molecule due to its planar, anti-aromatic configuration (Figure 2.2). Its well-defined triangular geometry makes it a rigid building block, ideal for crystallization into MOF structures. Annulenes are useful as a carbon-based linker for the construction of frameworks due to their shape-persistent geometry and unique electronic properties. The rigidity of annulenes increases when acetylenes are added into the π-electron perimeter.[3] Dehydrobenzannulenes add additional stability with an aromatic ring that breaks conjugation of the carboxylic acids with the annulene to prevent decarboxylation and reactivity as a Michael acceptor. Yoshito Tobe and Steven De Feyter have demonstrated the utility of molecular geometry directed networks by the use of non-covalent interactions to engineer two-dimensional Kagomé and Honeycomb networks using rhombohedral and trigonal shaped derivatives, respectively (Figure 2.3).[4] This macrocycle has three alkynes which can act as two or four electron donors to form bonds to a metal. The macrocycle is able to form organometallic complexes by metalation of the cavity with some low oxidation state transition metals such as Ni(0),[5] Cu(I),[6,7] Co(0),[8] and Ag(I).[9] Furthermore, reducing the complex of Ni(0) bis(1,5-cyclooctadiene) with alkali metals increases conductivity by four orders of magnitude.[10,11]

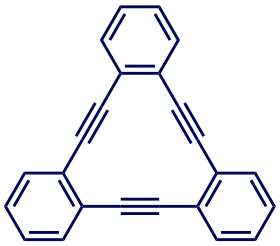

2.2

Figure 2.2. The 12]DBA macrocycle **2.2**.

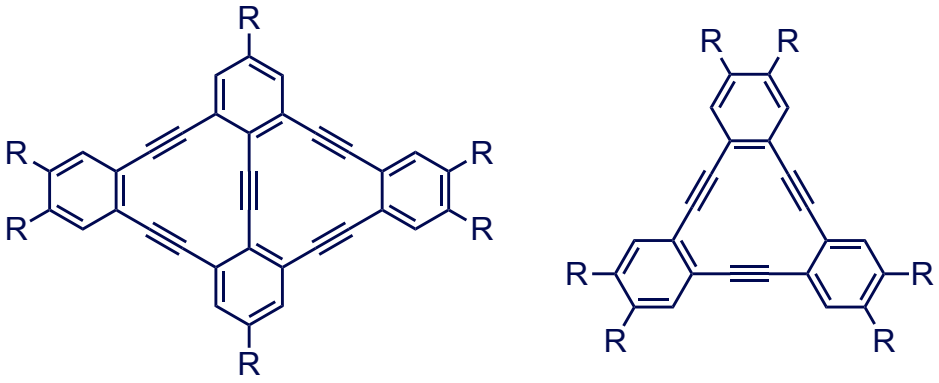

2.3 **2.4**

Figure 2.3 Rhombohedral **2.3** and trigonal **2.4** [12]DBA macrocycles used for molecular geometry directed 2D networks.

Carbon allotropes are of considerable interest to synthesize and study their properties. Examples of carbon allotropes include graphene, carbon nanotubes, fullerenes, diamond, and graphite. Naturally occurring carbon allotropes include graphite, diamond, and fullerenes. Graphynes, a family of non-natural carbon allotropes containing *sp*- and sp^2- hybridized carbon were first proposed by Baughman in 1987 (Figure 2.4).[12] Since then, considerable interest in simulating the mechanical, optical, and electronic properties of this theoretical family of allotropes has been hotly pursued despite the lack of structures successfully synthesized.[13] Small amounts of graphdiyne on Cu foil were synthesized in 2010 and so far represent the only successfully synthesized member of this family.[14] Although most proposed graphyne structures still remain elusive, successful attempts at subunits of and precursors to graphyne materials have been successfully synthesized by Haley (Figure 5).[15]

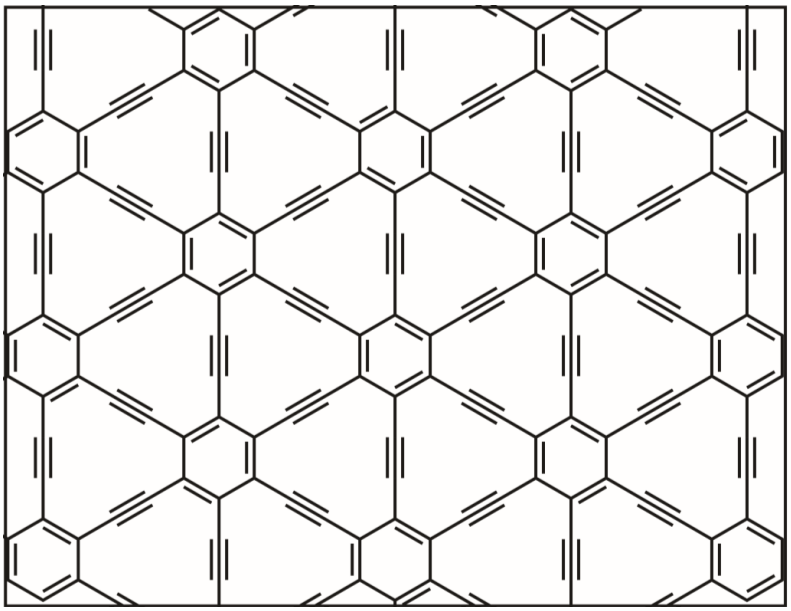

Figure 2.4. γ-Graphyne, a theoretical network composed entirely of *sp*- and sp^2-hybridized carbons.

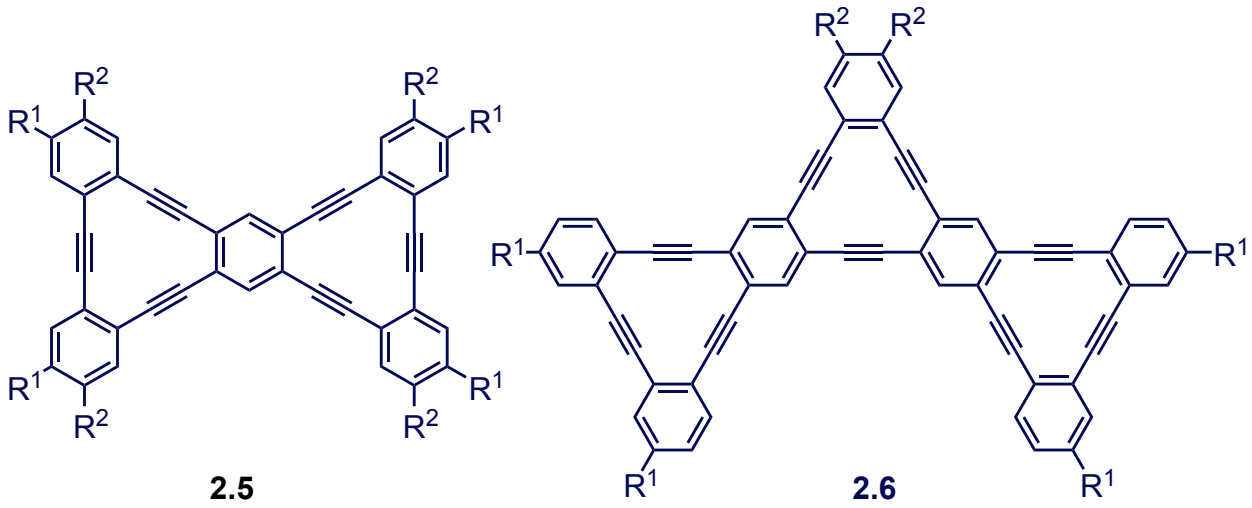

Figure 2.5. Some examples of isolated subunits of graphyne, biscyclyne **2.5** and tris[12]cyclne **2.6.**[15]

2.2.3 [12]DBA Synthetic Strategies

Several strategies for synthesizing [12]DBA analogues have been demonstrated. Diercks and Vollhardt prepared a [12]DBA by the 3-fold cyclization of hexaethynylbenzene with $CpCo(CO)_2$ followed by a thermal retrocyclization of the central benzene ring to form the macrocycle.[16] Alkyne metathesis has been used to prepare symmetrical [12]DBA cycles by Moore[17] and asymmetric [12]DBA macrocycles were synthesized by Tew; however, they were

unable to separate the isomers by chromatography.[18] The Castro-Stephens coupling[19] was first published in 1963 to synthesize diaryl acetylenes from aryl halides and copper acetylides and was later used by Hisaki[20] to synthesize [12]DBA analogues through a cyclotrimerization reaction.

2.3 Results & Discussion

2.3.1 Original [12]DBA Synthesis

The [12]DBA **2.1** was first synthesized by Hisaki following a general copper catalyzed cyclotrimerization of *o*-iodophenylacetylenes for the preparation of substituted [12]DBA analogues.[20] This synthetic route was used as a general outline and many steps were optimized or modified during the synthesis from the known procedures (Scheme 2.1). The carboxylic acid groups are protected as their methyl esters during the synthesis of the [12]DBA macrocycle. Commercially available *p*-aminobenzoic acid **2.7** was esterified with dimethyl carbonate to yield the methyl ester **2.8** in 95% yield. Benzyltriethylammonium dichloroiodate (BTEA•ICl_2) was used to selectively iodinate the ortho position of aniline to yield **2.9** in 96% yield. The pyrrolidine triazene **2.10** was synthesized instead of the diethylamine-triazene system synthesized by Hisaki in order to improve the crystallinity of the substrate to isolate the product by precipitation from the reaction solution. The aniline was converted to the pyrrolidine-capped triazene **2.10** by treatment with $NaNO_2$ in aqueous HCl to form the diazonium salt and was subsequently quenched with pyrrolidine to obtain the triazene **2.10**, which precipitated out of the reaction and was collected by filtration in 93% yield. Sonogashira coupling of **2.10** with trimethylsilylacetylene (TMSA) resulted in acetylene derivative **2.11**. followed by thermal iodination with methyl iodide in an autoclave yield the iodoaryl system **2.12**. Mild deprotection of the TMS-acetylene with K_2CO_3 in methanol yielded the macrocyclization precursor **2.13**.

Scheme 2.1. Original [12]DBA synthesis of the macrocyclization precursor **2.13**.

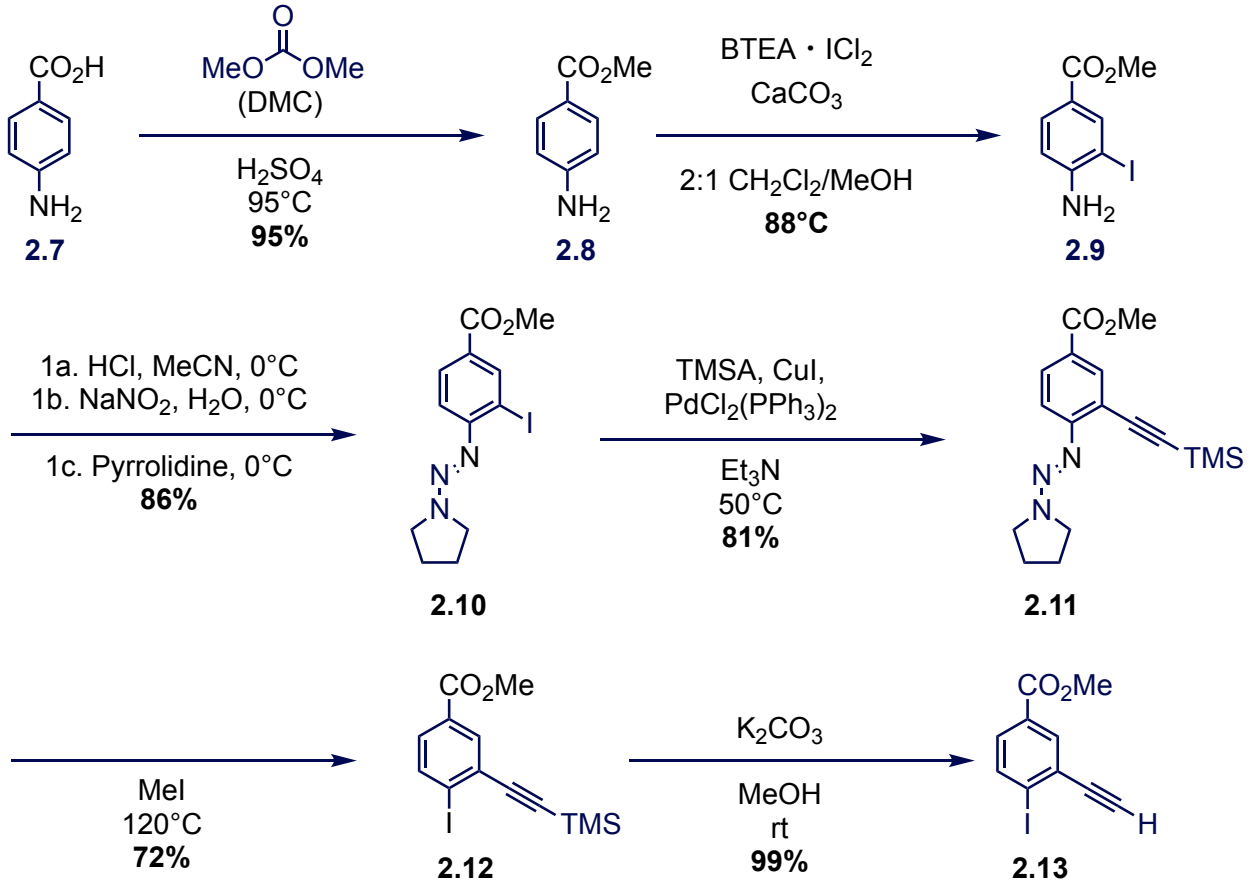

2.3.2 Macrocyclization

The methyl ester protected [12DBA **2.14** was obtained using modified Castro-Stephens coupling conditions (CuI, K_2CO_3, PPh_3, DMF, 120°C) in 33% yield based on ^{1}H NMR using an internal standard; however, tedious purification by column chromatography gives only 4% isolated yield of **14** (Scheme 2.2) due to the difficulty of removing PPh_3O and oligomer byprodcts. Thus, saponification of the methyl ester **2.14** to give the carboxylic acid **2.1** was never attempted initially due to the difficulty of obtaining enough material of precursor **2.13** for this final reaction.

Many attempts were made to optimize the macrocyclization reaction and purification to yield enough material for the subsequent synthesis of MOFs. The macrocyclization was optimized by using a concentration of 20 mM of [12]DBA substrate in DMF. Too concentrated of conditions lead to the formation of large oligomers. During purification, PPh_3O could not be completely precipitated away from the product due to their similar solubilities. The streaking of PPh_3O during flash column chromatography required three columns to purify the material and thus greatly affected the isolated yield.

Alternative reaction conditions were attempted in order to yield larger quantities of macrocycle **2.14**. One approach involved isolating the copper acetylide **2.15** and reacting it alone to ease the purification by avoiding the use of PPh_3. The macrocyclization precursor was converted to the copper acetylide **2.15** in 45% yield (Scheme 2.3). The isolated copper acetylide **15** was

reacted in pyridine at 120 °C but only the homocoupled dimer was isolated. Another approach involved using water-soluble ligands for the copper(II) in order to be easily removed during aqueous workup; however, only polymers were isolated from the reaction. Sonogashira coupling conditions were tried using $PdCl_2(PPh_3)_2$ catalyst at sub ambient temperatures but only polymers were isolated. Ultimately, the optimized Castro-Stephens conditions were the only reaction conditions that yielded isolable product, albeit in 4% yield.

Scheme 2.2. Optimized macrocyclization conditions of [12]DBA **2.14** from **2.13**.

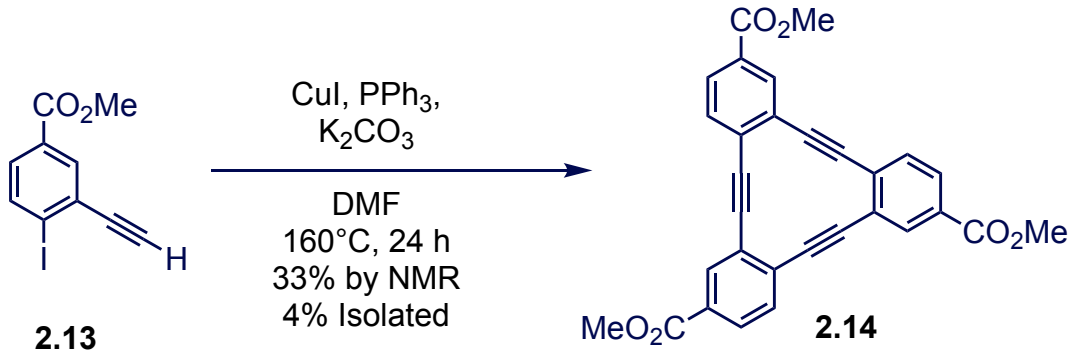

Scheme 2.3. Synthesis of copper acetylide **2.15** from *o*-iodophenylacetylene **2.13**.

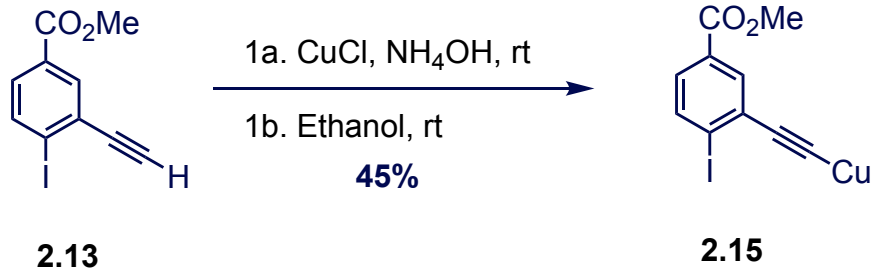

2.3.3 New [12]DBA Synthesis

Multigram scale amounts of macrocyclization precursor **2.13** were needed to optimize the modified Castro-Stephens coupling, a facile route to isolate the compound in high yield, large quantities, and short synthetic times was imperative for the success of the project. An alternative route to install the terminal alkyne functionality was designed. This is significant as it cuts the number of steps from six to three in order to access the macrocyclization precursor **2.13**. Furthermore, the original synthesis contained a number of undesirable steps that required metal-catalyzed cross couplings and scale-up limiting steps. The revised synthesis of the macrocyclization precursor **2.13** was designed by radical bromination of the commercially available toluene **2.16** followed by oxidation of the resulting benzyl bromide **2.17** to the aldehyde **2.18** in order to install the alkyne functionality by Seyferth-Gilbert homologation (Scheme 2.4).

Scheme 2.4. Revised synthesis of macrocyclization precursor **2.13**.

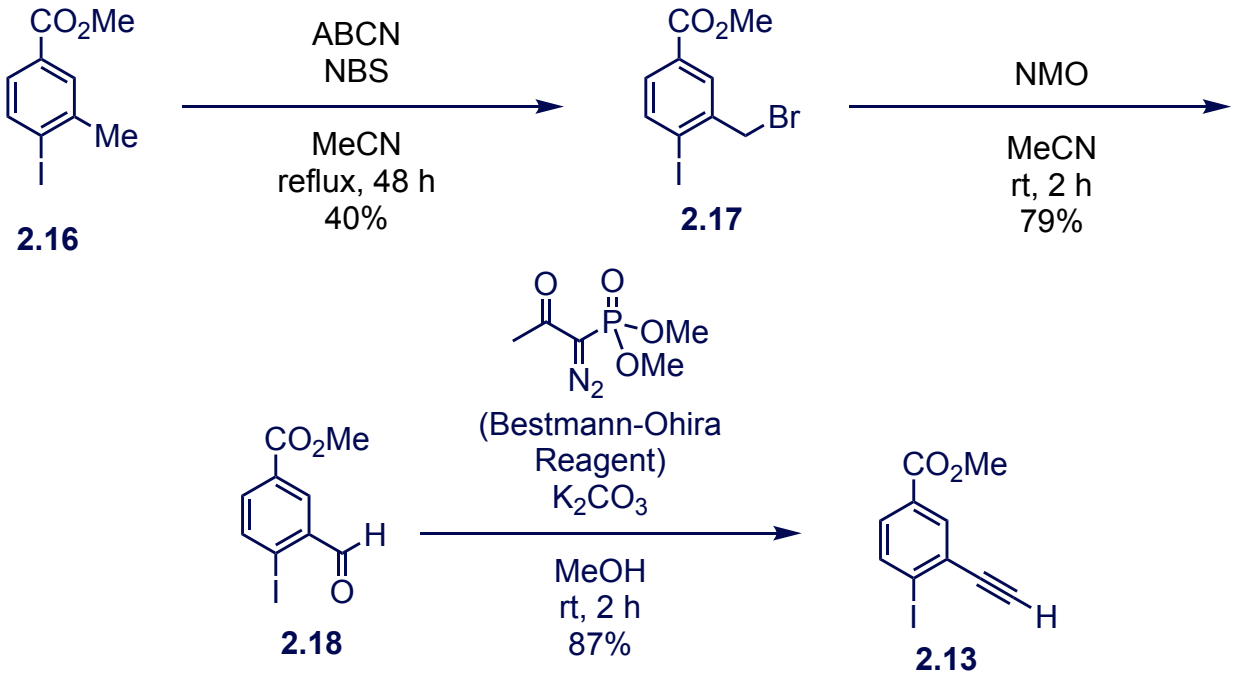

2.4 Conclusions and Outlook

The carboxylic acid functionalized [12]DBA was synthesized by the cyclotrimerization of *o*-iodophenylacetylenes. The isolated yield of this Modified Castro-Stephens coupling is low and reaction is unreliably reproducible at larger scales. Unreliable Castro-Stephens coupling and numerous synthetic steps to the cyclotrimerization precursor were prohibitive in the large-scale isolation of macrocycle. Large amounts of macrocyclization precursor were required to optimize the cyclotrimerization Castro-Stephens coupling reaction to obtain [12]DBA linker in gram scale quantities for exploratory MOF synthesis. This prompted a redesign in the synthetic strategy to shorten the synthesis by installing the terminal alkyne by homologation of the benzaldehyde rather than through a Sonogashira coupling.

The impracticality of isolating large quantities of macrocycle for the synthesis of MOFs was evidenced after considerable reaction trials, optimizations, and tedious purification. MOF gas sorption studies alone require gram scale of materials. Isolating the macrocycle in mg quantities is sufficient for crystallographic studies but not for full characterization or the study of the bulk properties and exploration of applications of the resulting materials. Small amounts of macrocycle were sufficient for crystallographic studies discussed in Chapter 3; however, preparing enough material for porosity, surface area, and gas sorption measurements was not feasible. It is hoped that the revised synthesis will give better isolated yields.

2.5 Experimental

2.5.1 General

All syntheses were performed under inert Ar atmosphere. ^{1}H and $^{13}C\{^{1}H\}$ NMR spectra were acquired on a Bruker DRX-500 or ARX-500 or AV-500 (500 MHz) spectrometer and chemical shifts were calculated using the solvent resonance as internal standards (^{1}H: 7.26 ppm for $CHCl_3$, 2.50 ppm for DMSO; $^{13}C\{^{1}H\}$: 77.00 ppm for $CDCl_3$, 39.51 ppm for DMSO-d_6). ^{1}H NMR data is reported as follows: chemical shift δ (ppm), multiplicity, coupling constant (Hz), and integration. ^{13}C NMR data is reported according to the chemical shift. Column chromatography was performed on silica gel purchased from Sorbent Technologies (standard grade, 60 Å, 40-63 μm). Analytical thin layer chromatography (TLC) was performed on Whatman 250 μm-thick silica gel 60 plates with a fluorescent indicator. TLC spots were visualized using either short-wave (254 nm) or long-wave (365 nm) UV light.

2.5.2 Materials

All commercial reagents were used as purchased unless otherwise specified. Silica gel used for flash column chromatography and plugs were purchased from Sorbent Technologies (standard grade, 60 Å, 40-63 μm). Thin layer chromatography (TLC) was performed on EMD silica gel 60 plates and visualized with a 254 nm light. Dichloromethane (CH_2Cl_2), tetrahydrofuran (THF), diethyl ether (Et_2O), and acetonitrile (MeCN) were distilled over calcium hydride (CaH_2) for CH_2Cl_2, and benzophenone for THF, Et_2O, and MeCN under argon immediately before use. Anhydrous *N,N*-dimethylformamide (DMF) and triethylamine (Et_3N) were obtained by passing them through an alumina column on a solvent purification system (SPS) under argon immediately before use. Methanol (MeOH) was stored over 4Å molecular sieves. *N*-Bromosuccinimide (NBS) was recrystallized immediately before use. Benzyltriethylammonium dichloroiodate (BTEA•ICl_2) was synthesized according to a literature procedure and stored in a dark glass bottle until use.[21] The Bestmann-Ohira reagent was synthesized according to a literature procedure and stored in the refrigerator until use.[22] All other solvents and reagents were purchased from commercial sources (Sigma Aldrich, Alfa Aesar, Acros) and used without any further purification.

2.5.3 Synthetic Procedures and Spectral Data

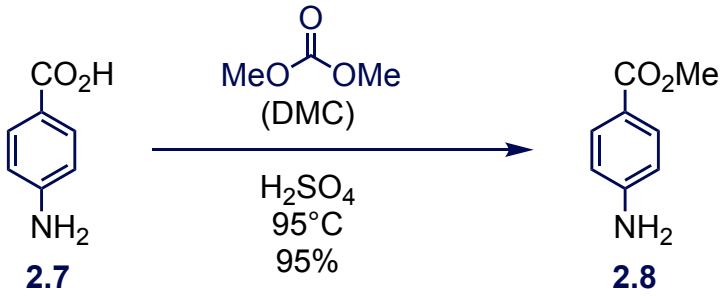

Synthesis of methyl 4-aminobenzoate (2.8): Commercially available *p*-aminobenzoic acid (**2.7**, 20 g, 145 mmol), dimethyl carbonate (45 mL), and H_2SO_4 (11.4 mL) were added to a round-bottom flask and the mixture was refluxed at 95 °C for 16 hours until a homogenous solution was obtained. The reaction was cooled to room temperature and $NaHCO_3$ (24 g in 240 mL of D.I. water) was added. The mixture was filtered and 21.0 g (95%) of a white powder was collected and used

without further purification. ^{1}H NMR (500 MHz, $CDCl_3$) δ 7.85 (d, J = 8.5 Hz, 2H), 6.63 (d, J = 8.5 Hz, 2H), 4.11 (broad s, 2H), 3.84 (s, 3H). ^{13}C NMR (400 MHz, $CDCl_3$) δ 167.2, 150.9, 131.6, 119.6, 113.8, 51.6.

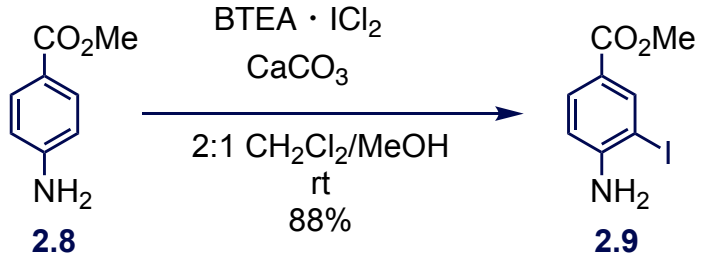

Synthesis of methyl 4-amino-3-iodobenzoate (2.9): Methyl 4-aminobenzoate (**2.8**, 570 mg, 3.77 mmol), BTEA•ICl_2 (2.50 g, 6.48 mmol), and $CaCO_3$ (566 mg, 5.65 mmol) were added to a dry round-bottom flask under argon. A 2:1 mixture of CH_2Cl_2:MeOH (34 mL) was added and the reaction was stirred at room temperature. The reaction was monitored by TLC in 1:1 EtOAc/Hexanes (product R_f = 0.79, starting material R_f = 0.63). The reaction mixture was filtered and the filtrate was reduced by half under reduced pressure. The resulting solution was washed with saturated $Na_2S_2O_3$ solution and the organic layer was dried over $MgSO_4$ before removing the solvent to give 191.9 mg (96%) of **2.9** as a brown powder. ^{1}H NMR (500 MHz, $CDCl_3$) δ 8.32 (d, J = 2 Hz, 1H), 7.80 (dd, J = 8.4 Hz, H), 7.70 (d, J = 8.4 Hz, 1H), 4.45 (broad s, 2H), 3.85 (s, 3H); ^{13}C NMR (400 MHz, $CDCl_3$) δ 165.8, 150.7, 141.0, 131.2, 121.2, 113.1, 82.1, 51.9.

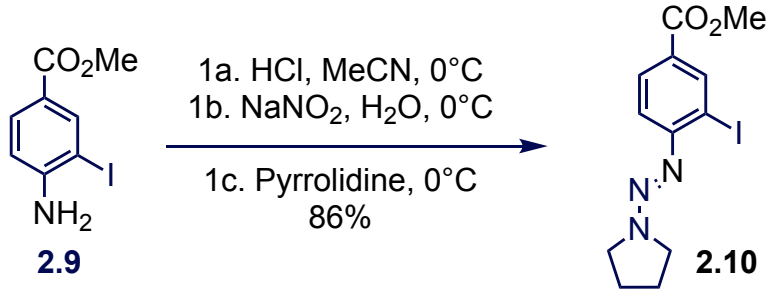

Synthesis of methyl 3-iodo-4-(pyrrolidin-1-yldiazenyl)benzoate (2.10). Followed a general procedure.[23] Methyl 4-amino-3-iodobenzoate (**2.9**, 2.77g, 10.0 mmol), 1M HCl (60 mL), and MeCN (60 mL) were added to a round-bottom flask and stirred until the solution was homogenous and then subsequently cooled to 0 °C in an ice-bath. A 0 °C solution of $NaNO_2$ in 5 mL of water was added dropwise and the mixture was allowed to stir for 1 hour in an ice bath before quenching with pyrrolidine (8.27 mL). The resulting mixture was filtered, rinsed with ice-cold water, and dried at 40 °C under reduced pressure for 24 hours to obtain 3.08 g (86%) of **2.10** as a beige powder. ^{1}H NMR (500 MHz, $CDCl_3$) δ 8.52 (d, J = 1 Hz, 1H), 7.94 (dd, J =8.5 Hz, 2 Hz, 1H), 7.42 (d, J = 8.5 Hz, 1H), 3.94 (broad s, 2H), 3.89 (s, 3H) 2.08 (s, 4H). ^{13}C NMR (400 MHz, $CDCl_3$) δ 165.9, 154.0, 140.8, 130.2, 127.6, 116.6, 95.5, 52.1.

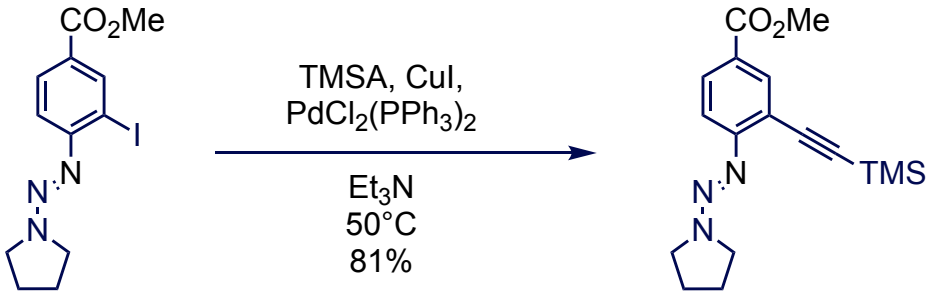

2.10 **2.11**

Synthesis of methyl 4-(pyrrolidin-1-yldiazenyl)-3-((trimethylsilyl)ethynyl)benzoate (2.11). Methyl 3-iodo-4-(pyrrolidin-1-yldiazenyl)benzoate (**2.10**, 5.12 g, 16.4 mmol) was added to a 3-necked flask under argon with $PdCl_2(PPh_3)_2$ (0.686 g, 0.979 mmol) and CuI (0.373 g, 1.96 mmol). Et_3N (163 mL) was added and allowed to stir at room temperature for 30 minutes before TMSA was added (3.26 mL, 22.9 mmol). The reaction was heated at 50 °C (with a reflux condenser to prevent the loss of TMSA) for 15 hours and was monitored by TLC and TMSA was added in 1 mL portions until no starting material remains by TLC. The reaction was cooled to room temperature and filtered through a celite plug with EtOAc before removing the solvent under reduced pressure. The residue was purified by flash column chromatography in an increasing gradient of 10-20% EtOAc in hexanes to yield 4.34 g (81%) of **2.11** as bright yellow, shiny flakes. ^{1}H NMR (500 MHz, $CDCl_3$) δ 8.16 (d, *J* = 1 Hz, 1H), 7.89 (dd, *J* = 1 Hz, 1H), 7.47 (d, *J* = 1 Hz, 1H), 3.96 (broad t, 2H), 3.89 (s, 3H) 3.75 (broad t, 2H) 2.06 (broad t, 4H), 0.26 (s, 9H); ^{13}C NMR (400 MHz, $CDCl_3$) δ 166.4, 156.0, 135.0, 130.2, 125.8, 117.5, 116.4, 102.3, 51.8, 51.2, 46.8, 23.8, 23.4, -0.06.

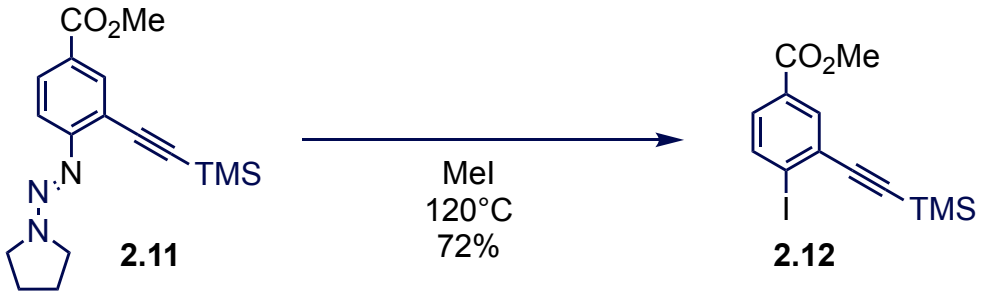

2.11 **2.12**

Synthesis of methyl 4-iodo-3-((trimethylsilyl)ethynyl)benzoate (2.12). Methyl 4-(pyrrolidin-1-yldiazenyl)-3-((trimethylsilyl)ethynyl)benzoate (**2.11**, 1.38 g, 4.17 mmol) was divided into teflon-lined autoclave and MeI (27.5 mL) was added. The autoclaves were sealed and placed in a 120 °C oven for 17 hours then allowed to cool to room temperature before opening. The MeI was allowed to evaporate and the residue was dissolved in hexanes and run through a large silica plug with hexanes and the solvent was removed under reduced pressure. A small amount of acetone was added to dissolve and slowly evaporated to give 1.07 g (72%) of **2.12** as clear, pale yellow needle crystals. ^{1}H NMR (500 MHz, $CDCl_3$) δ 8.09 (d, *J* = 1 Hz, 1H), 7.83 (d, *J* = 5 Hz, 1H), 7.60 (dd, *J* = 5 Hz, 1 Hz, 1H), 3.91(s, 3H), 0.30 (s, 9H); ^{13}C NMR (400 MHz, $CDCl_3$) δ 165.7, 138.9, 133.2, 130.0, 129.8, 129.7, 107.2, 105.4, 99.9, 52.3, -0.36.

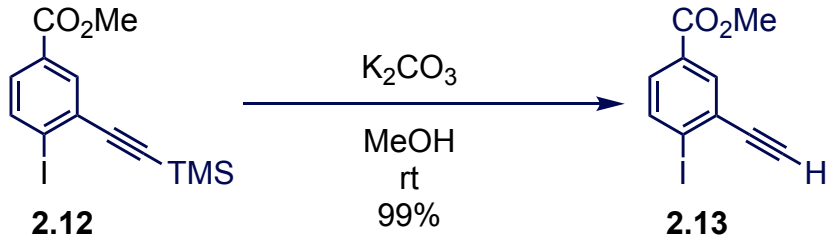

Synthesis of methyl 3-ethynyl-4-iodobenzoate (2.13). Methyl 4-iodo-3-((trimethylsilyl)ethynyl)benzoate (**2.12**, 850 mg, 2.37 mmol) and anhydrous K_2CO_3 (978 mg, 7.07 mmol) were added to a dry round-bottom flask with a stir bar. Anhydrous MeOH (3.9 mL) was added and the reaction was stirred at room temperature while monitoring reaction progress by TLC in 1:3 EtOAC/Hexanes. The MeOH was removed under reduced pressure and the residue was dissolved in CH_2Cl_2, poured into a separatory funnel with water and extracted 3x with CH_2Cl_2, washed 3x with water, and washed 1x with brine. The organic layer was dried over $MgSO_4$, filtered, and the solvent removed under reduced pressure to yield **2.13** as a light brown, crystalline powder 670 mg (99%). ^{1}H NMR (500 MHz, $CDCl_3$) δ 8.11 (d, J = 1 Hz, 1H), 7.83 (d, J = 10.5 Hz, 1H), 7.63 (dd, J = 10.5 Hz, 1 Hz, 1H), 3.90(s, 3H), 3.44 (s, 1H). ^{13}C NMR (400 MHz, $CDCl_3$) δ 165.9, 139.2, 134.1, 130.4, 130.1, 129.3, 106.6, 84.3, 82.0, 52.5.

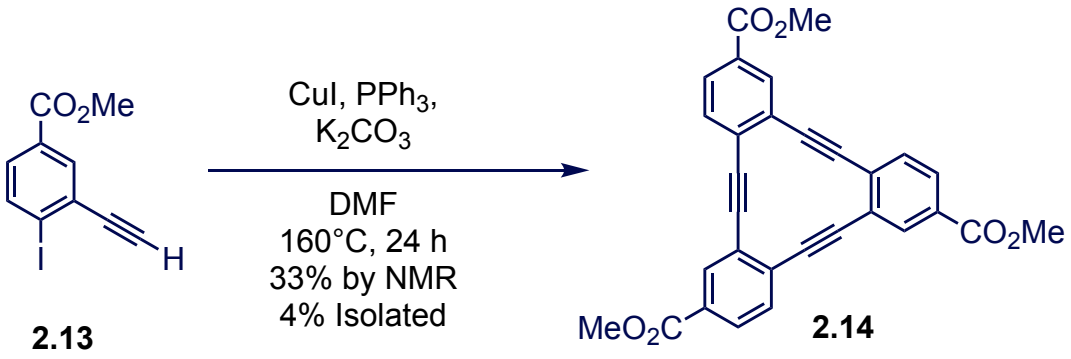

Synthesis of [12]Dehydrobenzoannulene trimethyl ester (2.14). 2.13 (50 mg, 0.1748 mmol), CuI (9.98 mg, 0.0524 mmol), PPh_3 (13.74 mg, 0.0524 mmol), and K_2CO_3 (72.46 mg, 0.5243 mmol) were added to a dry, two-neck round-bottom flask under argon atmosphere. DMF (8.74 mL) was added and the reaction was stirred at 160 °C for 24 hours. The reaction was cooled to room temperature and filtered through a celite plug with CH_2Cl_2. The resulting solution was poured into a separatory funnel with water and extracted 3x with CH_2Cl_2 and washed 3x with water, 1x with brine, and the organic layer was dried over $MgSO_4$, filtered, and the solvent removed under reduced pressure to leave a brown residue. The residue was purified by 3x FCC with CH_2Cl_2, followed by 2x (CH_2Cl_2 with 1% MeOH and 1% Et_3N) to yield 1 mg (4%) of **2.14** as a bright yellow powder. ^{1}H NMR (500 MHz, $CDCl_3$) δ 8.02 (d, J = 1.5 Hz, 1H), 7.81 (dd, J = 8 Hz, 1.5 Hz, 1H), 7.43 (d, J = 8 Hz, 1H), 3.92 (s, 3H).

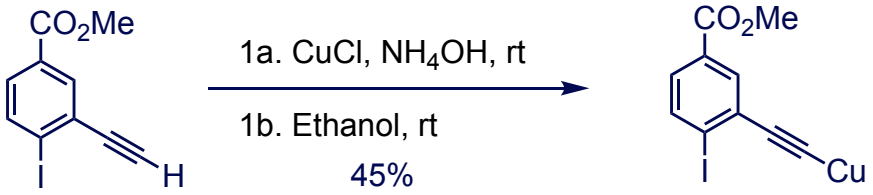

2.13 **2.15**

Synthesis ((2-iodo-5-(methoxycarbonyl)phenyl)ethynyl)copper (2.15). CuI (17.3 mg, 0.091 mmol) was added to a round-bottom flask under argon. NH_4OH (3 mL of a 28% aq. solution) was added and the solution immediately turned a bright, royal blue. A degassed solution of methyl 3-ethynyl-4-iodobenzoate (**2.13**, 26 mg, 0.091 mmol) in EtOH (0.4 mL) was added dropwise and a yellow precipitate formed immediately. The product was filtered and the washed 3x each with EtOH, water, and Et_2O. The product was dried overnight under reduced pressure to yield 14.4 mg (45%) of the product as a bright yellow powder.

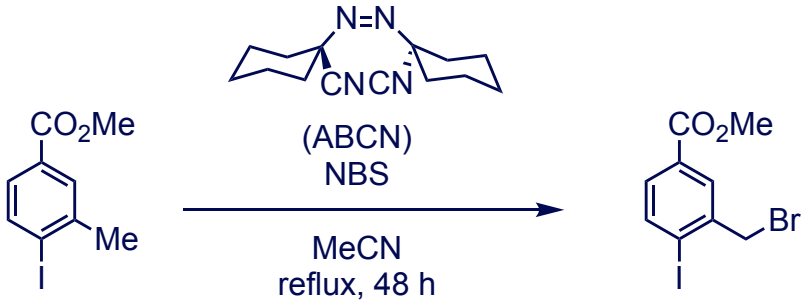

2.16 **2.17**

Synthesis of methyl 3-formyl-4-iodobenzoate (2.17). Methyl 4-iodo-3-methylbenzoate (**2.16**, 1.00 g, 3.62 mmol) and NBS (774 mg, 4.35 mmol) was added to a dry round-bottom flask fitted with a condenser and placed under argon atmosphere. Anhydrous MeCN (4.2 mL) and methyl 3-1,1'-azobis-(cyclohexanecarbonitrile) (ABCN) (20 mg, 0.083 mmol) was added to the flask and the reaction was stirred at room temperature while the monitoring reaction progress by TLC in 3% EtOAC/Hexanes. The crude reaction solution was purified by FCC in 3% EtOAC/Hexanes and the solvent was removed under reduced pressure to yield 170 mg of methyl 3-(bromomethyl)-4-iodobenzoate (**2.17**) as a solid. ^{1}H NMR (500 MHz, $CDCl_3$) δ 8.11 (d, J = 2.1 Hz, 1H), 7.95 (d, J = 8.2 Hz, 1H), 7.60 (dd, J = 8.2 Hz, 2.1 Hz, 1H), 4.62 (s, 2H), 3.92 (s, 3H). ^{13}C NMR (500 MHz, $CDCl_3$) δ 165.9, 140.7, 140.4, 131.0, 130.9, 130.5, 106.1, 52.4, 37.8.

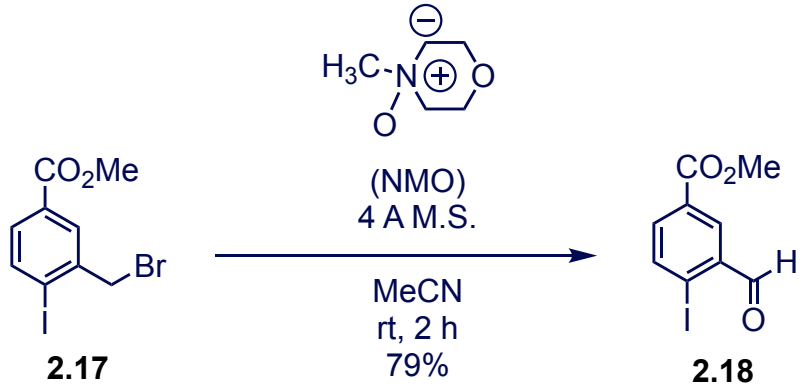

2.17 **2.18**

Synthesis of methyl 3-formyl-4-iodobenoate (2.18). A general procedure was followed.[24] NMO (683 mg, 5.83 mmol) was added to a dry Schlenk round-bottom flask with a stir bar and 4 Å molecular sieves and placed under argon atmosphere. Anhydrous MeCN (49 mL) and methyl 3-(bromomethyl)-4-iodobenzoate (**2.17**, 1.00 g, 2.82 mmol) was added to the flask and the reaction was stirred at room temperature while monitoring reaction progress by TLC in 20% EtOAC/Hexanes. The solution was filtered through a silica plug and the solvent was removed under reduced pressure to yield 643 mg (79%) of methyl 3-formyl-4-iodobenzoate (**2.18**) as a waxy solid. ^{1}H NMR (500 MHz, $CDCl_3$) δ 10.1 (s, 1H), 8.44 (d, J = 2.3 Hz, 1H), 8.03 (d, J = 8.2 Hz, 1H), 7.88 (dd, J = 8.2 Hz, 2.3 Hz, 1H), 3.93 (s, 3H). ^{13}C NMR (500 MHz, $CDCl_3$) δ 194.5, 165.4, 140.9, 135.3, 135.2, 130.9, 130.9, 104.8, 52.5.

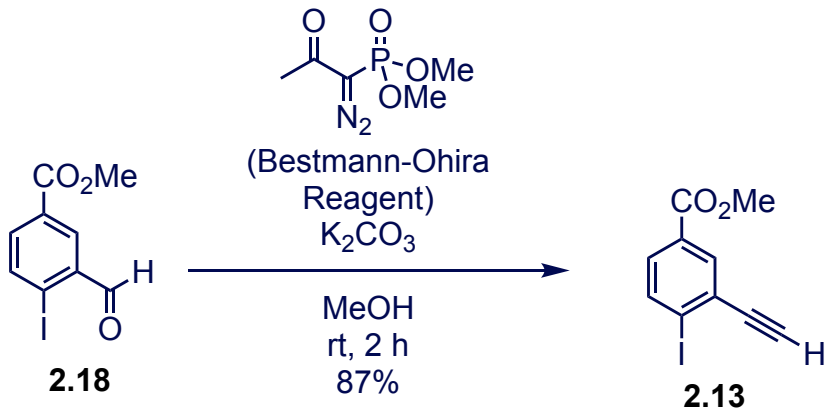

2.18 **2.13**

Synthesis of methyl 3-ethynyl-4-iodobenzoate (2.13). A general procedure was followed.[25] Methyl 3-formyl-4-iodobenzoate (**2.18**, 32 mg, 0.110 mmol), the Bestmann-Ohira reagent (24 mg, 0.125 mmol), and K_2CO_3 (28.8 mg, 0.208 mmol) was added to a dry scintillation vial with a stir bar. The vial was fitted with a septum cap and placed under argon atmosphere. Anhydrous MeOH (1.55 mL) and was added to the vial and the reaction was stirred at room temperature while monitoring the progress by TLC in 20% EtOAC/Hexanes. The solution was diluted with Et_2O, washed with a 5 wt% solution of sodium bicarbonate, dried over Na_2SO_4, and the solvent was removed under reduced pressure to yield 26 mg (87%) of methyl 3-ethynyl-4-iodobenzoate (**2.13**) as a solid. ^{1}H NMR (500 MHz, $CDCl_3$) δ 8.11 (d, J = 1 Hz, 1H), 7.83 (d, J = 10.5 Hz,

1H), 7.63 (dd, J = 10.5 Hz, 1 Hz, 1H), 3.90 (s, 3H), 3.44 (s, 1H). ^{13}C NMR (400 MHz, $CDCl_3$) δ 165.9, 139.2, 134.1, 130.4, 130.1, 129.3, 106.6, 84.3, 82.0, 52.5.

2.6 References and Notes

(1) Li, J.; Brill, T. B. Spectroscopy of Hydrothermal Reactions 20: Experimental and DFT Computational Comparison of Decarboxylation of Dicarboxylic Acids Connected by Single, Double, and Triple Bonds. *J. Phys. Chem. A* **2002**, *106*(41), 9491–9498.

(2) Bredas, J. L.; Adant, C.; Tackx, P.; Persoons, A.; Pierce, B. M. Third-Order Nonlinear Optical Response in Organic Materials: Theoretical and Experimental Aspects. *Chem. Rev.* **1994**, *94*(1), 243–278.

(3) Li, Y.; Rubin, Y.; Diederich, F.; Houk, K. N. Electronic and Structural Properties of the Cyclobutenodehydroannulenes. *J. Am. Chem. Soc.* **1990**, *112*(4), 1618–1623.

(4) Furukawa, S.; Uji-i, H.; Tahara, K.; Ichikawa, T.; Sonoda, M.; De Schryver, F. C.; Tobe, Y.; De Feyter, S. Molecular Geometry Directed Kagomé and Honeycomb Networks: Toward Two-Dimensional Crystal Engineering. *J. Am. Chem. Soc.* **2006**, *128*(11), 3502–3503.

(5) Ferrara, J. D.; Tessier-Youngs, C.; Youngs, W. J. Synthesis and characterization of the first transition metal complex of 1,2:5,6:9,10-tribenzocyclododeca-1,5,9-triene-3,7,11-triyne. *J. Am. Chem. Soc.* **1985**, *107*(23), 6719–6721.

(6) Ferrara, J. D.; Tessier-Youngs, C.; Youngs, W. J. Synthesis and characterization of a copper(I) triflate complex of 1,2:5,6:9,10-tribenzocyclododeca-1,5,9-triene-3,7,11-triyne. *Organometallics* **1987**, *6*(3), 676–678.

(7) Ferrara, J. D.; Tessier-Youngs, C.; Youngs, W. J. Synthesis and molecular structure of a trinuclear copper(I) cofacial bimacrocycle. *Inorg. Chem.* **1988**, *27*(13), 2201–2202.

(8) Djebli, A.; Ferrara, J. D.; Tessier-Youngs, C.; Youngs, W. J. The synthesis and structural characterization of a novel tetracobalt cluster of 5,6,11,12,17,18-hexadehydrotribenzo[*a,e,i*]-cyclododecine. *J. Chem. Soc., Chem. Commun.* **1988**, 548–549.

(9) Ferrara, J. D.; Djebli, A.; Tessier-Youngs, C.; Youngs, W. J. Synthesis and characterization of a silver(I) triflate sandwich complex of 1,2:5,6:9,10-tribenzocyclododeca-1,5,9-triene-3,7,11-triyne. The first example of a 12-membered macrocycle sandwich complex. *J. Am. Chem. Soc.* **1988**, *110*(2), 647–649.

(10) Ferrara, J. D.; Tessier-Youngs, C.; Youngs, W. J. A novel n-doped metallomacrocyclic conductor. *J. Am. Chem. Soc.* **1988**, *110*(10), 3326–3327.

(11) Ferrara, J. D.; Tanaka, A. A.; Fierro, C.; Tessier-Youngs, C. A.; Youngs, W. J. Synthesis and structural and theoretical characterization of a nickel(0) complex of tribenzocyclyne (TBC) and the preparation of a novel organometallic conductor. *Organometallics* **1989**, *8*(9), 2089–2098.

(12) Baughman, R. H.; Eckhardt, H.; Kertesz, M. Structure-property predictions for new planar forms of carbon: Layered phases containing sp^2 and *sp* atoms. *J. Chem. Phys.* **1987**, *87*(11), 6687–6699.

(13) For example, see: (a) Zhang, Y. Y.; Pei, Q. X.; Wang, C. M. Mechanical properties of graphynes under tension: A molecular dynamics study. *Appl. Phys. Lett.* **2012**, *101*, 081909. (b) Sevinçli, H.; Sevik, C. Electronic, phononic, and thermoelectric properties of graphyne sheets. *Appl. Phys. Lett.* **2014**, *105*, 223108. (c) Jing, Y.; Wu, G.; Guo, L.; Sun, Y.; Shen, J. Electronic transport properties of graphyne and its family. *Comput. Mater. Sci.* **2013**, *78*, 22–28. (d) Narita, N.; Nagai, S.; Suzuki, S.; Nakao, K. Electronic structure of

three-dimensional graphyne. *Phys. Rev. B* **2000**, *62*(16), 11146. (e) Cranford, S. W.; Buehler, M. J. Mechanical properties of graphyne. Carbon 2011, *49*(13), 4111–4121. (f) Chen, J.; Xi, J.; Wang, D.; Shuai, Z. Carrier Mobility in Graphyne Should Be Even Larger than That in Graphene: A Theoretical Prediction. *J. Phys. Chem. Lett*. **2013**, *4*(9) 1443–1448. (g) Wang, A.; Li, L.; Wang, X.; Bu, H.; Zhao, M. Graphyne-based carbon allotropes with tunable properties: From Dirac fermion to semiconductor. Diamond Relat. Mater. **2014**, *41*, 65–72.

(14) Li, G.; Li, Y.; Liu, H.; Guo, Y.; Li, Y.; Zhu, D. Architecture of graphdiyne nanoscale films. *Chem. Commun.* **2010**, *46*(19), 3256–3258.

(15) Johnson, C. A.; Lu, Y.; Haley, M. M. Carbon Networks Based on Benzocyclynes. 6. Synthesis of Graphyne Substructures via Directed Alkyne Metathesis. *Org. Lett.* **2007**, *9*(19), 3725–3728.

(16) Diercks, R.; Vollhardt, K. P. C. Tris(benzocyclobutadieno)benzene, the triangular [4]phenylene with a completely bond-fixed cyclohexatriene ring: cobalt-catalyzed synthesis from hexaethynylbenzene and thermal ring opening to 1,2:5,6:9,10-tribenzo-3,4,7,8,11,12-hexadehydro[12]annulene. *J. Am. Chem. Soc.* **1986**, *108*(11), 3150–3152.

(17) Zhang, W.; Brombosz, S. M.; Mendoza, J. L.; Moore, J. S. A High-Yield, One-Step Synthesis of *o*-Phenylene Ethynylene Cyclic Trimer via Precipitation-Driven Alkyne Metathesis. *J. Org. Chem.* **2005**, *70*(24), 10198–10201.

(18) Jiang, J.; Tew, G. N. Synthesis of Macrocycle Isomers via Metathesis Cyclization and Their Self-Assembly from Aqueous Solutions. *Org. Lett.* **2008**, *10*(20), 4393–4396.

(19) Stephens, R. D.; Castro, C. E. The Substitution of Aryl Iodides with Cuprous Acetylides. A Synthesis of Tolanes and Heterocyclics. *J. Org. Chem.* **1963**, *28*(12), 3313–3315.

(20) Hisaki, I.; Sakamoto, Y.; Shigemitsu, H.; Tohnai, N.; Miyata, M.; Seki, S.; Saeki, A.; Tagawa, S. Superstructure-Dependent Optical and Electrical Properties of an Unusual Face-to-Face, π-Stacked, One-Dimensional Assembly of Dehydrobenzo[12]annulene in the Crystalline State. *Chem. Eur. J.* **2008**, *14*(14), 4178–4187.

(21) Kosynkin, D. V.; Tour, J. M. Benzyltriethylammonium Dichloroiodate/Sodium Bicarbonate Combination as an Inexpensive, Environmentally Friendly, and Mild Iodination Reagent for Anilines. *Org. Lett.* **2001**, *3*(7), 991–992.

(22) Dayoub, W.; Doutheau, A. (*E*) Enol ethers from the stereoselective reduction of α-alkoxy-β-ketophosphonates and Wittig type reaction. *Sci. China: Chem.* **2010**, *53*(6), 1937–1945.

(23) Bui, C. T.; Flynn, B. L. J. Solid-Phase Synthesis of 2,3-Disubstituted Benzo[*b*]thiophenes and Benzo[*b*]selenophenes. *Comb. Chem.* **2006**, *8*(2), 163–167.

(24) Griffith, W. P.; Jolliffe, J. M.; Ley, S. V.; Springhorn, K. F.; Tiffin, P. D. Oxidation of Activated Halides to Aldehydes and Ketones by N-Methylmorpholine-N-Oxide. *Synth. Commun.* **2006**, *22*(13), 1967–1971.

(25) Müller, S.; Liepold, B.; Roth, G. J.; Bestmann, H. J An Improved One-pot Procedure for the Synthesis of Alkynes from Aldehydes. *Synlett* **1996**, 521–522.

CHAPTER 3

Synthesis of a Chiral Metal-Organic Framework with srs Topology from an Achiral [12]Dehydrobenzannulene Carboxylate Organic Linker

3.1 Abstract

The synthesis and structure determination of a chiral metal-organic framework (MOF) with $SrSi_2$ topology from an achiral [12]dehydrobenzannulene ([12]DBA) macrocyclic organic linker is presented. This double-walled framework features two macrocycles π-stacked and staggered face-to-face joined by a three Zn^{2+} center secondary building unit (SBU).

3.2 Introduction

The use of acetylene-containing organic linkers for the construction of MOFs is largely unexplored and prompts more research to be devoted to the development of these materials to study their structures, properties, and applications of the resulting frameworks.

3.2.1 Alkynes as a Building Unit

The element carbon can adopt three hybridization states of (sp^3, sp^2 and *sp*) with discrete geometries which leads to a variety of topological possibilities from their combinations due to their geometric differences. In contrast to sp^2-hybridized alkenes, alkynes do not suffer from geometry changes arising from the *cis*/*trans* isomerization. Additionally, the structural linearity of the *sp*-hybridized carbon-carbon triple bond is convenient in connecting structures and lengthening their unit cell dimensions.

3.2.2 Why Are *sp*-Hybridized Networks Useful to Study for MOF chemistry?

Our initial interest in the use of acetylene-containing organic linkers was for the study of gas uptake properties, in particular H_2. Acetylenes are attractive candidates for increasing the uptake of H_2 since the carbon-rich acetylene functionalities are lightweight and effectively increase surface area (increased edge to space ratio) due to their long and cylindrical shape, providing an ideal surface for the adsorption of H_2. Previous research in the Yaghi group has demonstrated that H_2 adsorption can be increased with a few basic parameters: frameworks must have a high surface area with an appropriate pore size (<10Å), interpenetration, coordinatively unsaturated metal sites, light building blocks, and functionalized ligands.[1] An important consideration in increasing hydrogen storage capacity is to increase the number of adsorptive sites on the framework by using long, slim functionalities while the faces and edges are exposed to increase the surface area available for van der Waals interactions between the gas substrate and the framework.[2,3] These van der Waals interactions are significant, especially in the case of low pressure H_2 storage, since at low pressures the H_2 molecules are more likely to be on the surface of the framework rather than the center of the pore. Thus, acetylene- containing frameworks with a high surface area and reasonable pore size should be advantageous for low pressure H_2 storage.

3.2.3 Previous Work Using Acetylenic MOFs

The use of acetylene-containing organic linkers in MOFs is largely unexplored and there are even fewer examples of their use for potential H_2 storage materials. The first example of an acetylene containing MOF was synthesized by Kim *et al*. from acetylenedicarboxylate **3.1** using non-solvothermal conditions with zinc nitrate in ethanol.[4] Triethylamine vapor-diffusion was used to deprotonate the link and an augmented diamond framework was formed. The structure is composed of two interpenetrating frameworks. Expanding on the use of acetylene-containing organic linkers in MOFs, Dr. David Tranchemontagne synthesized a series of linear, acetylene-containing organic linkers used to make IRMOF-61 (**3.2**), IRMOF-62 (**3.3**), and IRMOF-64 (**3.4**) with the number of conjugated acetylenes (n) equal to 1, 2, and 4 respectively (Figure 3.1).[5] Tranchemontagne demonstrated that hydrogen storage in MOFs can be improved by keeping a large surface area and decreasing the pore volume from IRMOF-61 to IRMOF-62 as evidenced by the increased wt% of H_2 that was stored, going from 1.04% to 1.72% (Table 3.1).

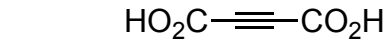

3.1

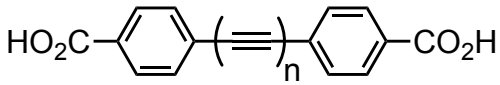

3.2 (n=1)
3.3 (n=2)
3.4 (n=4)

Figure 3.1. Acetylene dicarboxylate **3.1** used for the synthesis of IRMOF-0 (MOF-31) (top) and diphenylacetylene dicarboxylic acid ligands used for IRMOF-6x series **3.2** (IRMOF-61), **3.3** (IRMOF-62), and **3.4** (IRMOF-64) (bottom).

Another example of using acetylene-containing organic linkers for H_2 storage applications is 4,4′,4″-[benzene-1,3,5-triyl-tris(ethyne-2,1-diyl)]tribenzoate (BTE) which was used with a $Zn_4O(CO_2)_6$ SBU for the construction of MOF-180, **qom** topology, and additionally combined with biphenyl-4,4'-dicarboxylate (BPDC) to yield MOF-210, **toz** topology (Figure 3.2).[6] To date, MOF-180 has no reported H_2 absorption data, but MOF-210 exhibits exceptional H_2 uptake capacity with 176 mg g^{-1} at 77 K and 80 bar.

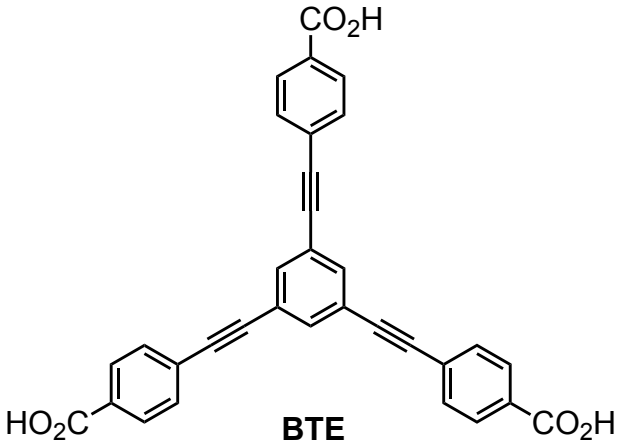

Figure 3.2. BTE linker used to make MOF-180 and MOF-210 (combined with BPDC).

More recently, the PCN-6x series of isoreticular acetylenic MOFs based on C_3 symmetric hexacarboxylate lisgands were synthesized by Yuan and coworkers (Figure 3.3).[7] The PCN-6x series are (3,24)-connected **rht**-type MOFs comprised of hexacarboxylate ligands and copper paddlewheel SBUs. Yaun and coworkers were unable to activate the largest member of their series, PCN-610, which collapsed upon removal of the solvent guest molecules. The structure was eventually activated by Hupp using a supercritical CO_2 technique and renamed NU-100.[8] Subsequent high pressure gas adsorption studies showed NU-100 had excellent high pressure H_2 uptake capabilities with 164 mg g^{-1} at 70 bar and 77 K, likely to due to the large surface area of the framework (6,143 m^2 g^{-1} Brunauer-Emmett-Teller (BET) surface area) and pore size (2.82 cm^3 g^{-1}); however, no gas adsorption studies were carried out at lower pressures (Table 3.1), presumably since the large pore volumes would make the material less than ideal for low pressure H_2 uptake. Many of these acetylene-containing MOFs were shown to have exceptional H_2 uptake capacities (Table 3.1) suggesting that acetylenes should be good for H_2 uptake due to their favorable edge to space ratio being long and slim and provide an ideal surface for the physioadsorption of H_2.

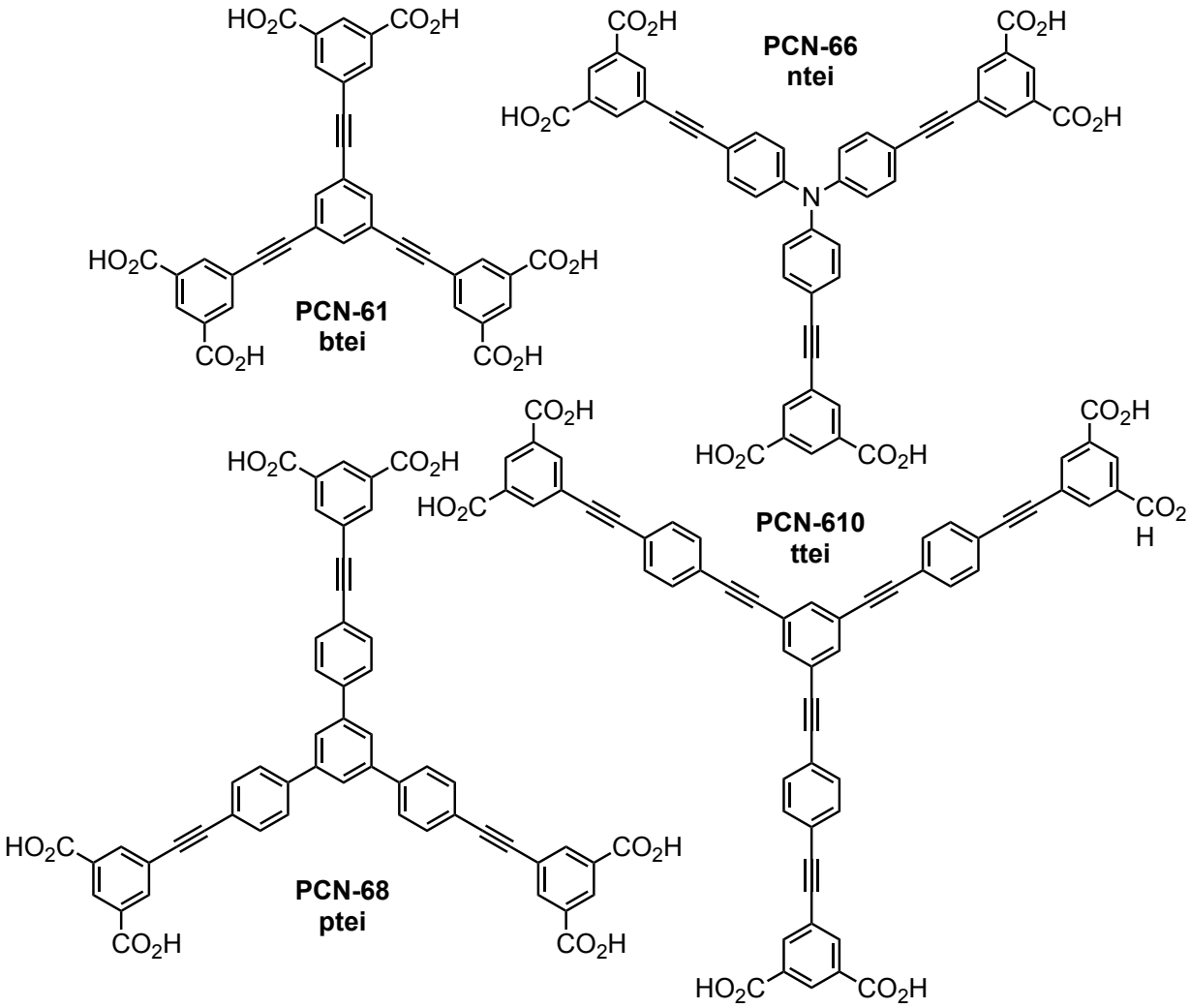

Figure 3.3. PCN-6x series of (3,24)-connected hexacarboxylate ligands **btei** (PCN-61), **ntei** (PCN-66), **ptei** (PCN-68), and **ttei** (PCN-610, aka NU-100).

Table 3.1. H_2 storage properties of acetylene-containing metal-organic frameworks.

MOF	Linker	SA_{BET} [$m^2\ g^{-1}$][a]	$SA_{Langmuir}$ [$m^2\ g^{-1}$][a]	Pore Volume [$cm^3\ g^{-1}$]	H_2 Uptake [wt%]	Total Uptake [$mg\ g^{-1}$]	Q_{ST} [$kJ\ mol^{-1}$]	Ref
IRMOF-61	**3.2**	1410	1580	1.66	1.04	ND	7.4	5
IRMOF-62	**3.3**	2420	2690	0.91	1.72	ND	7.3	5
PCN-61	**btei**	3000	3500	1.36	2.25	ND	6.36	7
PCN-66	**ntei**	4000	4600	1.63	1.79	ND	6.22	7
PCN-68	**ptei**	5109	6033	2.13	1.87	ND	6.09	7
PCN-610	**ttei**	6143	ND	2.82	ND	164	6.1	8
MOF-210	**BTE, BPDC**	6240	10400	3.60	ND	176	4.4	6

[a] Abbreviations: SA = apparent surface area, ND = not determined, Ref. = reference.

3.2.4 Crystal Engineering [12]DBA

The first example of crystal engineering with [12]DBA macrocycles was demonstrated in 2D by De Feyter on a surface where the molecular geometry of the [12]DBA macrocyclic core directed the formation of the network topology such that rhombi [12]DBA macrocycles formed Kagomé networks while the triangular [12]DBA macrocycles formed a honeycomb network.[9]

The planar configuration and rich density of sp^2-hybridized carbon atoms makes the [12]DBA macrocycle suitable for π-stacking. It has been demonstrated that [12]DBA forms a variety of stacking configurations depending upon the substitution of different appendages or solvent used to crystallize the macrocycle as a small molecule.[10]

The unique geometry of the triangular shape-persistent [12]DBA macrocycle can produce unique topologies and nets when combined with a variety of metal cation secondary building units by using the principles of reticular chemistry. Furthermore, the rigid, shape-persistent nature of the macrocycle is suitable for crystallizing periodic networks due to facile packing and reduced degrees of freedom.

3.3 Results & Discussion

3.3.1 Synthesis and Single Crystal Growth Optimization

Initial synthetic studies with the [12]DBA **2.1** focused on exploring conditions to crystallize the macrocycle into ordered, periodic networks. Zinc was initially chosen as the metal cluster cation due to zinc's well-known ability to adopt multiple coordination geometries leading to a wide array of secondary building units and nets.[11] After many synthetic attempts discussed in Chapter 2, a collaboration was started with Professors Hisaki and Miyata at the University of Osaka, Japan, to prepare MOFs with the DBA **2.1**. Using Hisaki's [12]DBA, Zn MOF-[12]DBA-1 was synthesized from **2.1** with $Zn(NO_3)_2 \cdot 6H_2O$ in DMF at 100 °C in a half dram vial in an isothermal oven to yield 0.3-0.4 mm bright yellow prismatic rhombohedral single crystals after 24 hours (Figure 3.4). At higher concentrations and lower temperatures of 80 °C, a second phase of material, orange prismatic single crystals is evident under the microscope and confirmed by PXRD analysis. This second phase can be inhibited from forming if the synthesis is carried out in diluted conditions at higher temperatures. This phase does not form single crystals therefore its structure resolution was not further pursued.

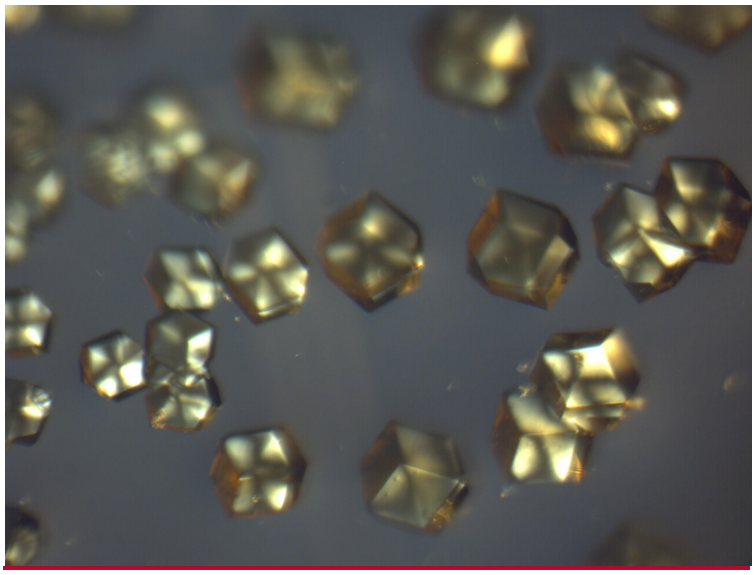

Figure 3.4. Single crystals of Zn MOF-[12]DBA-1 under optical microscope.

3.3.2 Crystallography and Structure Analysis

A single crystal of Zn MOF-[12]DBA-1 with a drop of DMF solvent was sealed inside a capillary with wax and diffraction data were collected using synchrotron radiation at Advanced Photon Source (APS). The structure was solved by single-crystal X-ray diffraction (SCXRD) and confirmed by computational models and powder X-ray diffraction (PXRD) (Figure 3.5). Some peaks in the simulated PXRD pattern are absent from the experimental pattern since not all of the predicted Bragg reflections are experimentally observed. This result is quite typical in nanoporous frameworks where crystallinity and long-range ordering are poor compared to other crystalline materials such as small molecules that are characterized by PXRD.

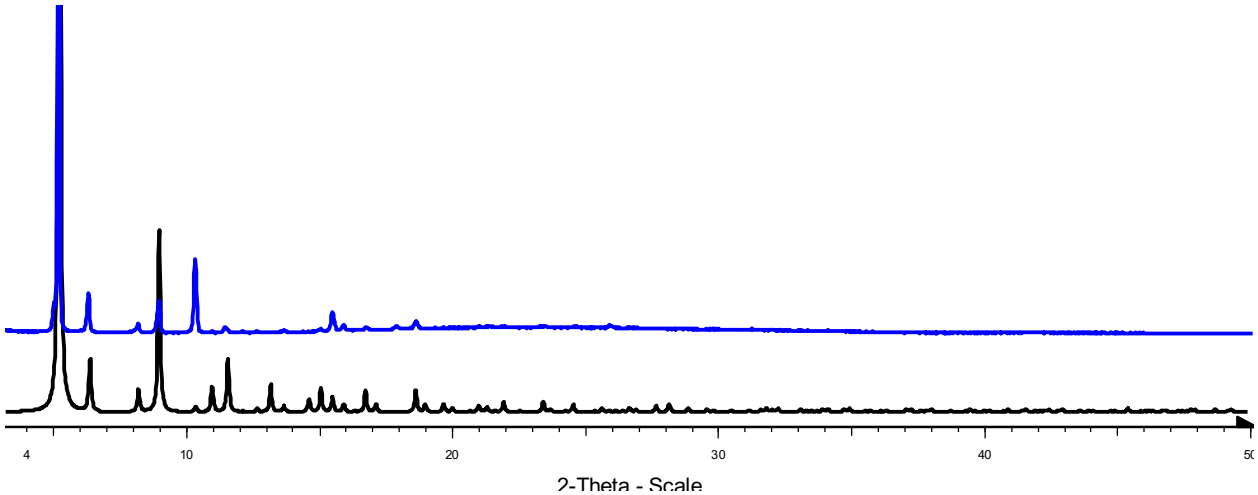

Figure 3.5. PXRD of Zn MOF-[12]DBA-1 single crystals (blue) compared to simulated pattern from Materials Studio (black).

Single-crystal X-ray diffraction studies revealed that Zn MOF-[12]DBA-1 crystallizes in the space group *P*4(*3*)32 (No. 212) with a = 24.12 Å and a molecular formula of [12]DBA$_2$Zn$_3$ to yield 3-D open frameworks with a (10,3)-connected $SrSi_2$ topology similar to crystals obtained by Chae et al.[12] The SBU is comprised of three Zn^{2+} cations—the central zinc is octahedrally bound to the carboxylate oxygens and two tetrahedrally coordinated to the central octahedral zinc and carboxylates (Figure 3.6). The tetrahedral zincs have terminating solvent ligands, presumably DMF or water, although disorder in the crystal structure does not allow for the determination of the identity of this ligand. If these solvent ligands can be removed by activation of the material, each SBU will contain two coordinately unsaturated metal sites that that may increase the H_2 uptake capacity by functioning as additional binding sites for H_2.

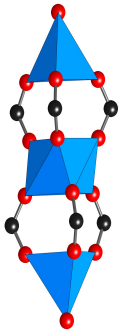

Figure 3.6. SBU of Zn MOF-[12]DBA-1 showing a central octahedral Zn^{2+} ion with two tetrahedral Zn^{2+} ions on its sides. Zn (blue), O (red), C (black).

Two [12]DBA macrocycles are stacked face-to-face, staggered 60°, with acetylene-arene π-stacking distance of approximately 3.48 Å, comparable to the reported mean value of 3.82 Å for other phenylacetylene shape-persistent macrocycles (Figure 3.7).[13] The inter-distance between each link is governed by the coordination to the octahedral and tetrahedral metal center and through π-π stacking. This smaller distance is likely due to the ability of the acetylene to more closely approach the aromatic ring. Hisaki demonstrated the [12]DBA macrocycle can form stacked face-to-face 1D assemblies.[10]

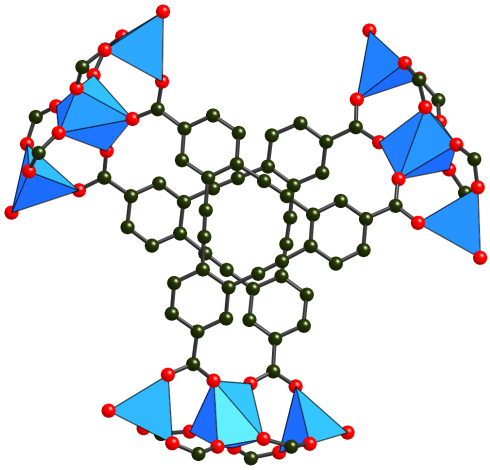

Figure 3.7. Space-filling representation of the trinuclear zinc SBU and the wall of face-to-face stacked macrocycles in Zn MOF-[12]DBA-1. Zn (blue), O (red), C (black).

First proposed by Wells,[14] this net can be interpenetrated by its enantiomeric form to create a racemate; however, the shape and bulkiness of the [12]DBA organic linker in this case likely prevents such interpenetration from forming. To determine the topology of Zn MOF-[12]DBA-1, each zinc cluster can be considered an octahedral SBU while the organic linker can be considered to be a trigonal SBU to produce the chiral $SrSi_2$ topology (Figures 3.8-3.10). **srs** is the RCSR symbol for the MOF where **srs** is derived from network of $SrSi_2$.[15] This net features 4-fold symmetry and a screw axis, leading to its chiral nature.

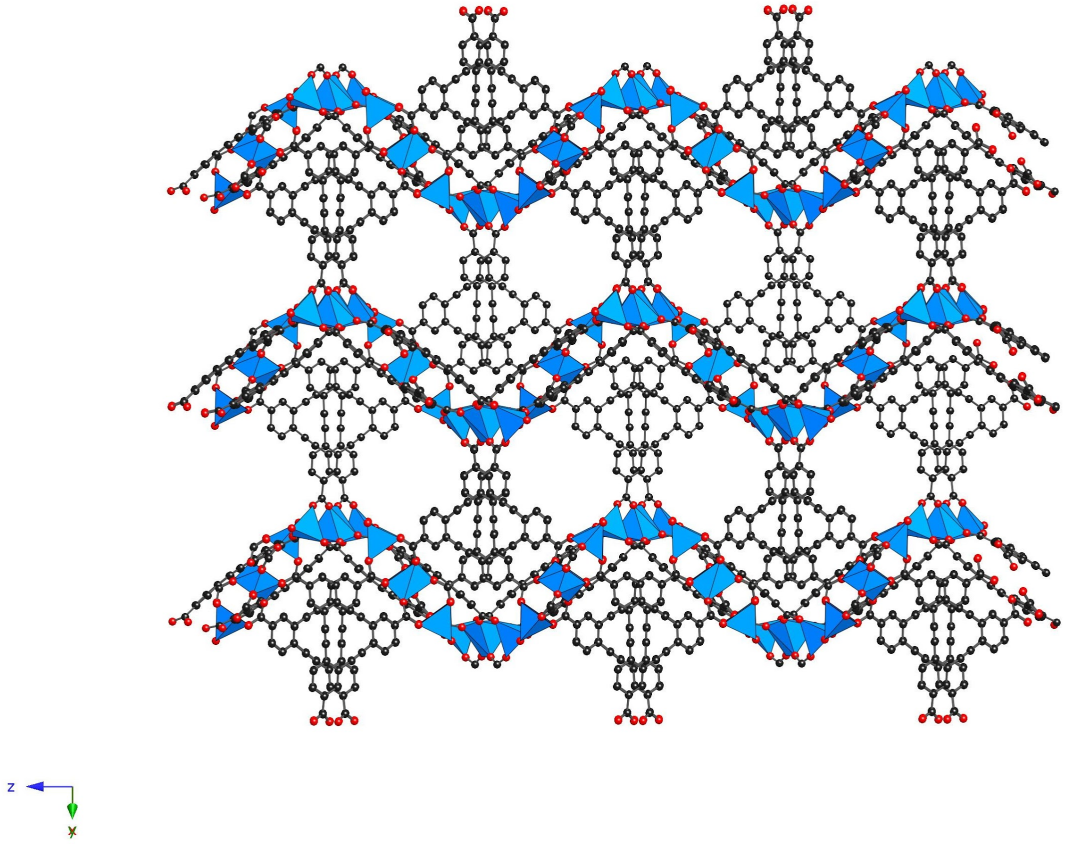

Figure 3.8. Representation of a calculated model crystal structure for Zn MOF-[12]DBA-1 showing $SrSi_2$ topological when viewed along the Y-axis. Zn (blue), O (red), C (black).

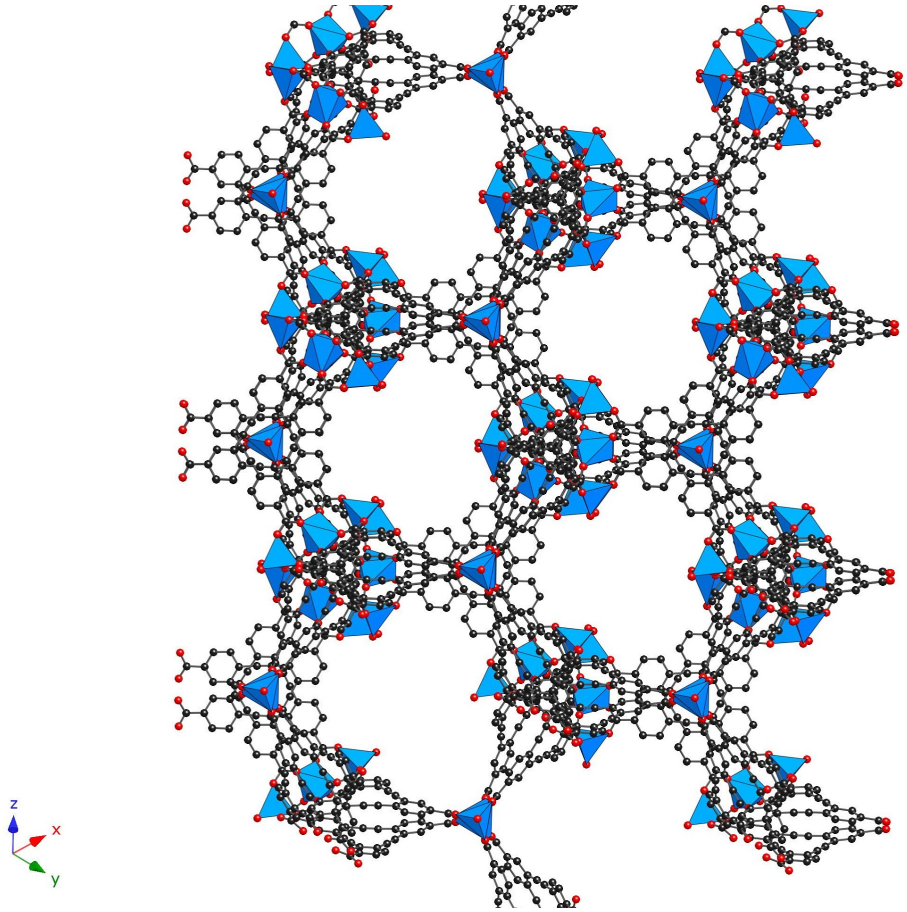

Figure 3.9. Representation of a calculated model crystal structure for Zn MOF-[12]DBA-1 showing chiral $SrSi_2$ topology. Zn (blue), O (red), C (black).

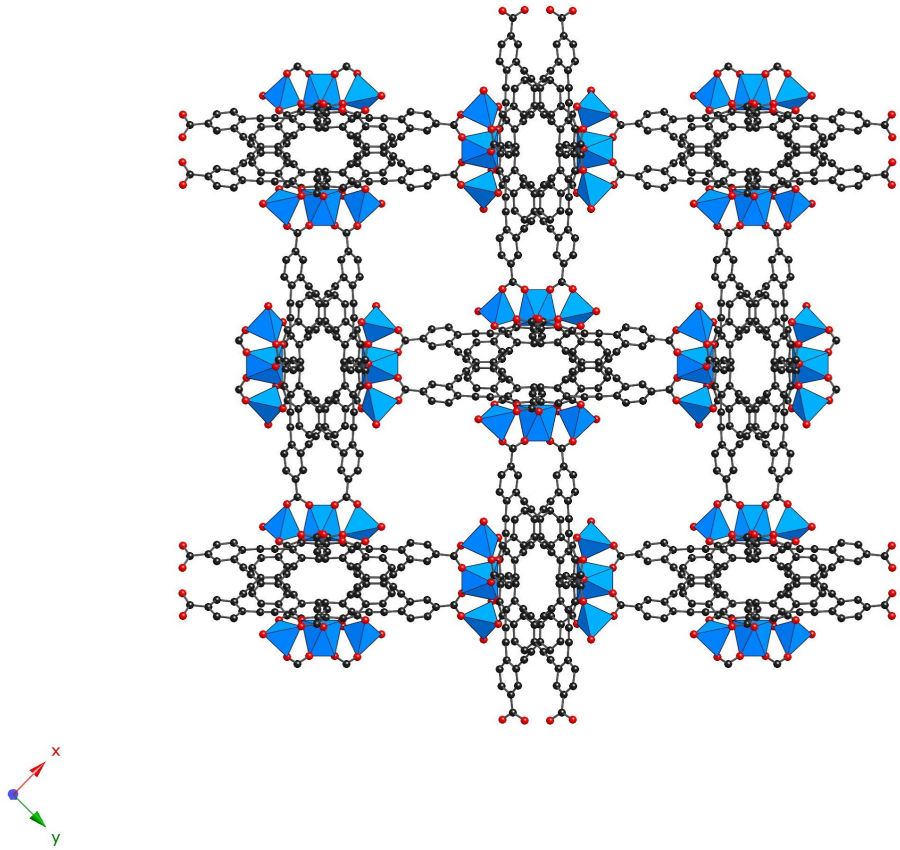

Figure 3.10. Representation of a calculated model crystal structure for Zn MOF-[12]DBA-1 showing $SrSi_2$ topology when viewed along the Z-axis. Zn (blue), O (red), C (black).

3.3.3 Surface Area Calculations and Nitrogen Isotherm

The structure of Zn MOF-[12]DBA-1 features 3D channels suitable for the uptake of small gas molecules. The largest sphere that can fit inside the channels is approximately 8 Å in diameter, ideal dimensions for low pressure H_2 storage by maximizing the surface area of the framework to promote physioadsorption on the surface while minimizing dead space in the pores (Figure 3.11).

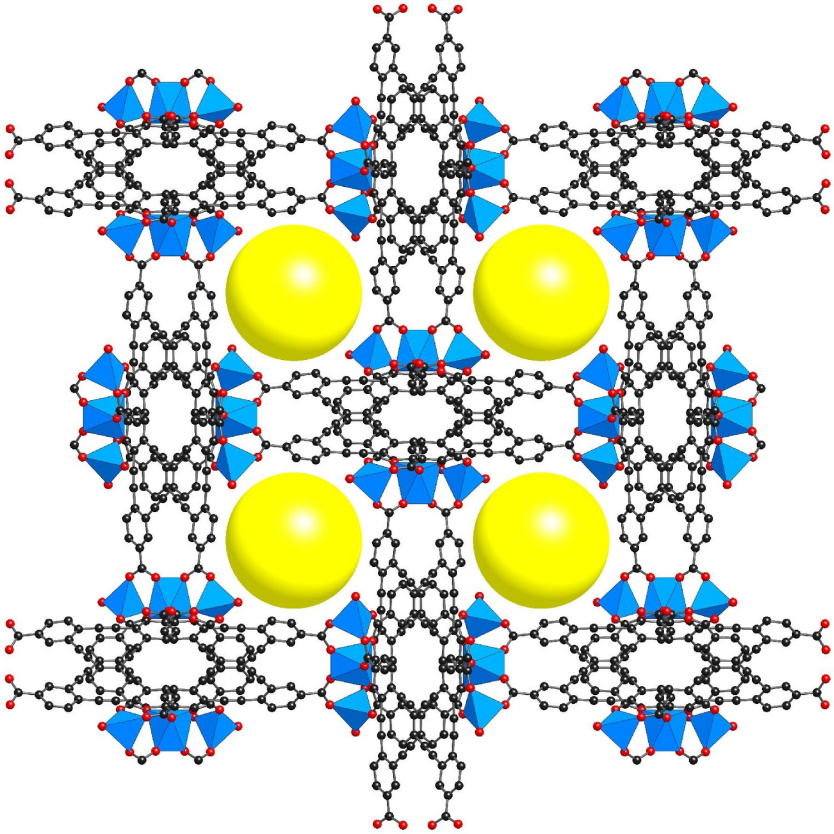

Figure 3.11. Crystal structure of Zn MOF-[12]DBA-1 showing a yellow sphere of diameter of 8 Å that represents the largest sphere that would occupy the channel without contacting the interior van der Waals surface. Zn (blue), O (red), C (black).

Calculations from BET models show that the surface area should be 3,600 $m^2 g^{-1}$; however, preliminary measurements yielded a surface area much lower than predicted of 380 $m^2 g^{-1}$ (Figure 3.12). Powder X-ray Diffraction (PXRD) patterns taken of the sample after N_2 isotherms demonstrate the structure had lost crystallinity.

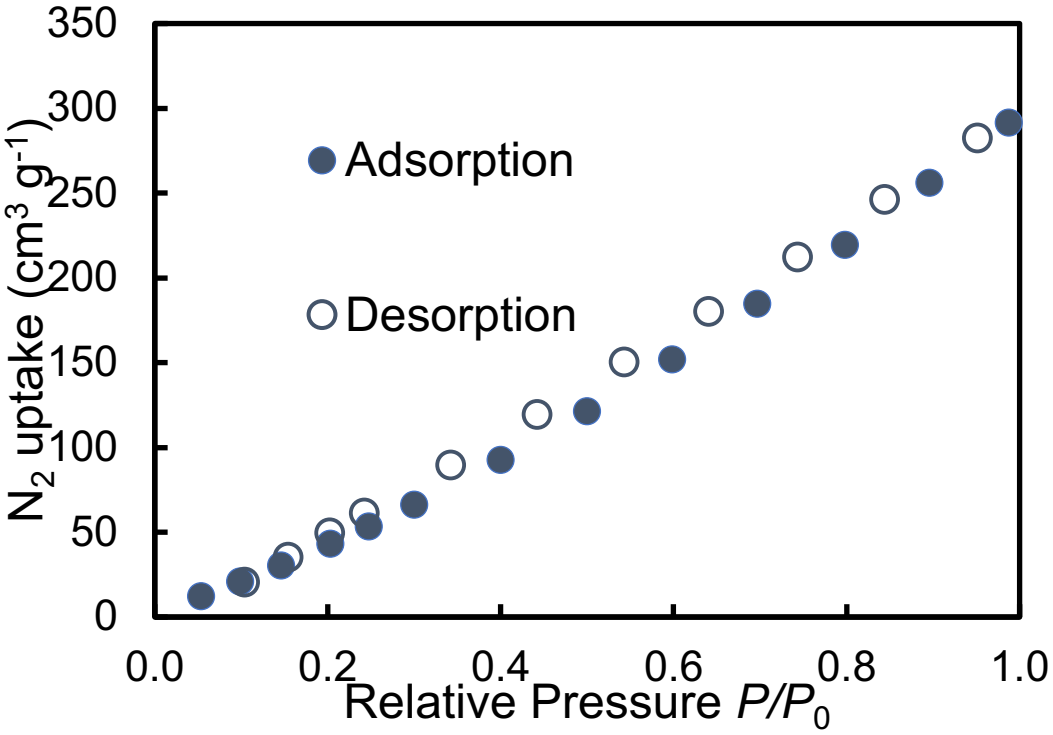

Figure 3.12. Nitrogen isotherm of Zn MOF-[12]DBA-1.

3.4 Conclusions and Outlook

Zn MOF-[12]DBA-1 was synthesized using the triangular shaped macrocycle, [12]DBA **2.1** with Zn^{2+} salts. The structure was determined by single crystal X-ray diffraction to give a chiral, non-interpenetrated **srs** topology. This structure features a rare double wall with two cycles staggered face-to-face and bound by the trinuclear zinc SBU. Zn MOF-[12]DBA-1 has 1D-channels, ideal for reversible gas uptake, as well as ideal pore size with a high surface area framework, ideal for the low pressure storage of H_2. Preliminary surface area measurements yielded a surface area of 380 m^2 g^{-1} which is much lower than the expected surface area of 3600 m^2 g^{-1}.

Zn MOF-[12]DBA-1 demonstrates the ability to use principles of reticular chemistry and crystal engineering to produce 3D graphyne-like structures using the [12]DBA macrocycle and MOFs as a crystallizing template. Furthermore, this rare double-walled structure is an opportunity to design and engineer structures with controlled orientation between two interacting molecules and warrants further investigation in possible niche properties and applications.

Future plans include activating Zn MOF-[12]DBA-1 by removing all solvent guests in order to carry out gas adsorption studies to measure the H_2 uptake capabilities as well as CO_2, CH_4. In addition, it would be of particular interest to solve the structure of and fully characterize the second phase of material (prismatic crystals) observed at lower temperatures and higher concentrations. These experiments will require multigram amounts of [12]DBA macrocycle **2.1** in order to fully realize.

3.5 Experimental

3.5.1 General

All reactions and characterization were carried out under ambient conditions unless otherwise noted.

3.5.2 Materials

All commercial reagents were used as purchased unless otherwise specified. **2.1** was provided by Dr. Ichiro Hisaki.[10] Zinc nitrate hexahydrate ($Zn(NO_3)_2$•$6H_2O$) was purchased from Sigma Aldrich Chemical Co. Anhydrous *N*,*N*-dimethylformamide (DMF) and tetrahydrofuran (THF) were purchased from EMD Chemicals DrySolv® system.

3.5.3 Synthetic Procedures

Zn MOF-[12]DBA-1. A solid mixture of $Zn(NO_3)_2 \cdot 6H_2O$ (4.68 mg, 2.47×10^{-5} mol) and [12]DBA **2.1** (1.13 mg, 2.61×10^{-6} mol) were dissolved in a 2-mL half dram vial with 0.50 mL of DMF. The vial was capped and heated in an isothermal oven held at 100 ºC for 24 h before removing and cooling to room temperature to yield 0.3-0.4 mm yellow-orange crystals on the side of the vial.

Activation of Zn MOF-[12]DBA-1 for N_2 Isotherms. The obtained crystals were immersed in anhydrous DMF and the solvent was exchanged with fresh DMF several times followed by anhydrous THF. The wet sample was then transfer to a super critical drier and was washed five times with liquid CO_2 and exchanged with fresh CO_2 five times at half hour intervals. The system was heat up to 45 ºC to bring about the supercritical state of the CO_2 which was bled after half hour in very slow flow rate to ambient pressure. The sample was then transferred to a vacuum chamber and evacuated to 20 mTorr at room temperature to yield a bright yellow-orange powder.

3.5.4 Powder X-ray Diffraction

Powder X-ray diffraction (PXRD) patterns were collected with a Bruker D8-Discover θ-2θ diffractometer operated at 40 kV and 40 mA with monochromated Cu K_α radiation (λ = 1.5406 Å) and with a scan speed of 1 sec/step and a step size of 0.05°. The simulated PXRD patterns were calculated from single crystal data using the PowderCell 2.3 software suite. The simulated powder diffraction patterns were compared to the powder diffraction patterns of the as synthesized samples for all MOFs for comparison.

3.5.5 Single crystal X-ray diffraction

Single crystal X-ray diffraction (SCXRD) data were collected at the Advanced Photon Source (APS) at the Argonne National Lab, Chicago. A yellow prismatic rhombohedral shaped crystal of MOF-[12]DBA was sealed with wax in a quartz capillary and mounted 125 mm from an ADSC Q315 detector.[16] The X-ray intensities, Kα radiation (λ = 1.0082 Å), were measured at 298 K with an exposure time of 2 seconds per frame and a transmission of 2%. Integration of the data in the cubic cell yielded a total of 4875 reflections of which 777 were unique. The structure was solved by least-squares methods and the subsequent difference Fourier syntheses and refined with the SHELXTL (v6.14) software package, using the cubic space group *P*4(3)32 with Z = 4. All non-hydrogen atoms of the nonsolvent portion of the structure were refined anisotropically.

Table 3.2. Crystal data for Zn MOF-[12]DBA-1.

Formula	$[Zn_3(CO_2)_6(H_2O)_2]L_3$
Temperature	298 K
Wavelength	1.0082 Å
Crystal System	Cubic
Space Group	*P*4(3)32 No. 212
Unit Cell Dimensions	a = 24.12 Å α = 90°
	b = 24.12 Å β = 90°
	c = 24.12 Å γ = 90°
Volume	14032 $Å^3$
Z	4
Density (calculated)	0.52 g cm^{-3}
F(000)	6120
Crystal Size	0.1 mm x 0.1 mm x 0.2 mm
Reflections Collected	4875
Independent Reflections	777
Resolution (completeness)	1.45 Å (100%)

3.5.6 Structure Modeling

Crystal models of Zn MOF-[12]DBA-1 were generated using Materials Studio through modification of the reported crystal structure of $Cd_3(TTCA)_2$•$6DMF$•$7H_2O$ (where TTCA = triphenylene-2,6,10-tricarboxlate).[12] Cd^{2+} was changed to Zn^{2+} and the atomic connectivity within the inorganic SBU remained the same. An oxygen molecule was included to complete the tetrahedral coordination environment of the Zn atoms since the identity of this ligand could not be resolved through experimental single crystal X-ray data. The TTCA ligand was exchanged for [12]DBA and an energetic minimization was then performed to optimize the geometry of the molecules, employing a smart algorithm and the universal force field implemented in the *Forcite* module of *Materials Studio* (*Materials Studio* v. 5.0.0.0, 2009, Accelrys Software Inc.). The unit cell parameters were also optimized until convergence was reached (energy convergence criteria: 10^{-4} kcal/mol). The powder X-ray diffraction patterns of the crystal structures were then calculated and compared with the experimental patterns.

3.6 References and Notes

(1) Rowsell, J. L.; Yaghi, O. M. Strategies for Hydrogen Storage in Metal-Organic Frameworks. *Angew. Chem., Int. Ed.* **2005**, *44*(30), 4670–4679.

(2) Chae, H. K.; Siberio-Pérez, D. Y.; Kim, J.; Go, Y.; Eddaoudi, M.; Matzger, A. J.; O'Keeffe, M.; Yaghi, O. M. A route to high surface area, porosity and inclusion of large molecules in crystals. *Nature* **2004**, *427*, 523–527.

(3) Rowsell, J. L. C.; Spencer, E. C.; Eckert, J.; Howard, J. A. K.; Yaghi, O. M. Gas Adsorption Sites in a Large-Pore Metal-Organic Framework. *Science* **2005**, *309*(5739), 1350–1354.

(4) Kim, J.; Chen, B.; Reineke, T. M.; Li, H.; Eddaoudi, M.; Moler, D. B.; O'Keefe, M.; Yaghi, O. M. Assembly of Metal-Organic Frameworks from Large Organic and Inorganic Secondary Building Units: New Examples and Simplifying Principles for Complex Structures. *J. Am. Chem. Soc.* **2001**, *123*(34), 8239–8247.

(5) Tranchemontagne, D. J. The Synthesis and Investigation of Alkyne-Containing Isoreticular Metal-Organic Frameworks for Hydrogen Storage and the Preliminary Investigation of Metal-Organic Framework for Gas Separation Applications, Ph. D. Thesis, University of California, Los Angeles, **2007**.

(6) Furukawa, H.; Ko, N.; Go, Y. B.; Aratani, N.; Choi, S. B.; Choi, E.; Yazaydin, A. Ö.; Snurr, R. Q.; O'Keeffe, M.; Kim, J.; Yaghi, O. Ultrahigh Porosity in Metal-Organic Frameworks. *Science*, **2010**, *329*(5990), 424–428.

(7) Yuan, D.; Zhao, D.; Sun, D.; Zhou, H.-C. An Isoreticular Series of Metal-Organic Frameworks with Dendritic Hexacarboxylate Ligands and Exceptionally High Gas-Uptake Capacity. *Angew. Chem., Int. Ed.* **2010**, *49*(31), 5357–5361.

(8) Farha, O. K.; Yazaydın, A. Ö.; Eryazici, I.; Malliakas, C. D.; Hauser, B. G.; Kanatzidis, M. G.; Nguyen, S. T.; Snurr, R. Q.; Hupp, J. T. *De novo* synthesis of a metal-organic framework material featuring ultrahigh surface area and gas storage capacities. *Nat. Chem.* **2010**, 2, 944–948.

(9) Furukawa, S.; Uji-I, H.; Tahara, K.; Ichikawa, T.; Sonoda, M.; De Schryver, F. C.; Tobe, Y.; De Feyter, S. Molecular Geometry Directed Kagomé Networks: Toward Two-Dimensional Crystal Engineering. *J. Am. Chem. Soc.* **2006**, *128*(11), 3502–3503.

(10) For example, see: Hisaki, I.; Sakamoto, Y.; Shigemitsu, H.; Tohnai, N.; Miyata, M.; Seki, S.; Saeki, A.; Tagawa, S. Superstructure-Dependent Optical and Electrical Properties of an Unusual Face-to-Face, π-Stacked, One-Dimensional Assembly of Dehydrobenzo[12]annulene in the Crystalline State. *Chem. Eur. J.* **2008**, *14*(14), 4178–4187.

(11) Tranchemontagne, D. J.; Mendoza-Cortés, J. L.; O'Keeffe, M.; Yaghi, O. M. Secondary building units, nets and bonding in the chemistry of metal-organic frameworks. *Chem. Soc. Rev.* **2009**, *38*(5), 1257–1283.

(12) Choi, J. Y.; Kim, J.; Furukawa, H.; Chae, H. K. Porous Chiral Metal Organic Carboxylate Frameworks with a Double-interwoven $SrSi_2$ Topology: $M_3(TTCA)_2$•6DMF•$7H_2O$ (TTCA = triphenylenetricarboxylate; M = Zn^{2+}, Cd^{2+}). *Chem. Lett.* **2006**, *35*(9), 1054–1055.

(13) Shetty, A. S.; Zhang, J.; Moore, J. S. Aromatic π-Stacking in Solution as Revealed through the Aggregation of Phenylacetylene Macrocycles. *J. Am. Chem. Soc*. **1996,** *118*(5), 1019–1027.

(14) Wells, A. F. The geometrical basis of crystal chemistry. Part 4. *Acta Crystallogr.* **1954**, *7*, 849–853.
(15) http://rcsr.net/nets/srs
(16) This research used resources of the Advanced Photon Source, a U.S. Department of Energy (DOE) Office of Science User Facility operated for the DOE Office of Science by Argonne National Laboratory under Contract No. DE-AC02-06CH11357. Special thanks to Dulio Cascio at the Molecular Biology Institute, UCLA with his help in single crystal X-ray diffraction and the folks at the Advanced Photon Source (APS) Beamline 24-ID-C and their DOE grants that made this data collection possible.

CHAPTER 4

Synthesis of a Double-Walled Metal-Organic Framework with apo Topology from the Eclipsed Stacking of Biphenyl [12]Dehydrobenzannulene Carboxylate Organic Linkers

4.1 Abstract

A biphenyl analogue of [12]DBA **2.1** was used to further explore the incorporation of the [12]DBA structural motif into MOFs. A new metal-organic framework (MOF) was synthesized and the structure of MOF-[12]DBA-2 was determined by SCXRD (single crystal X-ray diffraction) to reveal 3,6-connected **apo** topology. This MOF features two [12]DBA macrocycles eclipsed π-π stacked and joined by a heptanuclear zinc SBU (secondary building unit).

4.2 Introduction

MOF-[12]DBA-1 reported in Chapter 3 did not maintain permanent porosity after evacuation of the pores. Furthermore, the limited amount of the [12]DBA macrocycle **2.1** did not allow for characterization. A variation of the [12]DBA macrocycle **2.1** with an extra phenyl ring between the macrocycle core and the carboxylic acid groups to yield the [12]DBA **4.1**, featuring a biphenyl motif, was available from the laboratory of Dr. Ichiro Hisaki and Dr. Mikiji Miyata to target new MOFs with superior structural integrity and function (Figure 4.1).[1] Biphenyl has the ability for the additional aromatic ring to twist out of plane, possibly preventing aromatic stacking in the structure to obtain a low density framework of a single wall. This molecule also exhibits C_3-symmetry and predicts an isoreticular framework to MOF-[12]DBA-1 based on principles of reticular chemistry.

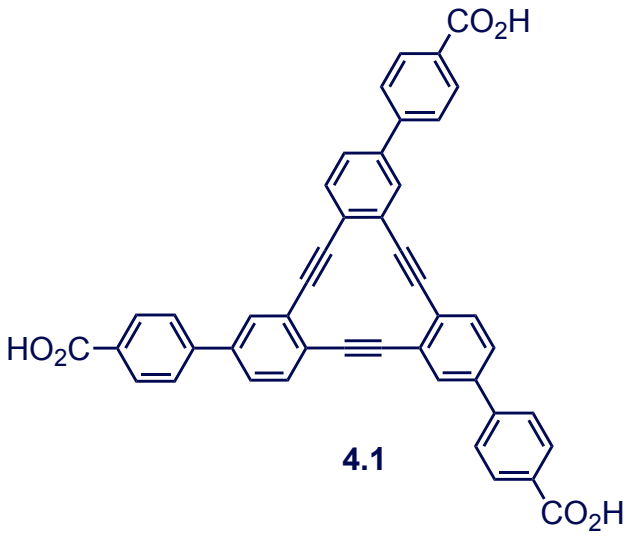

4.1

Figure 4.1. Structure of biphenyl [12]DBA **4.1**.

4.3 Results and Discussion

4.3.1 Synthesis and Single Crystal Growth of MOF-[12]DBA-1

Zinc was again chosen as the transition metal cation for MOF synthesis due to its high success in crystallizing a variety of organic linkers. The [12]DBA **4.1** was reacted with $Zn(NO_3)_2 \cdot 6H_2O$ in a 1:1 mixture of *N*,*N*-dimethylformamide (DMF) and *N*-methyl-2-pyrrolidone (NMP) at 120 °C for 24 hours. The same synthetic conditions used to fabricate MOF-[12]DBA-1 did not yield any crystalline material when used for **4.1**. Furthermore, the insolubility of **4.1** in DMF required the addition of NMP and higher reaction temperatures to isolate single crystals of MOF-[12]DBA-2 using solvothermal synthetic conditions (Figure 4.2).

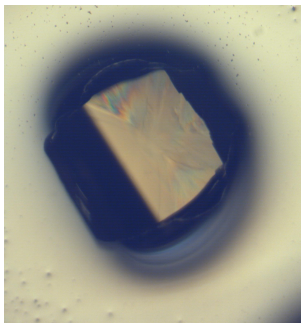

Figure 4.2. Single crystal of MOF-[12]DBA-2 under optical microscope.

4.3.2 Structure Determination and Refinement.

The structure of MOF-[12]DBA-2 was determined by SCXRD (Table 4.1). Single crystal X-ray data was collected to a resolution of 1.5 Å; however, the data was too poor to solve by direct methods. Charge-flipping techniques were used to locate the electron density of the zinc metal cluster. Further refinements utilizing the [12]DBA organic linker as a rigid body were performed to determine the location of the organics within the framework. The combination of techniques revealed the organic linker to SBU structural connectivity despite the poor resolution of the data. Additional crystallographic data sets were collected to improve the resolution; however, a resolution better than 1.5 Å was never achieved. The single crystals do not survive under cryogenic conditions and degrade rapidly after mounting.

It was determined that MOF-[12]DBA-2 crystallizes in the PBCN space group. This MOF features eclipsed π-πstacked, double-walled frameworks with 3,6-connected **apo** topology where the **apo** net is derived from the structure of α-PbO_2 (Figure 4.3).[2] The heptanuclear zinc SBU $Zn_7[O_2(CO_2)_{10}]$ of the MOF can only ligate 10 carboxylates and therefore does not have all 12 carboxylates coordinated to the metal cluster (Figure 4.4). This feature may explain the structural disorder of MOF-[12]DBA-2 and the difficulty to isolate single crystals suitable for structure determination by SCXRD. This is the same SBU as published with MOF-123 and MOF-246 (but with a ditopic linker).[3] There is some evidence in the PXRD patterns for an additional phase that appears to be less stable to air and/or drying. It is not clear if this is an additional phase or lattice transformation similar to that observed in MOF-123/MOF-246 from addition or removal of solvent ligands and thus warrants further investigation.

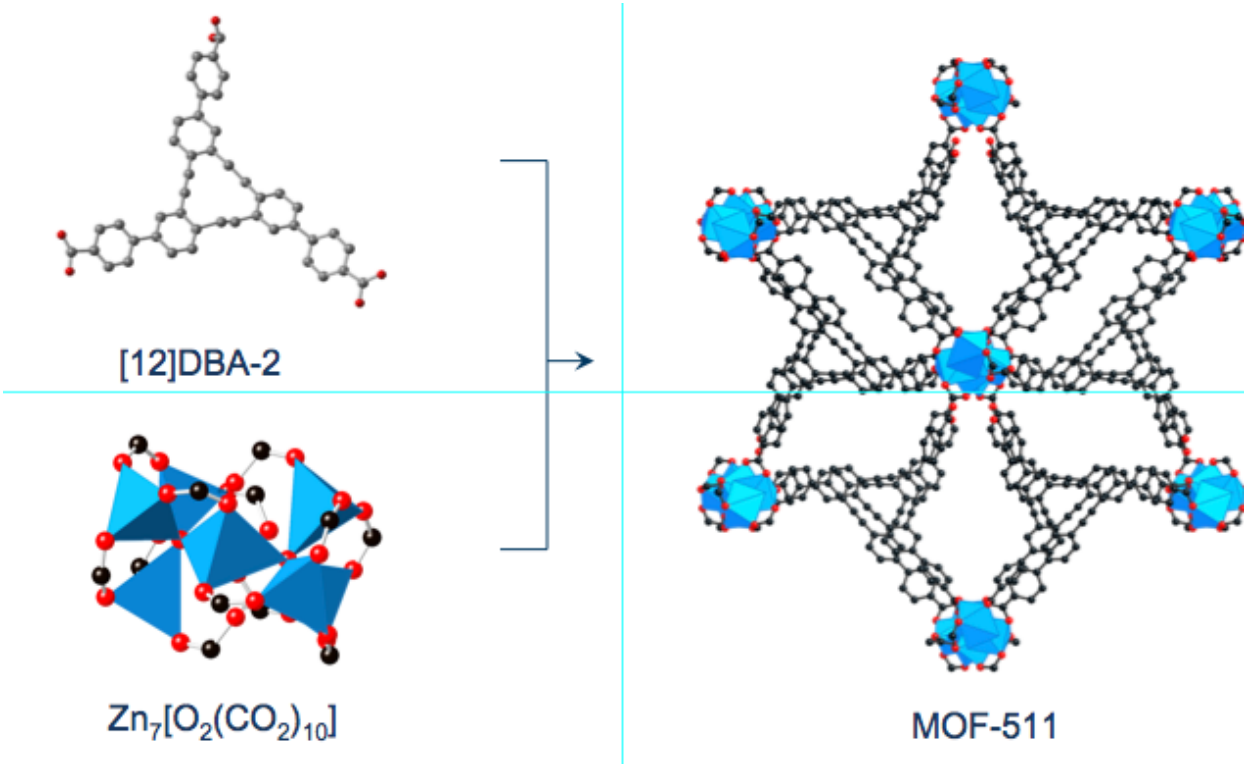

Figure 4.3. Space-filling representation of the formation of the 3,6-connected **apo** topology from the [12]DBA macrocycle **4.1** and the $Zn_7[O_2(CO_2)_{10}]$ SBU. Zn (blue), O (red), C (black). H atoms are omitted for clarity.

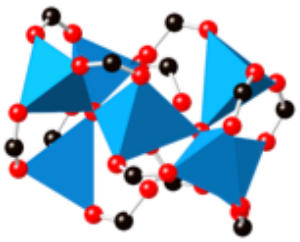

Figure 4.4. Space-filling representation of heptanuclear zinc SBU of MOF-[12DBA-2. Zn (blue), O (red), C (black).

The [12]DBA macrocycle **4.1** also exhibits C_3-symmetry identical to **2.1** and would be predicted by reticular chemistry principles to produce a MOF isoreticular to MOF-[12]DBA-1. Additionally, similar biphenyl [12]DBA macrocycles have previously been investigated in small molecule crystallographic studies to yield face-to-face, eclipsed π-π stacked dimers.[1] Interestingly, MOF-[12]DBA-2 instead crystallizes with face-to-bottom, eclipsed π-π stacked dimers to form double-walled cages (Figure 4.5).

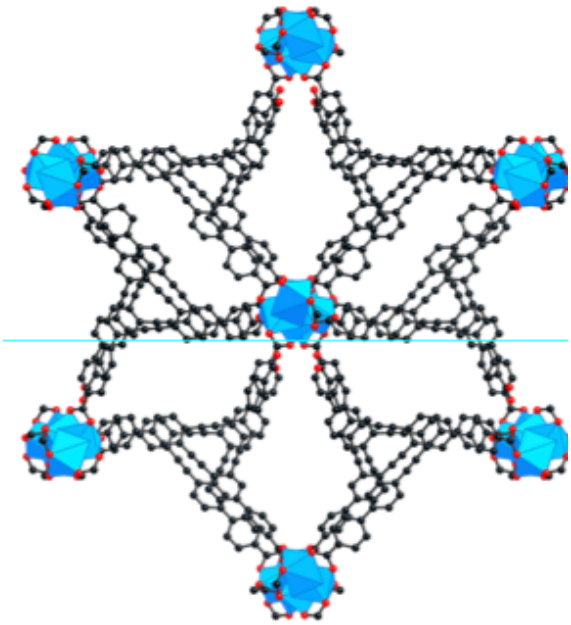

Figure 4.5. Space-filling representation of eclipsed [12]DBA macrocycle stacking connected by the heptanuclear zinc SBU of MOF [12]DBA-2. Zn (blue), O (red), C (black). H atoms are omitted for clarity.

Preliminary experiments incorporating Cu(I) and Ag(I) ions into the **apo** Zn MOF-[12]DBA-2 by post-synthetic diffusion were confirmed by PXRD and FT-IR. More conclusive data is required to confirm, locate, and quantify metal coordination within the MOF but there are definitive differences in FT-IR spectra and fluorescence properties after metal coordination. The PXRD patterns confirm the same structure and crystallinity of the framework are maintained after coordination. Additionally, the metal ions remain after washing several times and since the single crystals are still intact and it may be possible to obtain single-crystal x-ray data for the metalation.

4.4 Conclusions and Outlook

MOF-[12]DBA-2 was synthesized from the biphenyl [12]DBA organic linker −1 and Zn^{2+} ions. The structure was determined by SCXRD to reveal the MOF crystallizes with 3,6-connected **apo** topology and features two [12]DBA macrocycles eclipsed stacked and joined by a heptanuclear zinc SBU. It is particularly interesting that Zn MOF-[12]DBA-1 and Zn MOF-[12]DBA-2 are not isoreticular structures. Furthermore, they both form unusual double-walled frameworks with different macrocycle stacking orientations. Moving forward, reticular chemistry was employed to design a single-walled framework and is further discussed in Chapter 5. Future studies include the full characterization of the second MOF phase observed upon drying and to continue investigating the post synthetic diffusion of metals in the framework.

4.5 Experimental

4.5.1 General

All experimental characterization operations were performed in air, which led to the adsorption of water into the pores of samples.

4.5.2 Materials

Zinc nitrate hexahydrate ($Zn(NO_3)_2 \cdot 6H_2O$) was purchased from Sigma Aldrich. Anhydrous *N*,*N*-dimethylformamide (DMF) and *N*-methyl-2-pyrrolidone (NMP) were purchased from EMD Chemicals DrySolv® system. All reagents were used as purchased unless otherwise specified. The phenyl extended [12]DBA macrocycle **4.1** was synthesized in the laboratory of Dr. Ichiro Hisaki according to a previously reported literature procedure.[1]

4.5.3 Synthetic Procedures

Synthesis of Zn MOF-[12]DBA-2. 2.5 mg of the [12]DBA organic linker **4.1** was dissolved in 250 μL of NMP in a vial. 250 μL of a 0.13 mM solution of $Zn(NO_3) \cdot 6H_2O$ in DMF was added to the vial and 100 μL aliquots were added to half dram vials. The contents of the vial were further diluted with 100 μL of a 1:1 solution of DMF/NMP and placed in a 120 °C isothermal oven for 24 hours to yield single crystals of Zn MOF-[12]DBA-2 on the side of the vial.

4.5.4 Powder X-ray Diffraction

Powder X-ray diffraction (PXRD) data were collected using a Rigaku MiniFlex benchtop X-ray diffractometer with Cu $K\alpha_1$ radiation (λ = 1.5406 Å, 600 W, 30 kV, 15 mA) (Figure 4.6). All samples were mounted on a sample holder by dropping crystals and then leveling the sample surface with a spatula. Diffracted radiation was detected using a hybrid pixel array detector (HPAD).

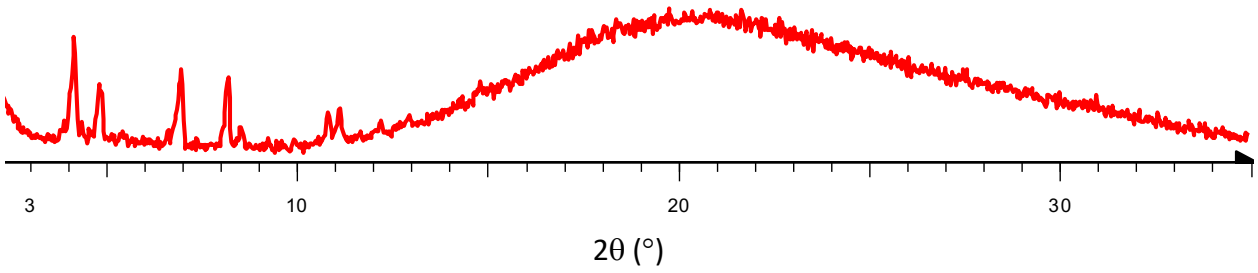

Figure 4.6. PXRD pattern of as-synthesized MOF-[12]DBA-2.

4.5.5 Single Crystal X-ray Diffraction

SCXRD data was collected at the University of California, Berkley ChexRay Facility. A 0.2 mm x 0.1 mm x 0.1 mm yellow single crystal was on mounter on a Bruker APEX II QUAZAR diffractometer (Mo K_α radiation λ = 0.70926 Å) under a cryostream of 100 K. 52,860 reflections were collected, 13,263 of which were unique.

4.5.6 Structure Resolution[4]

The structure resolution was too poor to solve by direct methods with SHELXTL (v.6.14); however, a preliminary unit cell and space group were obtained with XPREP. SUPERFLIP software was used to employ charge flipping techniques to locate areas of highest electron density, i.e. the zinc metal cluster. Further refinements in SHELXTL were performed using the organic linker as a rigid body determined the locations of the organic linkers to reveal the SBU to organic linker net connectivity.

Table 4.1. Crystal data for Zn MOF-[12]DBA-2.

Formula	$[Zn_7O_2(CO_2)_{10}]L_4$
Temperature	100 K
Crystal System	Orthorhombic
Space Group	PBCN No. 60
Unit Cell Dimensions	a = 22.9 Å α = 90°
	b = 40.2 Å β = 90°
	c = 44.9 Å γ = 90°
Volume	41,290 Å^3
Z	4
Density (calculated)	0.50 g cm^{-3}
Crystal Size	0.2 mm x 0.1 mm x 0.1 mm
Reflections Collected	52,860
Independent Reflections	13,263
Resolution (completeness)	1.5 Å (100#%)

4.6 References and Notes

(1) Hisaki, I.; Senga, H.; Sakamoto, Y.; Tsuzuki, S.; Tohnai, N.; Miyata, M. Specific Interaction between Chloroform and the Pockets of Triangular Annulene Derivatives Providing Symmetry Carry-Over Crystallization. *Chem. Eur. J.* **2009**, *15*(48), 13336–13340.

(2) http://rcsr.anu.edu.au/nets/apo

(3) Choi, S. B.; Furukawa, H.; Nam, H. J.; Jung, D.-K.; Jhon, Y. H.; Walton, A.; Book, D.; O'Keeffe, M.; Yaghi, O. M.; Kim, J. Reversible Interpenetration in a Metal-Organic Framework Triggered by Ligand Removal and Addition. *Angew. Chem., Int. Ed.* **2012**, *51*(35), 8791–8795.

(4) Special thank you to Dr. Felipe Gandara for assistance in the resolution of the structure.

CHAPTER 5

Synthesis of Isoreticular [12]Dehydrobenzannulene Containing Cu and Zn Metal-Organic Frameworks with rht Topology

5.1 Abstract

Reticular chemistry was used to design and synthesize Zn and Cu isoreticular [12]DBA containing metal-organic frameworks (MOFs) by targeting the **rht** topology. The Zn MOF-[12]DBA-3 structure was solved by single crystal X-ray diffraction (SCXRD) while the Cu MOF-[12]DBA-3 structure was solved by matching the experiment powder X-ray diffraction (PXRD) pattern with the simulated pattern.

5.2 Introduction

Initial synthetic studies with [12]DBA discussed in Chapter 3 and Chapter 4 focused on exploring conditions to crystallize the [12]DBA macrocycles **2.1** and **4.1** into extended networks. Both MOF [12]DBA-1 and MOF-[12]DBA-2 crystallized with unusual double-walled structures due to the exceptional π-stacking ability of the [12]DBA organic linkers. An approach utilizing reticular chemistry was adopted moving forward to target a single-walled MOF.

The **rht** net was designed using reticular chemistry principles to yield a MOF with no possible macrocycle stacking in the framework wall to yield a single-walled framework in contrast to the MOF-[12]DBA-1 and MOF-[12]DBA-2 which both formed unusual double-walled structures due to the excellent π-stacking ability of the [12]DBA organic linkers. The **rht** net was targeted to yield single-walled MOF structure. This net utilizes a paddlewheel SBU and trigonal ligands to produce a 3,24-connected network.[1]

5.3 Results and Discussion

5.3.1 Design of Isophthalate [12]DBA Organic Linker for rht Net

The [12]DBA organic linker **5.1** featuring isophthalate moieties was synthesized at Osaka University by Dr. Ichiro Hisaki. The isophthalate motif and C_3-symmetric organic linker to coordinate to paddlewheel SBU are characteristic for constructing the 3,24-connected **rht** net.

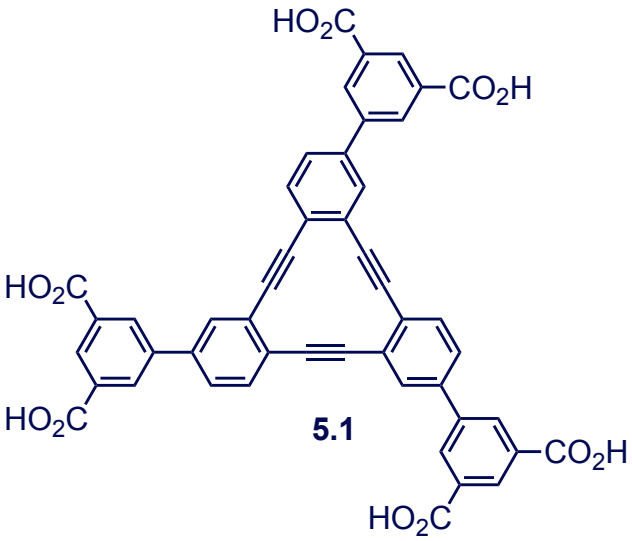

Figure 5.1. Isophthalate functionalized biphenyl [12]DBA **5.1.**

5.3.2 Synthesis of Zn and Cu rht MOFs

Again Zn^{2+} cations were initially chosen for metal cluster cation due to zinc's ability to adopt to adopt a paddle-wheel SBU and thus **rht** net. Bright yellow, cubic single crystals of the Zn MOF-[12]DBA-3 were grown (Figure 5.2) from a 3:1 mixture of DMF/NMP with zinc nitrate hexahydrate salts in an isothermal oven at 100 °C.

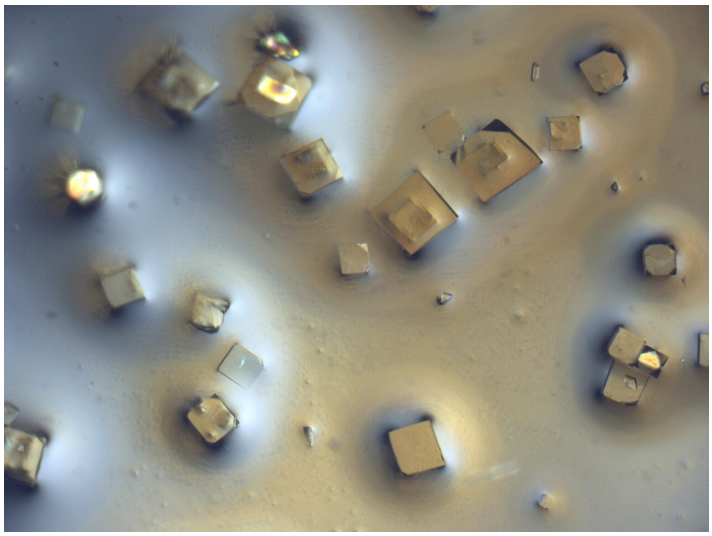

Figure 5.2. Single crystals of Zn MOF-[12]DBA-3 under optical microscope.

Initially, only microcrystalline powder of Cu MOF-[12]DBA-3 was isolated using preliminary synthetic procedures tried by our collaborator, Dr. Ichiro Hisaki. The [12]DBA isophthalate linker **5.1** is not soluble in DMF alone. Additionally, the addition of HBF_4 significantly lowers the solubility of **5.1**. With trial and error, single crystals were obtained from

modified conditions by playing with the synthetic conditions that control the formation of the Cu paddlewheel SBU (Figure 5.3).[2] Further optimization of the single crystal growth conditions is recommended in order to grow crystals suitable for structure determination by SCXRD (Figure 5.4).

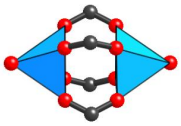

Figure 5.3. Paddlewheel $M_2[O_2(CO_2)_4]$ (M = Cu^{2+}/Zn^{2+}) SBU. M (blue), O (red), C (black). Terminal ligands are omitted for clarity.

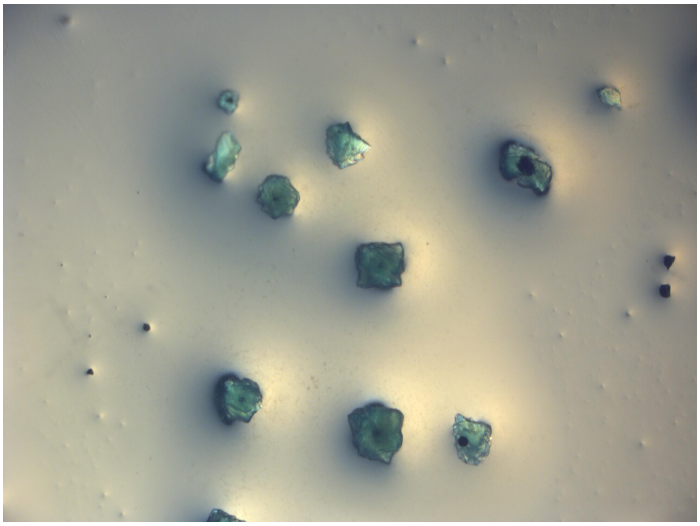

Figure 5.4. Crystals of Cu MOF-[12]DBA-3 unsuitable for SCXRD under optical microscope.

5.3.3 Confirmation of Zn rht Structure by PXRD and SCXRD Analysis

Single crystals of the Zn MOF-[12]DBA-3 were mounted on the beamline and an excellent data set to 0.7 Å was collected. This MOF diffracts really well and is very stable in air. Initially, the powder X-ray diffraction (PXRD) pattern was misleading because of the lack of congruence between experimental and simulated powder patterns. This is largely due to the highly crystalline nature of the MOF which leads to preferred orientations of the crystallites which results in high intensities of some Bragg diffraction peaks (Figure 5.5).

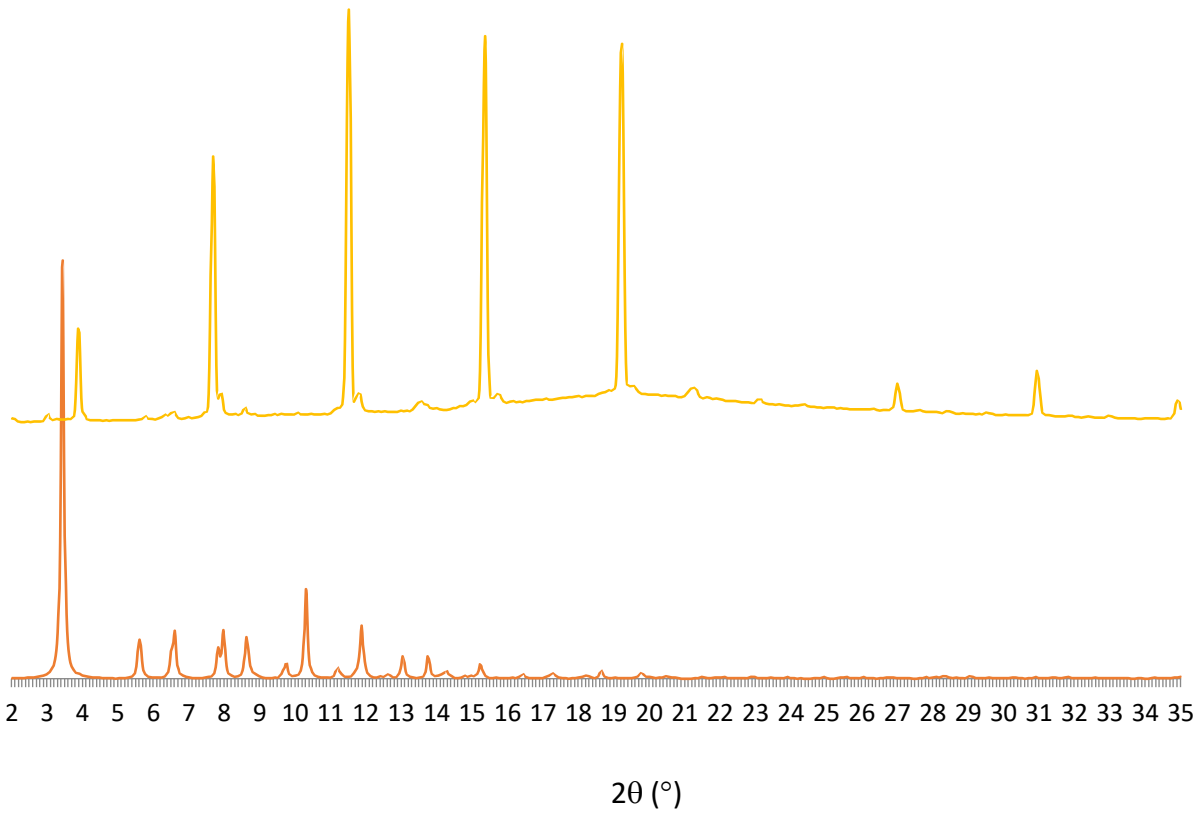

Figure 5.5 Comparison of the experimental PXRD pattern of Zn MOF-[12]DBA-3 (yellow) with the simulated MOF diffraction pattern (red).

5.3.4 Confirmation of Cu rht Structure by PXRD Analysis

Though single crystals of Cu MOF-[12]DBA-3 were eventually obtained, the crystal quality was still poor and requires further optimization; therefore, the structure was solved by PXRD rather SCXRD (Figure 5.6) due to time limitations of the project. The PXRD pattern shows the poor crystallinity of the Cu MOF-[12]DBA-3 as several Bragg reflections are absent from the experimental data. Cu MOF-[12]DBA-3 with **rht** topology was targeted for better chance of activation for gas adsorption studies; however, time limitations of the projected prevented the completion of this critical experiment.

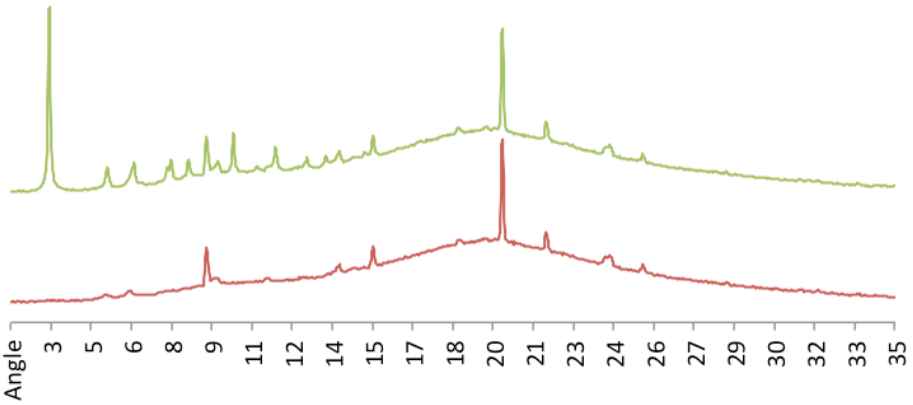

Figure 5.6. Comparison of the experimental PXRD pattern of Cu MOF-[12]DBA-3 (red) with the simulated MOF diffraction pattern (green).

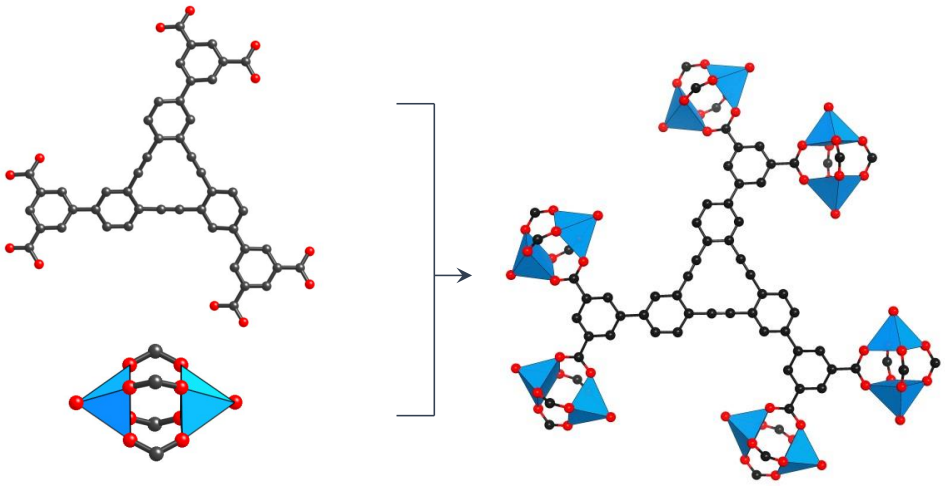

Figure 5.7. Formation of the single walls in the 3,24-connected **rht** net from the combination of the paddlewheel $Zn_2[O_2(CO_2)_4]$ SBU and the isophthalate [12]DBA organic linker **5.1**. Zn/Cu (blue), O (red), C (black). H atoms and terminal ligands protruding into the pores are omitted for clarity.

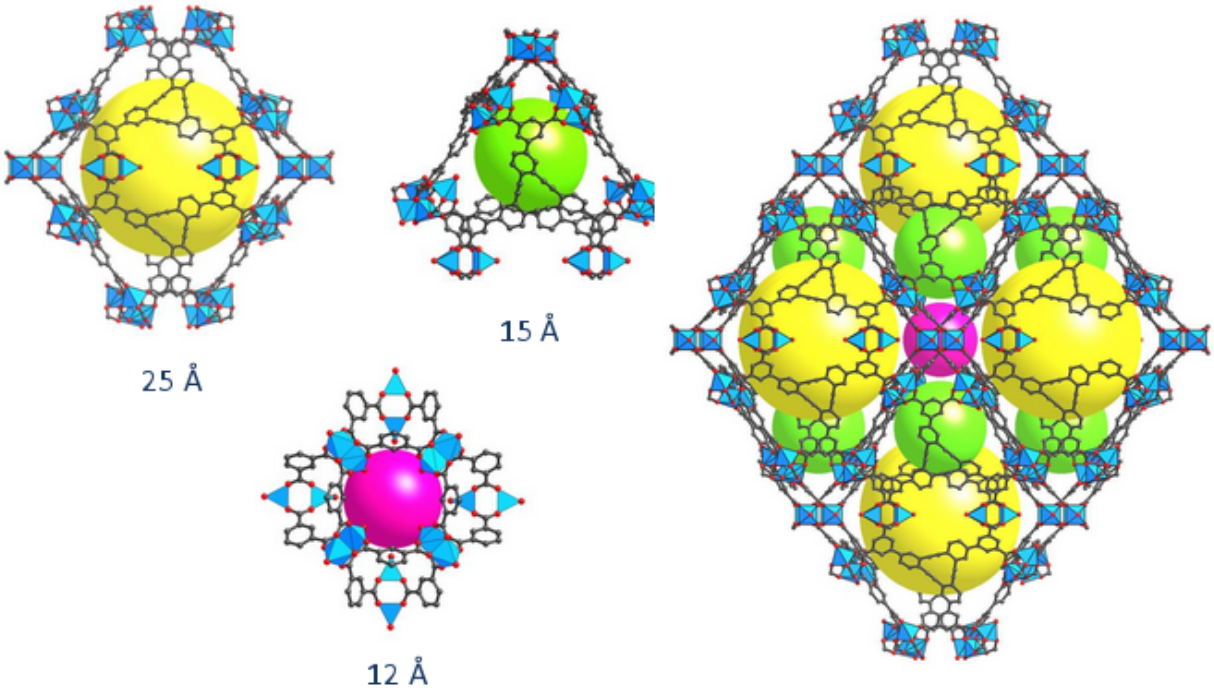

Figure 5.8. Space filling representation of the three cages of **rht** MOF-[12]DBA-3 showing a sphere with a diameter in Å that represents the largest sphere that would occupy the channel without contacting the interior van der Waals surface. Zn/Cu (blue), O (red), C (black). H atoms and terminal ligands protruding into the pores are omitted for clarity.

5.4 Conclusions and Outlook

The **rht** net was designed and synthesized using both copper and zinc metal cations. The zinc structure was solved by SCXRD and isoreticular copper structure was solved by PXRD and models. These MOFs exhibit a single wall and are especially stable in air.

All linkers were crystallized successfully with Zn^{2+} cations to yield single crystals suitable for structure determination by SCXRD (Figure 5.9). Initially only microcrystalline powder of the Cu **rht** MOF was isolated and the structure was confirmed by PXRD. Traditional conditions for the growth of single crystals of the Cu **rht** MOF only yielded an amorphous or microcrystalline powder initially; however modifying the reaction conditions led to the formation of single crystals. The [12]DBA isophthalate linker **5.1** is not soluble in DMF alone and the solvent volume is very small. Additionally, the addition of HBF_4 significantly lowers the solubility. With trial and error, single crystals were obtained from modified conditions to increase linker solubility. The single crystal synthesis of the **srs** MOF was optimized and crystals were sealed in a capillary to prevent drying. The **apo** MOF did not diffract well only allowing resolution to 1.5 Å, even on high intensity beam lines. Charge flipping structure solving techniques were used to locate electron density of metal clusters. Further structure refinement was necessary using ligands as rigid bodies. Single crystals of the Zn **rht** MOF mounted on the beam line and yielded an excellent data set to 0.7 Å. This MOF diffracts really well and is very stable in air. Confirmation of the Cu **rht** structure by modeling and PXRD analysis since single crystals were only achieved recently.

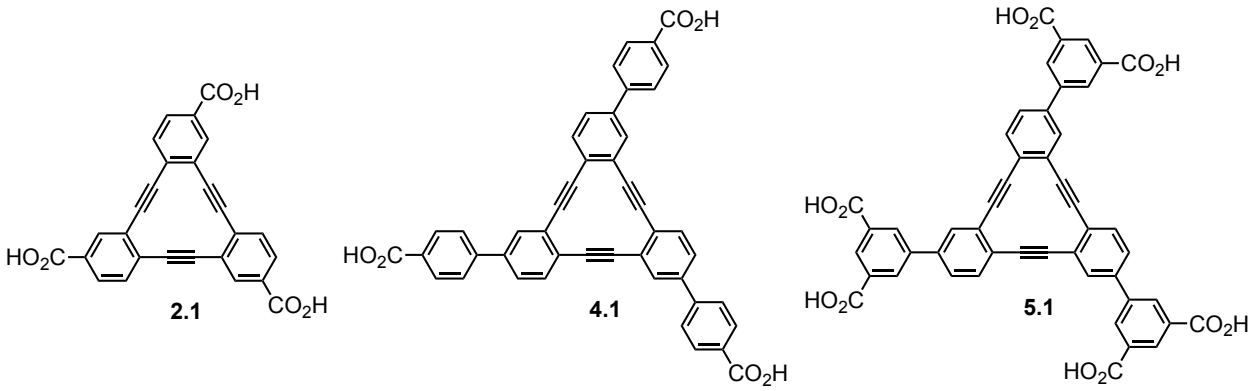

Figure 5.9. Comparison of [12]DBA links **2.1** (MOF-[12]DBA-1), **4.1** (MOF-[12]DBA-2), and **5.1** (MOF-[12]DBA-3).

Table 5.1. Summary of [12]DBA MOFs synthesized.

	Zn MOF-1	Zn MOF-2	Zn MOF-3	Cu MOF-4
Linker (L)	**2.1**	**4.1**	**5.1**	**5.1**
Formula	$[Zn_3L_3(H_2O)_2]$	$[Zn_7O_2]L_4$	$[Zn_2(H_2O)_2]L_2$	$[Cu_2(H_2O)_2]L_2$
Density (g/m^3)	0.52	0.50	0.58	0.58
Est. SA (m^2/g)	3,600	3,300	3,900	3,900
Void space	74%	73%	72%	72%
Space Group	*P*4(*3*)32	PBCN	*I* 4/m	*I* 4/m
Topology	**srs**	**apo**	**rht**	**rht**
Cell Vol. $(Å)^3$	14,050	41,290	47,260	46,610
Crystal system	cubic	orthorhombic	tetragonal	tetragonal
a (Å)	24.1	22.9	31.8	31.9
b (Å)	24.1	40.2	31.8	31.9
c (Å)	24.1	44.9	46.7	45.7
$\alpha = \beta = \gamma$	90°	90°	90°	90°

SA = surface area.

All of these MOFs solvent exchange well to lower boiling point solvents and are stable for extended periods of time immersed in solvent; however, crystallinity is not retained after evacuating the solvent guests from the Zn MOFs, even with supercritical CO_2 activation to avoid capillary forces upon evacuation causing these nets to collapse. Some structures inherently lack structural integrity due to weak SBUs, structural disorder, or large open nets and these factors ultimately determine the rigidity of the resulting net. MOF activation takes trial and error to find

the right conditions, especially with SBUs that are not fully coordinated and have open metal sites. The **rht** MOF seems more stable to drying in air so hopefully will be more robust to activation despite unsuccessful initial attempts with Zn SBUs. The Cu **rht** MOF has been synthesized and ready to test for activation. Experimentally, these nets are more robust to activation.

Frameworks were investigated to synthesize carbon allotrope mimics into 3D, crystalline material and study resulting topologies by x-ray crystallography. A strategy to synthetically approach carbon networks or mimics was developed using the concepts behind constructing porous frameworks through solvothermal synthesis. Carbon based subunits were designed and synthesized as the organic linker to link up with SBUs in porous frameworks to create novel architectures and expand the field by synthesizing non-commercially available linkers to incorporate functionalized organic linkers into MOFs to study. [12]DBA linkers were designed due to their rigid, shape-persistent structure and high thermal stability suitable for the solvothermal synthesis of frameworks. These linkers represent a subunit of larger carbon graphyne networks to build into 3D architectures using frameworks as a building scaffold. These hybrid organic-inorganic materials are carbon rich and synthetically feasible due to the solvothermal synthetic methods to yield crystalline frameworks. Resulting frameworks are crystalline, and robust in solution making them ideal candidates for study by x-ray crystallography. It will be of particular interest to synthesize and study materials with delocalized π systems for their applications in the next generation of carbon-based optoelectronic devices. Additionally, these porous structures are ideal for gas storage applications due to their light weight and low density. The ultimate goal would be to form nets constructed exclusively from C-C bond forming reactions. Among the new targeted COF materials, the carbon-carbon bond-based materials composed exclusively of carbon and hydrogen are of significant interest for potential applications ranging from optoelectronics to gas storage; however, they have been synthetically challenging to produce hindering the viability of studying these materials.

Future work includes the activation of [12]DBA MOFs by removing solvent guests to evacuate the pores and then to measure hydrogen adsorption isotherms at 77 K and 298 K. One specific target of this work is to study the hydrogen storage capabilities of these MOFs complexed with metals at ambient temperatures (233-333 K) and moderate pressures (up to 100 bar) for mobile vehicle applications. It has been shown that several MOFs can store sufficient hydrogen to meet the U.S. Department of Energy (DOE) requirements for 2015 of 5.5 wt% or 40 g L^{-1} at 77 K for benchmark MOFs; however, the storage of hydrogen in these materials at ambient temperatures still fall far below the DOE requirements due to the weak binding of hydrogen to the framework surface. Thus we propose using a Kubas-type interaction with the coordinatively unsaturated metal complexes of MOF-[12]DBA sites in the frameworks will increase the binding energy of the hydrogen.

In summary, this work outlines a strategy to develop a new generation of ordered, porous hydrocarbon-rich frameworks. The approach described is highly modular and provides plenty of opportunity for tuning structure and functionalities. This general study could be applied to COFs that have higher connectivity or structural complexity. It would be of particular interest to synthesize graphyne. Despite considerable interest, a lack of synthetic routes has prevented its fabrication and study, but Haley has synthesized a few substructures.[3] There is a great chance to form highly ordered materials utilizing the crystallinity of framework materials and this would be one of only a few instances in which graphyne-like carbon networks with long-range order are possible. With the development of this new synthetic application of framework synthetic

methodology to all carbon network, COFs may be granted a larger role in materials fabrication. These nets vary in their chemical and thermal stability affecting crystallinity and thus ability to be studied by x-ray crystallography. These frameworks have been highlighted for their applications in evacuated form for gas guests; however, few applications have highlighted the frameworks' exceptional stability in solution despite some delicate evacuated structures.

5.5 Experimental

5.5.1 General

All syntheses were performed under inert Ar atmosphere. All reagents were used as purchased unless otherwise specified.

5.5.2 Materials

Zinc nitrate hexahydrate ($Zn(NO_3)_2 \cdot 6H_2O$) was purchased from Sigma Aldrich Chemical Co. Copper nitrate hexahydrate ($Cu(NO_3)_2 \cdot 2.5H_2O$) was purchased from Alfa Aesar and Sigma Aldrich Chemical Co. Fluoroboric acid (HBF_4) was purchased from Spectrum Chemicals. Anhydrous *N*,*N*-dimethylformamide (DMF) and *N*-methyl-2-pyrrolidone (NMP), benzene, and THF were purchased from EMD Chemicals DrySolv® system. All commercial reagents were used as purchased unless otherwise specified. Isophthalate [12]DBA **5.1** was synthesized in the laboratory of Dr. Ichiro Hisaki.[4]

5.5.3 Synthetic Procedures

Synthesis of Zn MOF-[12]DBA-3

5.1 (6.4 mg, 0.0081 mmol) and zinc nitrate hexahydrate (18 mg, 0.094 mmol) were added to a dram vial. 300 μL of anhydrous 3:1 solution of DMF/NMP in a dram vial and the vial was placed in an isothermal oven. After heating at 100 ºC for 6 h, yellow crystals formed on the walls of the vial.

Synthesis of Cu MOF-[12]DBA-3

5.1 (1.1 mg, 1.4 μmol) was dissolved in 1 mL of anhydrous DMF. 30 μL of a 50% solution by weight of fluoroboric acid in water was added and the vial was sonicated for 10 mins. $Cu(NO_3)_2 \cdot 2.5H_2O$ (8.5 mg) was added and the vial was sonicated for another 10 mins before placing in an isothermal oven. After heating at 100 ºC for 24 h, cubic green crystals.

5.5.4 Powder X-ray Diffraction

Powder X-ray diffraction (PXRD) data were collected using a Rigaku MiniFlex benchtop X-ray diffractometer with Cu $K\alpha_1$ radiation (λ = 1.5406 Å, 600 W, 30 kV, 15 mA). All samples were mounted on a sample holder by dropping crystals and then leveling the sample surface with a spatula. Diffracted radiation was detected using a hybrid pixel array detector (HPAD).

5.5.5 Single Crystal X-ray Diffraction

Single crystal X-ray diffraction data was collected at the Advance Light Source (ALS) beamline 11.3.1.[5] Detailed unit cell parameters dimensions of the initial structural models are listed in Table 5.2.

Table 5.2. Crystal data for Zn MOF-[12]DBA-3.

Formula	$[Zn_2(CO_2)_4(H_2O)_2]L_2$
Temperature	100 K
Crystal System	Tetragonal
Space Group	*I*4/m No. 87
Unit Cell Dimensions	a = 31.8 Å $\alpha = 90°$
	b = 31.8 Å $\beta = 90°$
	c = 46.7 Å $\gamma = 90°$
Volume	47,260 $Å^3$
Density (calculated)	0.58 g cm^{-3}
Crystal Size	0.1 mm x 0.1 mm x 0.1 mm
Resolution (completeness)	0.7 Å (100%)

5.5.6 Structure Modeling

Crystal models were generated in Materials Studio v 6.0 using atomic coordinates and space group I4 / m collected from single crystal x-ray data and refined in Olex2. Bonds were built between atoms using the Build model with a bond-length tolerance of 0.76-1.1. Bonds types were modified as needed so that aromatic rings contained six partially double bonded C-C bonds. Carboxylate ligands were modified to contain two partially double bonded C-O bonds. Coordinated DMF ligands were added to the axial positions of the zinc paddlewheel secondary building unit. The unit cell was optimized using the Geometry Optimization task in the Forcite Calculation module. Using successive algorithms of steepest descent, ABNR, and Quasi-Newton when convergence was reached and the unit cell parameters did not change upon further geometry optimization. For each optimization, a universal forcefield was used with atom-based van der Waals and Ewald electrostatic interactions. The van der Waals cut off distance was 18.5Å. The final tetragonal unit cell had dimensions of a = b = 29.857170 Å and c = 45.767467 Å.

5.6 References and Notes

(1) http://rcsr.net/nets/rht

(2) For example, see: (a) Lin, X.; Telepeni, I.; Blake, A. J.; Dailly, A.; Brown, C. M.; Simmons, J. M.; Zoppi, M.; Walker, G. S.; Thomas, K. M.; Mays, T. J.; Hubberstey, P.; Champness, N. R.; Schröder, M. High Capacity Hydrogen Adsorption in Cu(II) Tetracarboxylate Framework Materials: The Role of Pore Size, Ligand Functionalization, and Exposed Metal Sites. *J. Am. Chem. Soc.* **2009**, *131*(6) 2159–2171. (b) Tan, C.; Yang, S.; Champness, N. R.; Lin, X.; Blake, A. J.; Lewis, W.; Schröder, M. High capacity gas storage by a 4,8-connected metal-organic polyhedral framework. *Chem. Commun.* **2011**, *47*(15), 4487–4489. (c) Lin, X.; Jia, J.; Zhao, X.; Thomas, K. M.; Blake, A. J.; Walker, G. S.; Champness, N. R.; Hubberstey, P.; Schröder, M. High H_2 Adsorption by Coordination-Framework Materials. *Angew. Chem., Int. Ed.* **2006**, *45*(44), 7358–7364. (d) Yuwono, V. M.; Burrows, N. D.; Soltis, J. A.; Penn, R. L. Orientation Aggregation: Formation and Transformation of Mesocrystal Intermediates Revealed. *J. Am. Chem. Soc.* **2009**, *132*(7), 2163–2165. (e) Farha, O. K.; Yazaydin, Ö.; Eryazici, I.; Malliakas, C. D.; Hauser, B. G.; Kanatzidis, M. G.; Nguyen, S. T.; Snurr, R. Q.; Hupp, J. T. *De novo* synthesis of a metal-organic framework material featuring ultrahigh surface area and gas storage capacities. *Nature Chem.* **2010**, *2*, 944–948. (f) Zhou, Y.; Park, M.; Hong, S.; Lah, M. S. A designed metal-organic framework based on a metal-organic polyhedron. *Chem. Commun.* **2008**, 2340–2342. (g) Yan, Y.; Telepeni, I.; Yang, S.; Lin, X.; Kockelmann, W. Dailly, A.; Blake, A. J.; Lewis, W.; Walker, G. S.; Allan, D. R.; Barnett, S. A.; Champness, N. R.; Schröder, M. *J. Am. Chem. Soc.* **2010**, *132*(12), 4092–4094. (h) Hong, S.; Oh, M.; Park, M.; Yoon, J. W.; Chang, J.-S.; Lah, M. S. Large H_2 storage capacity of a new polyhedron-based metal-organic framework with high thermal and hygroscopic stability. *Chem. Commun.* **2009**, 5397–5399.

(3) Johnson, C. A.; Lu, Y.; Haley, M. M. Carbon Network Based on Benzocyclynes. 6. Synthesis of Graphyne Substructures via Directed Alkyne Metathesis. *Org. Lett.* **2007**, *9*(19), 3725–3728.

(4) Department of Material and Life Science, Graduate School of Engineering, Osaka University, Yamadaoka, Suita, Osaka, 565-0871, Japan.

(5) This research used resources of the Advanced Light Source, which is a DOE Office of Science User Facility under contract no. DE-AC02-05CH11231.

CHAPTER 6

Mechanochemical Synthesis of a Boroxine Covalent Organic Framework

6.1 Abstract

The mechanochemical synthesis of a boroxine covalent organic framework (COF) is presented.

6.2 Introduction

6.2.1 Introduction to Mechanochemistry

Mechanochemical synthetic methods were originally developed in the late 19th century for the production of metal alloys where ball milling and grinding were used to grind pure metals into fine powders to mix into homogenous samples. In the early 20th century, mechanochemistry was used in solid state chemistry and engineering laboratories for the industrial production of cement, silicate, concrete, and refractory materials. More recently, mechanochemistry has re-emerged in the academic literature as a complement and alternative to solution-based chemistries for the fabrication of solid-state materials.[1] Novel materials tend to require high reaction temperatures and are not suitable even in high boiling point solvents. Furthermore, solubility issues persist for larger macromolecules making the production of self-assembled structures in solution unfeasible due to small crystallites precipitating from the solution. Additionally, solvent based reactions are scale limiting, especially for industrial productions.

Ball-milling has already been employed to synthesize a variety of metal-organic framework (MOFs).[2] To a lesser extent, COFs have also been prepared by mechanochemical methods and provide an opportunity for materials design and discovery. In 2013 the first mechanochemical synthesis of a COF was published and in subsequent years only a few additional papers have been published demonstrating the value of using mechanochemistry for materials discovery and the opportunity for growth of this field.[3] COF-1 was the first COF to be published by Côté and Yaghi in 2005 and features a boroxine core from the reversible condensation of 1,4-diboronic acid,[4] and since then several boroxine COFs have been prepared in solution,[4] on surfaces,[5] and by microwave heating;[6] however, to the best of our knowledge, no COFs featuring a boroxine core have been synthesized by mechanochemical methods.

6.2.2 Diketopiperidines as Functional Building Blocks

2,5-Diketopiperazine is a cyclic dipeptide formed from the head-to-tail cyclization of two α-amino acids (Figure 6.1).[7] The rigid heterocyclic core of 2,5-diketopiperazine can be obtained from natural sources including marine organisms where it arises from biosynthetic processes.[8] It has been demonstrated to be an important molecular scaffold for biological and pharmaceutical activities.[9] The C_2-symmetric six-membered ring also makes a useful building block for materials chemistry.

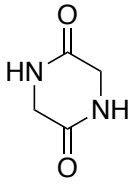

6.1

Figure 6.1. Structural motif of 2,5-diketopiperazine **6.1**.

6.3 Results and Discussion

Synthesis of monomer **6.5** is shown in Scheme 6.1. Glycine anhydride **6.1** is acylated to yield the *N*-acyl protected 2,5-diketopiperazine **6.2** by refluxing in acetic anhydride. The boronic acid **6.3** is protected with a pinacol group before the two-fold aldol addition with **6.2** to yield the unsaturated 2,5-diketopiperidine **6.5**.

Scheme 6.1. Small molecule synthesis of monomer **6.5**.

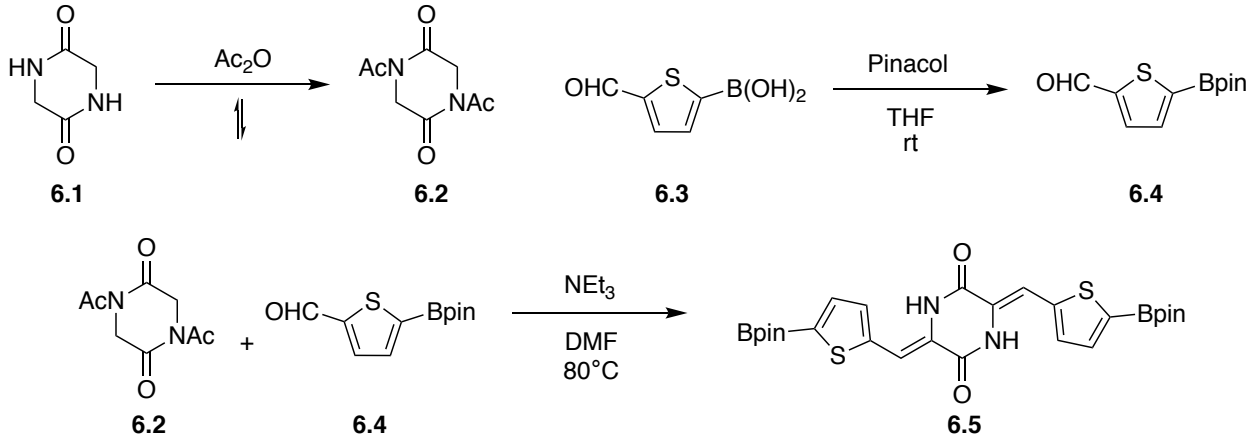

While at the Advanced Light Source (ALS) facility, 1-2 mg of the pinacol protected boronate ester **6.5** was added to a mortar and ground with a pestle for 30 seconds until a very fine powder was achieved (Scheme 6.2).[10] The ground substrate was immediately placed between two layers of Kapton then mounted and diffracted on the 12.2.2 beamline with synchrotron radiation to reveal a low angle peak at $2\theta = 3.2°$. Using Bragg's Law, $n\lambda=2d\sin\theta$, we can determine the $2\theta = 3.2°$ peak corresponds to a d-spacing of 15 Å which is in-line with nanoporous materials. Due to the large d-spacing or distance between lattice planes in these framework materials, small angles of 2θ are characteristic of this group of materials. Small molecules tend to crystallize with small d-spacing and thus larger angles of 2θ are observed. It is notable that the substrate appears to increase in crystallinity over time as the PXRD intensities are sharper in the diffraction patterns collected several hours after the initial grinding. More experiments are suggested to confirm this initial observation. It is important to note this experiment was carried out in ambient conditions leading to the absorption of moisture where water may be an important contribution factor to the crystalline transformation.

Scheme 6.2. Mechanochemical synthesis of COF **6.6** from monomer **6.5**.

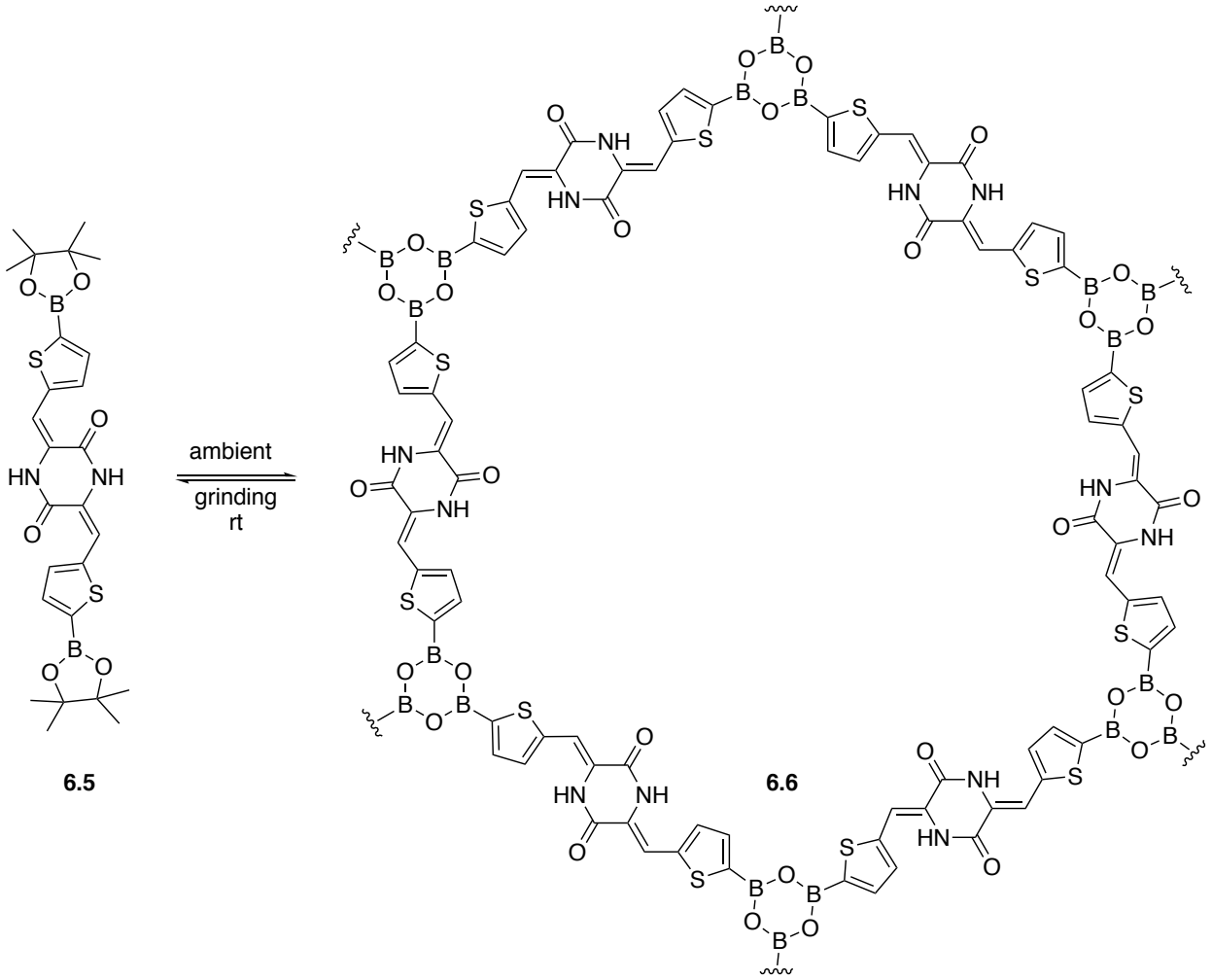

6.4 Conclusions and Outlook

A preliminary study of a boroxine covalent organic framework fabricated by mechanochemical synthesis was done, with the product characterized by powder X-ray diffraction studies at the ALS 12.2.2 beamline. This mechanochemical synthesis of boroxine COFs demonstrates the ability to diversify the fabrication of this class of organic crystalline materials. Future experiments at beamline 12.2.2 utilizing a diamond anvil cell to study the lattice formation as a function of time and pressure would be of particular interest and would reveal more information about the mechanism of framework construction and if the lattice formation/deformation is reversible. Full characterization of the COF (FT-IR, EA, CP-MAS, etc.) is required to confirm the structure of the COF to rule out large oligomers, polymers, or other network topologies.

6.5 Experimental

6.5.1 General

All organic syntheses were performed in dry glassware under inert N_2 atmosphere unless otherwise noted. ^1H and ^{13}C NMR spectra were acquired on a Bruker Avance II 500 MHz NMR spectrometer and chemical shifts were calculated using the solvent resonance as internal standards (^1H: 7.26 ppm for $CHCl_3$; ^{13}C: 77.00 ppm for $CDCl_3$). ^1H NMR data is reported as follows: chemical shift δ (ppm), multiplicity, coupling constant (Hz), and integration. ^{13}C NMR data is reported according to the chemical shift. Analytical thin layer chromatography (TLC) was performed on silica gel TLC plates with a fluorescent indicator. TLC spots were visualized using either short-wave (254 nm) or long-wave (365 nm) UV light.

6.5.2 Materials

All reagents were used as purchased unless otherwise specified. *N,N*-dimethylformamide (DMF), triethylamine (TEA), and tetrahydrofuran (THF) were purchased from commercial sources and distilled in a solvent purification system (SPS) immediately before use.

6.5.3 Synthetic Procedures and Spectral Data

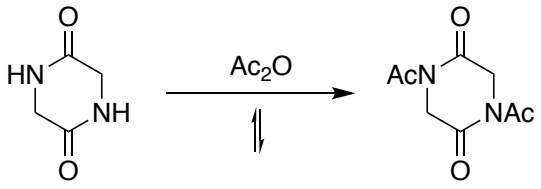

6.1 **6.2**

Synthesis of 1,4-diacetylpiperazine-2,5-dione (6.2). 200 mL of acetic anhydride was added to a 500-mL round-bottom flask with a condenser under N_2 atmosphere containing glycine anhydride (**6.1**, 10.0 g, 87.6 mmol)**.** The reaction was refluxed at 140 °C for 20 h before cooling to room temperature and removing the solvent under reduced pressure. The crude mixture was recrystallized with acetone followed by ethyl acetate/hexanes and dried under high vacuum. ^1H NMR (500 MHz, $CDCl_3$) δ 2.59 (s, 6H), 4.60 (s, 4H).

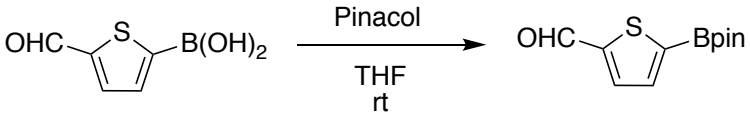

6.3 **6.4**

Synthesis of 5-(4,4,5,5-tetramethyl-1,3,2-dioxaborolan-2-yl)thiophene-2-carbaldehyde (6.4). The boronic acid (**6.3**, 2.10 mmol, 500 mg) and pinacol (2.10 mmol, 248 mg) were added to a 2-necked round-bottom flask with a stir bar and placed under N_2 atmosphere. 15 mL of THF was added and the reaction was stirred vigorously at room temperature. The reaction was monitored by TLC adding additions of 250 mg of pinacol dissolved in 15 mL of THF until all the boronic acid has been consumed. The solvent was removed under reduced pressure and the product was used without further purification. ^1H NMR (500 MHz, $CDCl_3$) δ 1.36 (s, 12H), 7.66 (d, J = 3.6 Hz,

1H), 7.80 (d, J = 3.6 Hz, 1H), 9.98 (s, 1H); ^{13}C NMR (500 MHz, $CDCl_3$) δ 24.7, 84.8, 135.6, 137.2, 148.9, 183.0.

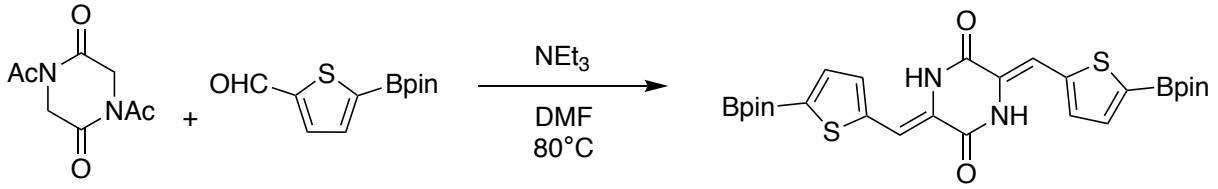

6.2 **6.4** **6.5**

Synthesis of (*3Z*,*6Z*)-3,6-bis((5-(4,4,5,5-tetramethyl-1,3,2-dioxaborolan-2-yl)thiophen-2-yl(methylene)piperazine-2,5-dione (6.5). DMF (10 mL) and TEA (280 μL) were sparged with N_2 in a 25-mL round-bottom flask. Aldehyde (**6.4**, 300 mg, 1.26 mmol) and the DKP (**6.2**, 100 mg, 0.505 mmol) were added to a separate round-bottom flask fitted with a condenser and placed under N_2 atmosphere. The DMF/TEA solution was transferred via a canula and the reaction was heated at 80°C for 19 h. 300 μL of TEA was added and the reaction was continued to stir at 90°C for an additional 24 h. The reaction was cooled to room temperature and the precipitate was collected by filtration and used without further purification. ^{1}H NMR (500 MHz, $CDCl_3$) δ 1.37 (s, 24H), 7.25 (d, J = 0.7 Hz, 2H), 7.32 (dd, J = 3.6, 0.7 Hz, 2H), 7.63 (d, J = 3.6 Hz, 2H), 8.30 (s, 2H); ^{13}C NMR (500 MHz, $CDCl_3$), δ 24.8, 84.6, 109.5, 124.0, 131.8, 137.8, 141.6, 156.7.

6.5.4 NMR Spectra

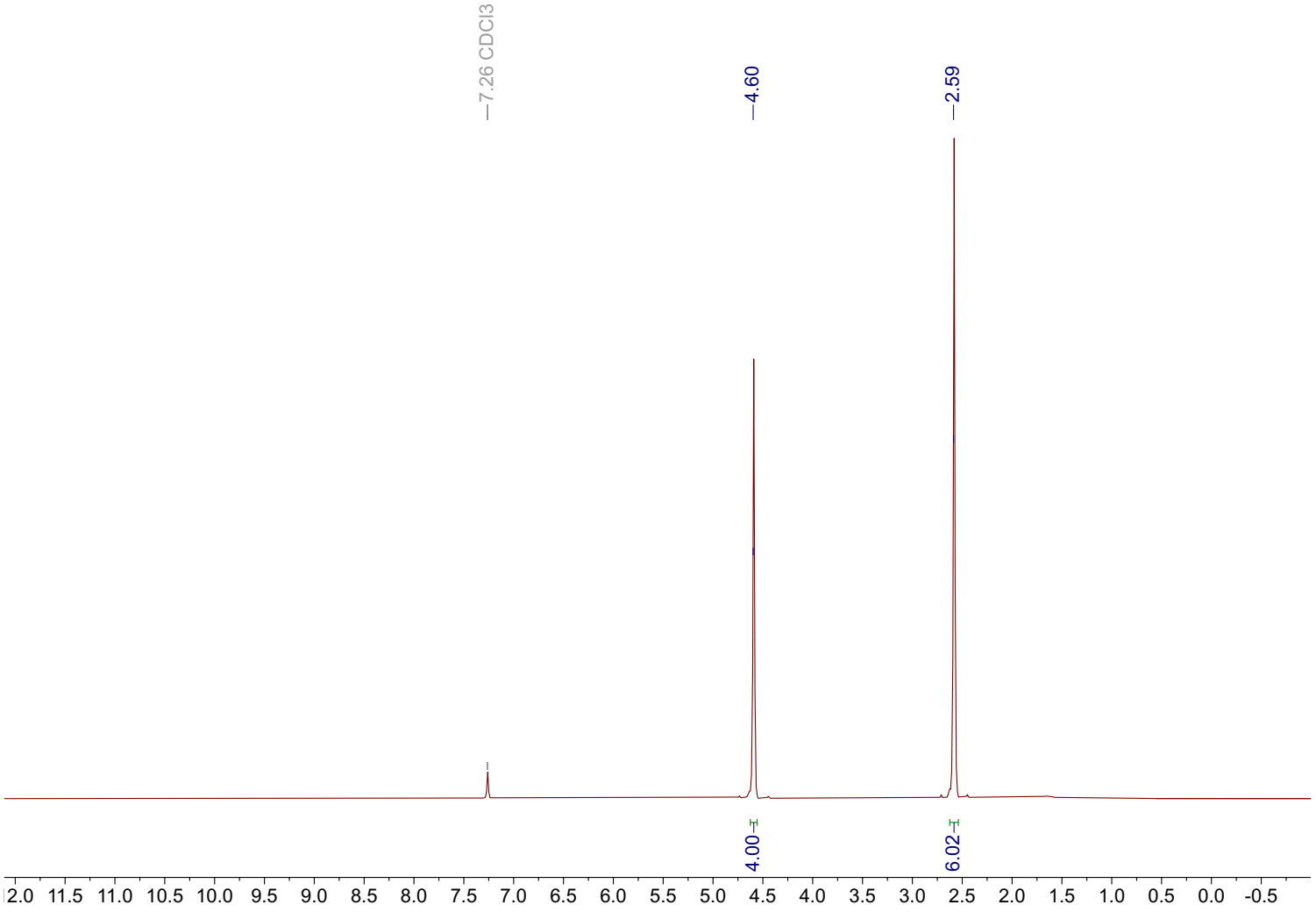

Figure 6.2. ^{1}H NMR spectrum of compound **6.2** (500 MHz, $CDCl_3$).

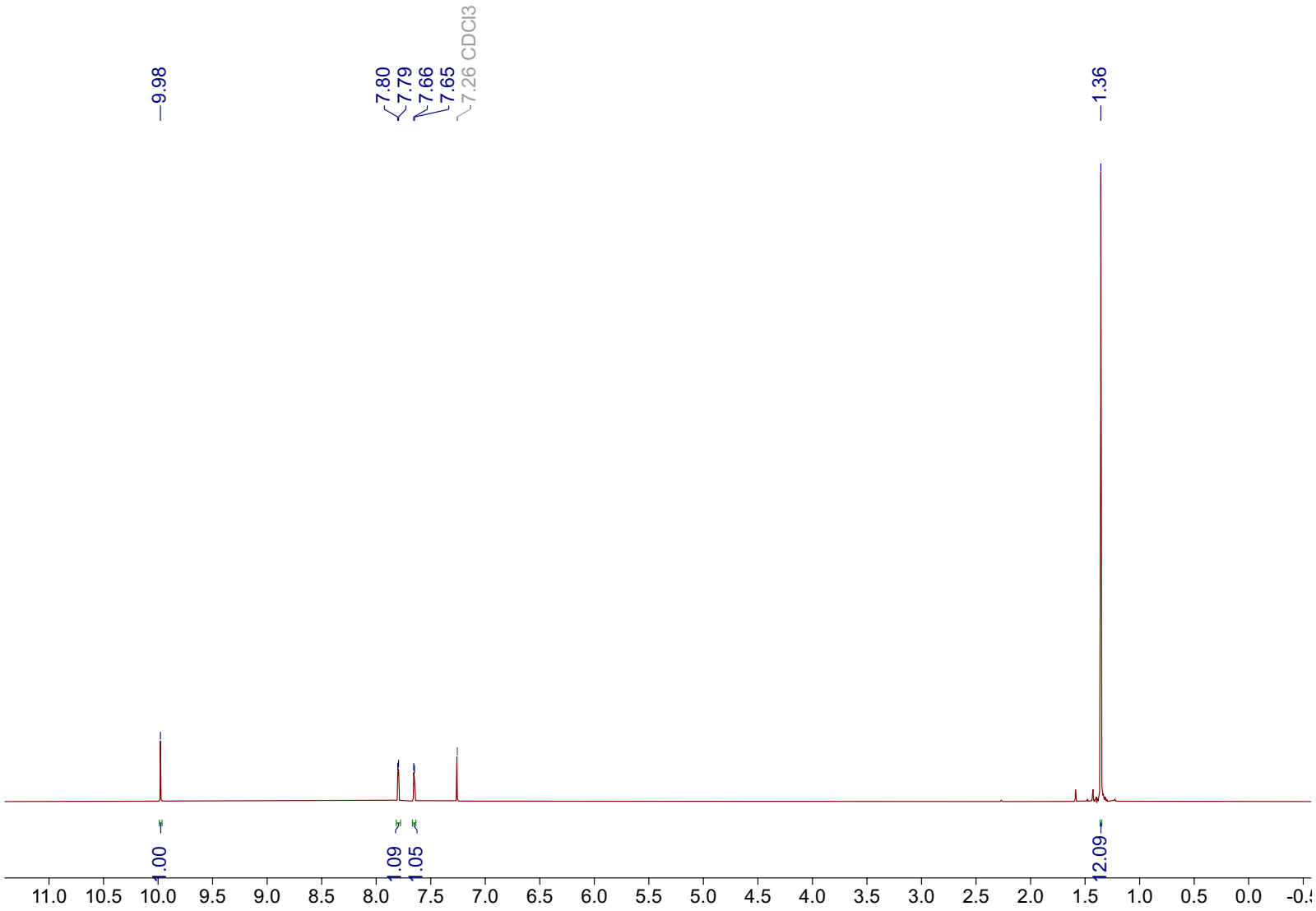

Figure 6.3. ^{1}H NMR spectrum of compound **6.4** (500 MHz, $CDCl_3$).

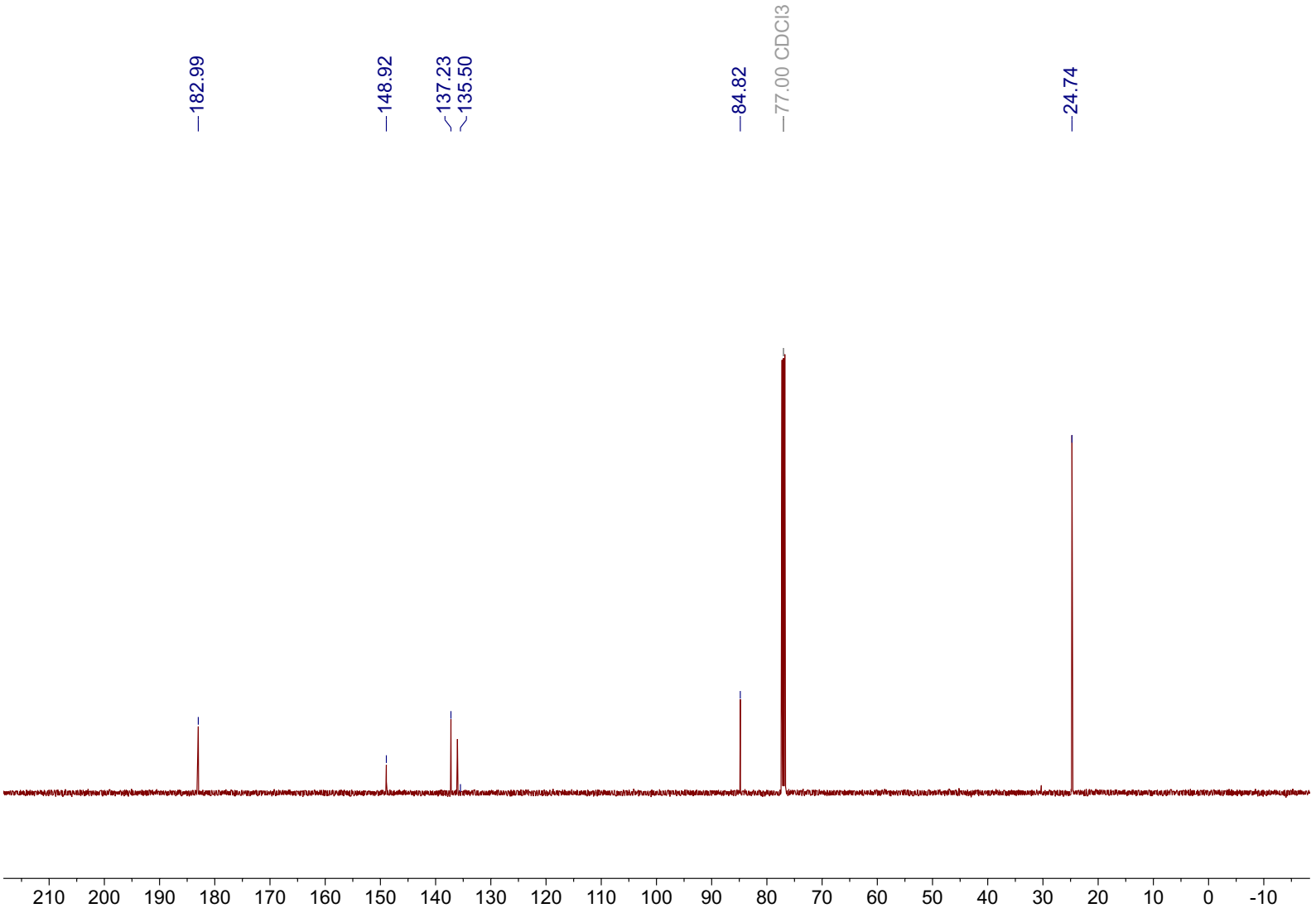

Figure 6.4. ^{13}C NMR spectrum of compound **6.4** (500 MHz, $CDCl_3$).

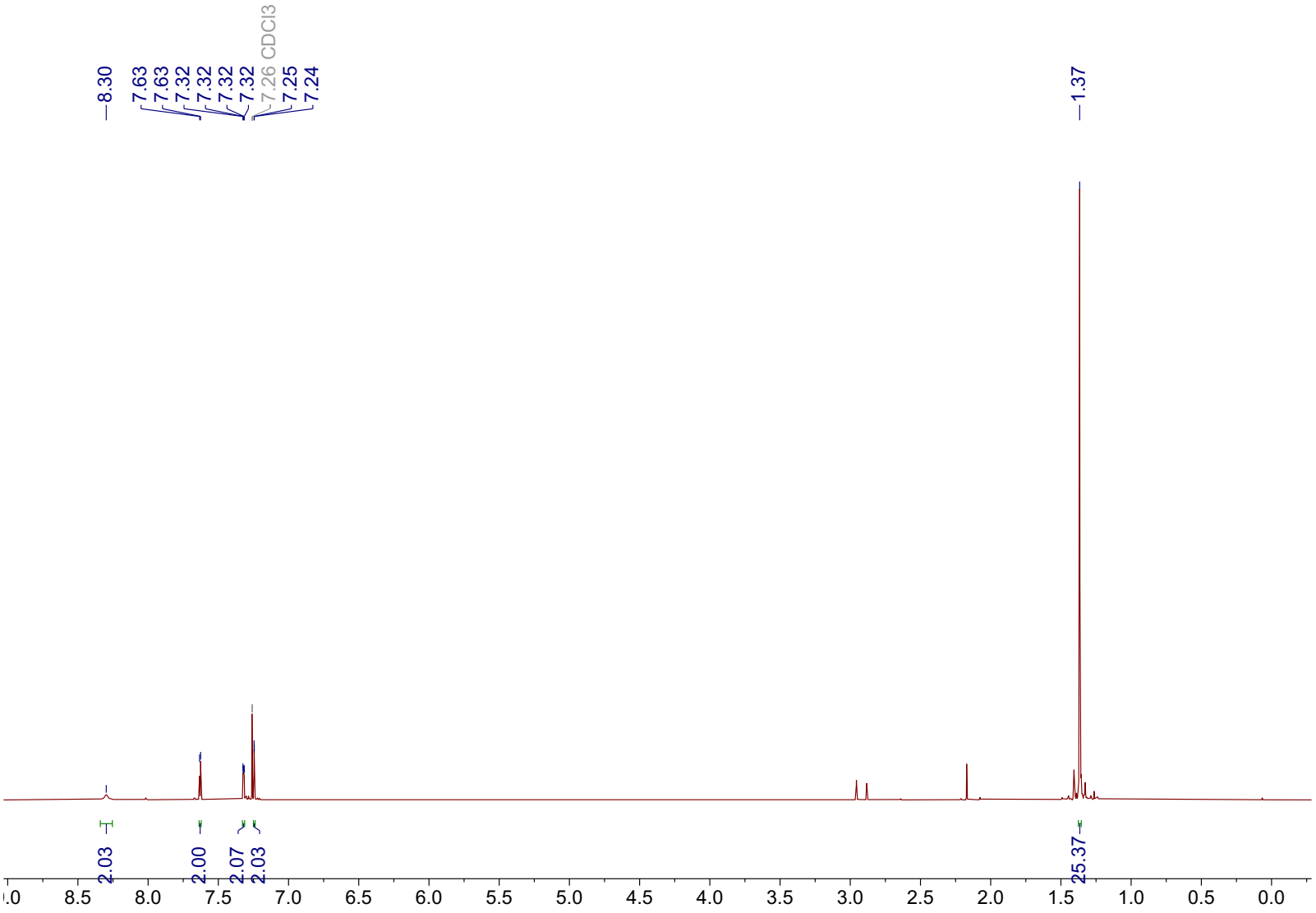

Figure 6.5. ^{1}H NMR spectrum of compound **6.5** (500 MHz, $CDCl_3$).

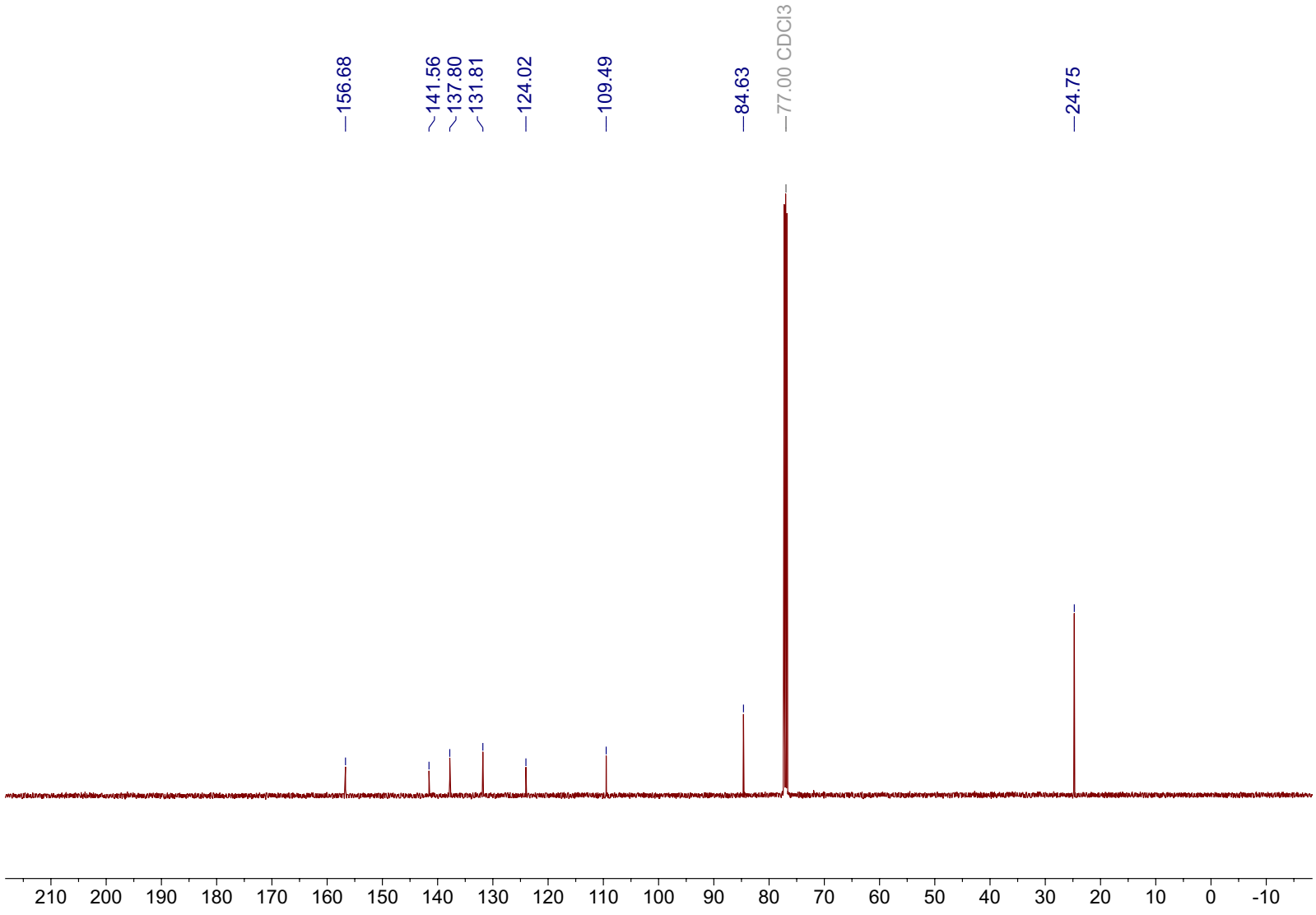

Figure 6.6. ^{13}C NMR spectrum of compound **6.5** (500 MHz, $CDCl_3$).

6.5.5 Mechanochemical Synthesis of a Boroxine Covalent Organic Framework

Synthesis of COF (6.3.6). 6.3.6 was synthesized by grinding a few mg of monomer **6.3.5** in a mortar and pestle.

6.5.6 Crystallography and Structure Analysis

Sample prep for PXRD. A few mg of freshly ground COF **6.6** was placed between two Kapton film layers.

PXRD data acquisition. A mar345 detector was used to collect one standard image with 120 s exposure time at a detector distance of 300 mm using CeO_2 as a reference standard for calibration. One standard image with 240 s exposure time at a detector distance of 300 mm and incident energy of 15 keV (λ = 0.825028 Å). Images were processed using Dioptas software.

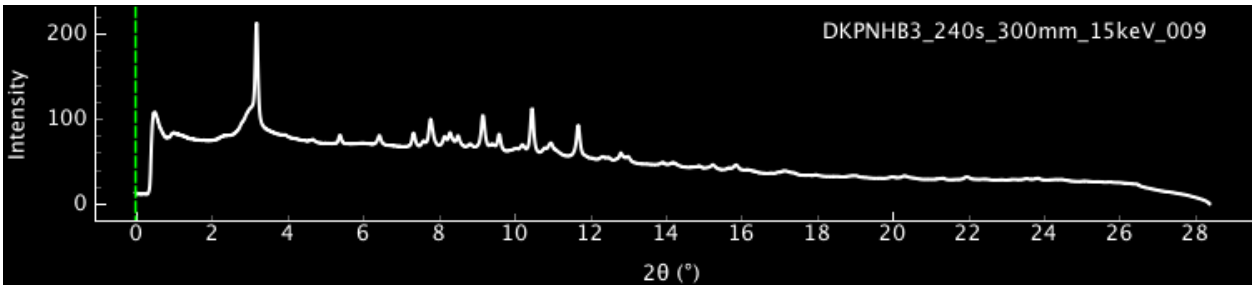

Figure 6.7. PXRD pattern of product **6.6** from the grinding of **6.5**.

6.6 References and Notes

(1) Xu, C.; De, S.; Balu, A. M.; Ojeda, M.; Luque, R. Mechanochemical synthesis of advanced nanomaterials for catalytic applications. *Chem. Commun.* **2015**, *51*(31), 6698–6713.

(2) (a) Coudert, F.-X.; Responsive Metal-Organic Frameworks and Framework Materials: Under Pressure, Taking the Heat, in the Spotlight, with Friends. *Chem. Mater.* **2015**, *27*(6), 1905–1914. (b) Chen, D.; Zhao, J.; Zhang, P.; Dai, S. Mechanochemical synthesis of metal-organic frameworks. *Polyhedron*, **2019**, *162*, 59-64.

(3) (a) Biswal, B. P.; Chandra, S.; Kandambeth, S.; Lukose, B.; Heine, T.; Banerjee, R. Mechanochemical Synthesis of Chemically Stable Isoreticular Covalent Organic Frameworks. *J. Am. Chem. Soc.* **2013**, *135*, 5328–5331. (b) Liao, Y.; Li, J.; Thomas, A. General Route to High Surface Area Covalent Organic Frameworks and Their Metal Oxide Composites as Magnetically Recoverable Adsorbents and for Energy Storage. *ACS Macro Lett.* **2017**, *6*(12), 1444–1450. (c) Lv, H.; Zhao, X.; Niu, H.; He, S.; Tang, Z.; Wu, F.; Giesy, J. P. Ball milling synthesis of covalent organic frameworks as a highly active photocatalyst for degradation of organic contaminants. *J. Hazard. Mater.* **2019**, *369*, 494–502. (d) Chen, H.; Zhang, Y.; Xu, C.; Cao, M. Dou, H.; Zhang, X. Two π-Conjugated Covalent Organic Frameworks with Long-Term Cyclability at High Current Density for Lithium Ion Battery. *Chem. Eur. J.* **2019**, *25*(68), 15472–15476. (e) Shinde, D. B.; Aiyappa, H. B.; Bhadra, M.; Biswal, B. P.; Wadge, P.; Kandambeth, S.; Garai, B.; Kundu, T.; Kurungol, S.; Banerjee, R. A mechanochemically synthesized covalent organic framework as a proton-conducting solid electrolyte. *J. Mater. Chem. A*. **2016**, *4*(7), 2682–2690. (f) Zhao, X.; Pachfule, P.; Li, S.; Langenhahn, T.; Ye, M.; Tian, G.; Schmidt, J.; Thomas, A. Silica-Templated Covalent Organic Framework-Derived Fe-N-Doped Mesoporous Carbon as Oxygen Reduction Electrocatalyst. *Chem. Mater.* **2019**, *31*(9), 3274–3280.

(4) Côté, A. P.; Benin, A. I.; Ockwig, N. W.; O'Keeffe, M.; Matzger, A. J.; Yaghi, O. M. Porous, Crystalline, Covalent Organic Frameworks. *Science* **2005**, *310*(5751), 1166–1170.

(5) (a) Dienstmaier, J. F.; Medina, D. D.; Dogru, M.; Knochel, P.; Bein, T.; Heckl, W. M.; Lackinger, M. Isoreticular Two-Dimensional Covalent Organic Frameworks Synthesized by On-Surface Condensation of Diboronic Acids. *ACS Nano* **2012**, *6*(8), 7234–7242. (b) Zwaneveld, N. A. A.; Pawlak, R.; Abel, M.; Catalin, D.; Gigmes, D.; Bertin, D.; Porte, L. Organized Formation of 2D Extended Covalent Organic Frameworks at Surfaces. *J. Am. Chem. Soc.* **2008**, *130*(21), 6678–6679. (c) Ourdjini, O.; Pawlak, R.; Abel, M.; Clair, S.; Chen, L.; Bergeon, N.; Sassi, M.; Oison, V.; Debierre, J.-M.; Coratger, R.; Porte, L. Substrate-mediated ordering and defect analysis of a surface covalent organic framework. *Phys. Rev. B* **2011**, *84*(12), 125421.

(6) Campbell, N. L.; Clowes, R.; Ritchie, L. K.; Cooper, A. I. Rapid Microwave Synthesis and Purification of Porous Covalent Organic Frameworks. *Chem. Mater.* **2009**, *21*(2), 204–206.

(7) (a) Dinsmore, C. J.; Beshore, D. C. Recent advances in the synthesis of diketopiperazines. *Tetrahedron*, **2002**, *58*(17) 3297–3312. (b) Borthwick, A. D. 2,5-Diketopiperidines: Synthesis, Reactions, Medicinal Chemistry, and Bioactive Natural Products. *Chem Rev.* **2012**, *112*, 3641–3716.

(8) Huang, R.-M.; Yi, X.-X.; Zhou, Y.; Su, X.; Peng, Y.; Gao, C.-H. An Update on 2,5-Diketopiperazines from Marine Organisms. *Mar. Drugs* **2014**, *12*, 6213–6235.
(9) Rational and combinatorial tailoring of bioactive cyclic dipeptides. Giessen, T. W.; Marahiel, M. A. *Front. Microbiol.* **2015**, *6*, 1–11.
(10) Beamline 12.2.2 at the Advanced Light Source is a DOE Office of Science User Facility under contract no. DE-AC02-05CH11231.

Bibliography

Baughman, R. H.; Eckhardt, H.; Kertesz, M. Structure-property predictions for new planar forms of carbon: Layered phases containing sp^2 and *sp* atoms. *J. Chem. Phys.* **1987**, *87*(11), 6687–6699.

Ben, T.; Ren, H.; Ma, S.; Cao, D.; Lan, J.; Jing, X.; Wang, W.; Xu, J.; Deng, F.; Simmons, J. M.; Qiu, S.; Zhu, G. Targeted Synthesis of a Porous Aromatic Framework with High Stability and Exceptionally High Surface Area. *Angew, Chem., Int. Ed.* **2009**, *48*(50), 9457–9460.

Biswal, B. P.; Chandra, S.; Kandambeth, S.; Lukose, B.; Heine, T.; Banerjee, R. Mechanochemical Synthesis of Chemically Stable Isoreticular Covalent Organic Frameworks. *J. Am. Chem. Soc.* **2013**, *135*, 5328–5331.

Borthwick, A. D. 2,5-Diketopiperidines: Synthesis, Reactions, Medicinal Chemistry, and Bioactive Natural Products. *Chem Rev.* **2012**, *112*, 3641–3716.

Bredas, J. L.; Adant, C.; Tackx, P.; Persoons, A.; Pierce, B. M. Third-Order Nonlinear Optical Response in Organic Materials: Theoretical and Experimental Aspects. *Chem. Rev.* **1994**, *94*(1), 243–278.

Bui, C. T.; Flynn, B. L. J. Solid-Phase Synthesis of 2,3-Disubstituted Benzo[*b*]thiophenes and Benzo[*b*]selenophenes. *Comb. Chem.* **2006**, *8*(2), 163–167.

Campbell, N. L.; Clowes, R.; Ritchie, L. K.; Cooper, A. I. Rapid Microwave Synthesis and Purification of Porous Covalent Organic Frameworks. *Chem. Mater.* **2009**, *21*(2), 204–206.

Chae, H. K.; Siberio-Pérez, D. Y.; Kim, J.; Go, Y.; Eddaoudi, M.; Matzger, A. J.; O'Keeffe, M.; Yaghi, O. M. A route to high surface area, porosity and inclusion of large molecules in crystals. *Nature* **2004**, *427*, 523–527.

Chen, D.; Zhao, J.; Zhang, P.; Dai, S. Mechanochemical synthesis of metal-organic frameworks. *Polyhedron*, **2019**, *162*, 59-64.

Chen, H.; Zhang, Y.; Xu, C.; Cao, M. Dou, H.; Zhang, X. Two π-Conjugated Covalent Organic Frameworks with Long-Term Cyclability at High Current Density for Lithium Ion Battery. *Chem. Eur. J.* **2019**, *25*(68), 15472–15476.

Chen, J.; Xi, J.; Wang, D.; Shuai, Z. Carrier Mobility in Graphyne Should Be Even Larger than That in Graphene: A Theoretical Prediction. *J. Phys. Chem. Lett.* **2013**, *4*(9) 1443–1448.

Choi, J. Y.; Kim, J.; Furukawa, H.; Chae, H. K. Porous Chiral Metal Organic Carboxylate Frameworks with a Double-interwoven $SrSi_2$ Topology: $M_3(TTCA)_2$•6DMF•$7H_2O$ (TTCA = triphenylenetricarboxylate; M = Zn^{2+}, Cd^{2+}). *Chem. Lett.* **2006**, *35*(9), 1054–1055.

Choi, S. B.; Furukawa, H.; Nam, H. J.; Jung, D.-K.; Jhon, Y. H.; Walton, A.; Book, D.; O'Keeffe, M.; Yaghi, O. M.; Kim, J. Reversible Interpenetration in a Metal-Organic Framework Triggered by Ligand Removal and Addition. *Angew. Chem., Int. Ed.* **2012**, *51*(35), 8791–8795.

Côté, A. P.; Benin, A. I.; Ockwig, N. W.; O'Keeffe, M.; Matzger, A. J.; Yaghi, O. M. Porous, Crystalline, Covalent Organic Frameworks. *Science* **2005**, *310*(5751), 1166–1170.

Coudert, F.-X.; Responsive Metal-Organic Frameworks and Framework Materials: Under Pressure, Taking the Heat, in the Spotlight, with Friends. *Chem. Mater.* **2015**, *27*(6), 1905–1914.

Cranford, S. W.; Buehler, M. J. Mechanical properties of graphyne. Carbon 2011, *49*(13), 4111–4121.

Dayoub, W.; Doutheau, A. (*E*) Enol ethers from the stereoselective reduction of α-alkoxy-β-ketophosphonates and Wittig type reaction. *Sci. China: Chem.* **2010**, *53*(6), 1937–1945.

Diederich, F.; Kivala, M. All-Carbon Scaffolds by Rational Design. *Adv. Mater.* **2010**, *22*(7), 803–812.

Dienstmaier, J. F.; Medina, D. D.; Dogru, M.; Knochel, P.; Bein, T.; Heckl, W. M.; Lackinger, M. Isoreticular Two-Dimensional Covalent Organic Frameworks Synthesized by On-Surface Condensation of Diboronic Acids. *ACS Nano* **2012**, *6*(8), 7234–7242.

Diercks, R.; Vollhardt, K. P. C. Tris(benzocyclobutadieno)benzene, the triangular [4]phenylene with a completely bond-fixed cyclohexatriene ring: cobalt-catalyzed synthesis from hexaethynylbenzene and thermal ring opening to 1,2:5,6:9,10-tribenzo-3,4,7,8,11,12-hexadehydro[12]annulene. *J. Am. Chem. Soc.* **1986**, *108*(11), 3150–3152.

Dinsmore, C. J.; Beshore, D. C. Recent advances in the synthesis of diketopiperazines. *Tetrahedron*, **2002**, *58*(17) 3297–3312.

Djebli, A.; Ferrara, J. D.; Tessier-Youngs, C.; Youngs, W. J. The synthesis and structural characterization of a novel tetracobalt cluster of 5,6,11,12,17,18-hexadehydrotribenzo[*a,e,i*]-cyclododecine. *J. Chem. Soc., Chem. Commun.* **1988**, 548–549.

Eddaoudi, M.; Moler, D. B.; Li, H.; Chen, B.; Reineke, T. M.; O'Keeffe, R.; Yaghi, O. M. Modular Chemistry: Secondary Building Units as a Basis for the Design of Highly Porous and Robust Metal-Organic Carboxylate Frameworks. *Acc. Chem. Res.* **2001**, *34*(4), 319–330.

Farha, O. K.; Yazaydin, Ö.; Eryazici, I.; Malliakas, C. D.; Hauser, B. G.; Kanatzidis, M. G.; Nguyen, S. T.; Snurr, R. Q.; Hupp, J. T. *De novo* synthesis of a metal-organic framework material featuring ultrahigh surface area and gas storage capacities. *Nature Chem.* **2010**, *2*, 944–948.

Ferrara, J. D.; Djebli, A.; Tessier-Youngs, C.; Youngs, W. J. Synthesis and characterization of a silver(I) triflate sandwich complex of 1,2:5,6:9,10-tribenzocyclododeca-1,5,9-triene-3,7,11-triyne. The first example of a 12-membered macrocycle sandwich complex. *J. Am. Chem. Soc.* **1988**, *110*(2), 647–649.

Ferrara, J. D.; Tanaka, A. A.; Fierro, C.; Tessier-Youngs, C. A.; Youngs, W. J. Synthesis and structural and theoretical characterization of a nickel(0) complex of tribenzocyclyne (TBC) and the preparation of a novel organometallic conductor. *Organometallics* **1989**, *8*(9), 2089–2098.

Ferrara, J. D.; Tessier-Youngs, C.; Youngs, W. J. A novel n-doped metallomacrocyclic conductor. *J. Am. Chem. Soc.* **1988**, *110*(10), 3326–3327.

Ferrara, J. D.; Tessier-Youngs, C.; Youngs, W. J. Synthesis and characterization of the first transition metal complex of 1,2:5,6:9,10-tribenzocyclododeca-1,5,9-triene-3,7,11-triyne. *J. Am. Chem. Soc.* **1985**, *107*(23), 6719–6721.

Ferrara, J. D.; Tessier-Youngs, C.; Youngs, W. J. Synthesis and characterization of a copper(I) triflate complex of 1,2:5,6:9,10-tribenzocyclododeca-1,5,9-triene-3,7,11-triyne. *Organometallics* **1987**, *6*(3), 676–678.

Ferrara, J. D.; Tessier-Youngs, C.; Youngs, W. J. Synthesis and molecular structure of a trinuclear copper(I) cofacial bimacrocycle. *Inorg. Chem.* **1988**, *27*(13), 2201–2202.

Furukawa, H.; Cordova, K. E.; O'Keeffe, M.; Yaghi, O. M. The Chemistry and Applications of Metal-Organic Frameworks. *Science* **2013**, *341*(6149).

Furukawa, H.; Go, Y. B.; Ko, N.; Park, Y. K.; Uribe-Romo, F. J.; Kim, J.; O'Keeffe, M.; Yaghi, O. M. Isoreticular Expansion of Metal-Organic Frameworks with Triangular and Square Building Units and the Lowest Calculated Density for Porous Crystals. *Inorg. Chem.* **2011**, *50(*18), 9147–9152.

Furukawa, H.; Ko, N.; Go, Y. B.; Aratani, N.; Choi, S. B.; Choi, E.; Yazaydin, A. Ö.; Snurr, R. Q.; O'Keeffe, M.; Kim, J.; Yaghi, O. Ultrahigh Porosity in Metal-Organic Frameworks. *Science*, **2010**, *329*(5990), 424–428.

Furukawa, S.; Uji-i, H.; Tahara, K.; Ichikawa, T.; Sonoda, M.; De Schryver, F. C.; Tobe, Y.; De Feyter, S. Molecular Geometry Directed Kagomé and Honeycomb Networks: Toward Two-Dimensional Crystal Engineering. *J. Am. Chem. Soc.* **2006**, *128*(11), 3502–3503.

Geim, A. K.; Novoselov, K. S. The rise of graphene. *Nat. Mater.* **2007**, *6*, 183–191.

Giessen, T. W.; Marahiel, M. A. Rational and combinatorial tailoring of bioactive cyclic dipeptides. *Front. Microbiol.* **2015**, *6*, 1–11.

Griffith, W. P.; Jolliffe, J. M.; Ley, S. V.; Springhorn, K. F.; Tiffin, P. D. Oxidation of Activated Halides to Aldehydes and Ketones by N-Methylmorpholine-N-Oxide. *Synth. Commun.* **2006**, *22*(13), 1967–1971.

Haley, M. M. Synthesis and properties of annulenic subunits of graphyne and graphdiyne nanoarchitectures. *Pure Appl. Chem.* **2008**, *80*(3), 519–532.

Hisaki, I.; Sakamoto, Y.; Shigemitsu, H.; Tohnai, N.; Miyata, M.; Seki, S.; Saeki, A.; Tagawa, S. Superstructure-Dependent Optical and Electrical Properties of an Unusual Face-to-Face, π-Stacked, One-Dimensional Assembly of Dehydrobenzo[12]annulene in the Crystalline State. *Chem. Eur. J.* **2008**, *14*(14), 4178–4187.

Hisaki, I.; Senga, H.; Sakamoto, Y.; Tsuzuki, S.; Tohnai, N.; Miyata, M. Specific Interaction between Chloroform and the Pockets of Triangular Annulene Derivatives Providing Symmetry Carry-Over Crystallization. *Chem. Eur. J.* **2009**, *15*(48), 13336–13340.

Hong, S.; Oh, M.; Park, M.; Yoon, J. W.; Chang, J.-S.; Lah, M. S. Large H_2 storage capacity of a new polyhedron-based metal-organic framework with high thermal and hygroscopic stability. *Chem. Commun.* **2009**, 5397–5399.

Huang, R.-M.; Yi, X.-X.; Zhou, Y.; Su, X.; Peng, Y.; Gao, C.-H. An Update on 2,5-Diketopiperazines from Marine Organisms. *Mar. Drugs* **2014**, *12*, 6213–6235.

Jing, Y.; Wu, G.; Guo, L.; Sun, Y.; Shen, J. Electronic transport properties of graphyne and its family. *Comput. Mater. Sci.* **2013**, *78*, 22–28.

Jiang, J.; Tew, G. N. Synthesis of Macrocycle Isomers via Metathesis Cyclization and Their Self-Assembly from Aqueous Solutions. *Org. Lett.* **2008**, *10*(20), 4393–4396.

Johnson, C. A.; Lu, Y.; Haley, M. M. Carbon Network Based on Benzocyclynes. 6. Synthesis of Graphyne Substructures via Directed Alkyne Metathesis. *Org. Lett.* **2007**, *9*(19), 3725–3728.

Kim, J.; Chen, B.; Reineke, T. M.; Li, H.; Eddaoudi, M.; Moler, D. B.; O'Keefe, M.; Yaghi, O. M. Assembly of Metal-Organic Frameworks from Large Organic and Inorganic Secondary Building Units: New Examples and Simplifying Principles for Complex Structures. *J. Am. Chem. Soc.* **2001**, *123*(34), 8239–8247.

Kosynkin, D. V.; Tour, J. M. Benzyltriethylammonium Dichloroiodate/Sodium Bicarbonate Combination as an Inexpensive, Environmentally Friendly, and Mild Iodination Reagent for Anilines. *Org. Lett.* **2001**, *3*(7), 991–992.

Kroto, H. W.; Heath, J. R.; O'Brien, S. C.; Curl, R. F.; Smalley, R. E. C_{60}: Buckminsterfullerene. *Nature* **1985**, *318*, 162–163.

Li, G.; Li, Y.; Liu, H.; Guo, Y.; Li, Y.; Zhu, D. Architecture of graphdiyne nanoscale films. *Chem. Commun.* **2010**, *46*(19), 3256–3258.

Li, J.; Brill, T. B. Spectroscopy of Hydrothermal Reactions 20: Experimental and DFT Computational Comparison of Decarboxylation of Dicarboxylic Acids Connected by Single, Double, and Triple Bonds. *J. Phys. Chem. A* **2002**, *106*(41), 9491–9498.

Li, Y.; Rubin, Y.; Diederich, F.; Houk, K. N. Electronic and Structural Properties of the Cyclobutenodehydroannulenes. *J. Am. Chem. Soc.* **1990**, *112*(4), 1618–1623.

Liao, Y.; Li, J.; Thomas, A. General Route to High Surface Area Covalent Organic Frameworks and Their Metal Oxide Composites as Magnetically Recoverable Adsorbents and for Energy Storage. *ACS Macro Lett.* **2017**, *6*(12), 1444–1450.

Lin, X.; Jia, J.; Zhao, X.; Thomas, K. M.; Blake, A. J.; Walker, G. S.; Champness, N. R.; Hubberstey, P.; Schröder, M. High H_2 Adsorption by Coordination-Framework Materials. *Angew. Chem., Int. Ed.* **2006**, *45*(44), 7358–7364.

Lin, X.; Telepeni, I.; Blake, A. J.; Dailly, A.; Brown, C. M.; Simmons, J. M.; Zoppi, M.; Walker, G. S.; Thomas, K. M.; Mays, T. J.; Hubberstey, P.; Champness, N. R.; Schröder, M. High Capacity Hydrogen Adsorption in Cu(II) Tetracarboxylate Framework Materials: The Role of Pore Size, Ligand Functionalization, and Exposed Metal Sites. *J. Am. Chem. Soc.* **2009**, *131*(6) 2159–2171.

Lv, H.; Zhao, X.; Niu, H.; He, S.; Tang, Z.; Wu, F.; Giesy, J. P. Ball milling synthesis of covalent organic frameworks as a highly active photocatalyst for degradation of organic contaminants. *J. Hazard. Mater.* **2019**, *369*, 494–502.

Müllen, K. Chemistry in a Materials World. *Angew. Chem., Int. Ed.* **2015**, *54*(35), 10040–10042.

Müller, S.; Liepold, B.; Roth, G. J.; Bestmann, H. J An Improved One-pot Procedure for the Synthesis of Alkynes from Aldehydes. *Synlett* **1996**, 521–522.

Narita, N.; Nagai, S.; Suzuki, S.; Nakao, K. Electronic structure of three-dimensional graphyne. *Phys. Rev. B* **2000**, *62*(16), 11146.

Novoselov, K. S.; Geim, A. K.; Morozov, S. V.; Jiang, D.; Zhang, Y.; Dubonos, S. V.; Grigorieva, I. V.; Firsov, A. A. Electric Field Effect in Atomically Thin Carbon Films. *Science* **2004**, *306*(5696), 666–669.

O'Keeffe, M.; Peskov, M. A.; Ramsden, S. J.; Yaghi, O. M. The Reticular Chemistry Structure Resource (RCSR) Database of, and Symbols for, Crystal Nets. *Accts. Chem. Res.* **2008**, *41*(12), 1782–1789.

Ourdjini, O.; Pawlak, R.; Abel, M.; Clair, S.; Chen, L.; Bergeon, N.; Sassi, M.; Oison, V.; Debierre, J.-M.; Coratger, R.; Porte, L. Substrate-mediated ordering and defect analysis of a surface covalent organic framework. *Phys. Rev. B* **2011**, *84*(12), 125421.

Peh, S. B.; Wang, Y.; Zhao, D. Scalable and Sustainable Synthesis of Advanced Porous Materials. *ACS Sustainable Chem. Eng.* **2019**, *7*(4), 3647–3670.

Rahman, G.; Najaf, Z.; Mehmood, A.; Bilal, S.; Shah, A.; Mian, S. A.; Ali, G. An Overview of the Recent Progress in the Synthesis and Applications of Carbon Nanotubes. *C* **2019**, *5*(1), 3.

Rowsell, J. L.; Yaghi, O. M. Strategies for Hydrogen Storage in Metal-Organic Frameworks. *Angew. Chem., Int. Ed.* **2005**, *44*(30), 4670–4679.

Rowsell, J. L. C.; Spencer, E. C.; Eckert, J.; Howard, J. A. K.; Yaghi, O. M. Gas Adsorption Sites in a Large-Pore Metal-Organic Framework. *Science* **2005**, *309*(5739), 1350–1354.

Sakamoto, J.; van Heijst, J.; Lukin, O.; Schluter, A. D. Two-Dimensional Polymers: Just a Dream of Synthetic Chemists? *Angew. Chem., Int. Ed.* **2009**, *48*(6), 1030–1069.

Saveleva, M. S.; Eftekhari, K.; Abalymov, A.; Douglas, T. E. L.; Volodkin, D.; Parakhonskiy, B. V.; Skirtach, A. G. Hierarchy of Hybrid Materials–The Place of Inorganics-*in*-Organics in it, Their Composition and Applications. *Front. Chem.* **2019**, *7*, 179.

Sevinçli, H.; Sevik, C. Electronic, phononic, and thermoelectric properties of graphyne sheets. *Appl. Phys. Lett.* **2014**, *105*, 223108.

Shetty, A. S.; Zhang, J.; Moore, J. S. Aromatic π-Stacking in Solution as Revealed through the Aggregation of Phenylacetylene Macrocycles. *J. Am. Chem. Soc*. **1996,** *118*(5), 1019–1027.

Shinde, D. B.; Aiyappa, H. B.; Bhadra, M.; Biswal, B. P.; Wadge, P.; Kandambeth, S.; Garai, B.; Kundu, T.; Kurungol, S.; Banerjee, R. A mechanochemically synthesized covalent organic framework as a proton-conducting solid electrolyte. *J. Mater. Chem. A*. **2016**, *4*(7), 2682–2690.

Stephens, R. D.; Castro, C. E. The Substitution of Aryl Iodides with Cuprous Acetylides. A Synthesis of Tolanes and Heterocyclics. *J. Org. Chem.* **1963**, *28*(12), 3313–3315.

Tan, C.; Yang, S.; Champness, N. R.; Lin, X.; Blake, A. J.; Lewis, W.; Schröder, M. High capacity gas storage by a 4,8-connected metal-organic polyhedral framework. *Chem. Commun.* **2011**, *47*(15), 4487–4489.

Thomas, A. Functional Materials: From Hard to Soft Porous Frameworks. *Angew. Chem., Int. Ed.* **2010**, *49*(45), 8328–8344.

Tranchemontagne, D. J. The Synthesis and Investigation of Alkyne-Containing Isoreticular Metal-Organic Frameworks for Hydrogen Storage and the Preliminary Investigation of Metal-Organic Framework for Gas Separation Applications, Ph. D. Thesis, University of California, Los Angeles, **2007**.

Tranchemontagne, D. J.; Mendoza-Cortés, J. L.; O'Keeffe, M.; Yaghi, O. M. Secondary building units, nets and bonding in the chemistry of metal-organic frameworks. *Chem. Soc. Rev.* **2009**, *38*(5), 1257–1283.

Waller, P. J.; Gándara, F.; Yaghi, O. M. Chemistry of Covalent Organic Frameworks. *Acc. Chem. Res.* **2015**, *48*(12), 3053–3063.

Wang, A.; Li, L.; Wang, X.; Bu, H.; Zhao, M. Graphyne-based carbon allotropes with tunable properties: From Dirac fermion to semiconductor. Diamond Relat. Mater. **2014**, *41*, 65–72.

Wang, J.; Deng, S.; Liu, Z.; Liu, Z. The Rare Two-Dimensional Materials with Dirac Cones. *Natl. Sci. Rev.* **2015**, *2*(1), 22–39.

Wells, A. F. The geometrical basis of crystal chemistry. Part 4. *Acta Crystallogr.* **1954**, *7*, 849–853.

Xu, C.; De, S.; Balu, A. M.; Ojeda, M.; Luque, R. Mechanochemical synthesis of advanced nanomaterials for catalytic applications. *Chem. Commun.* **2015**, *51*(31), 6698–6713.

Yaghi, O. M. Reticular Chemistry–Construction, Properties, and Precision Reactions of Frameworks. *J. Am. Chem. Soc.* **2016**, *138*(48), 15507–15509.

Yan, Y.; Telepeni, I.; Yang, S.; Lin, X.; Kockelmann, W. Dailly, A.; Blake, A. J.; Lewis, W.; Walker, G. S.; Allan, D. R.; Barnett, S. A.; Champness, N. R.; Schröder, M. *J. Am. Chem. Soc.* **2010**, *132*(12), 4092–4094.

Yuan, D.; Zhao, D.; Sun, D.; Zhou, H.-C. An Isoreticular Series of Metal-Organic Frameworks with Dendritic Hexacarboxylate Ligands and Exceptionally High Gas-Uptake Capacity. *Angew. Chem., Int. Ed.* **2010**, *49*(31), 5357–5361.

Yuwono, V. M.; Burrows, N. D.; Soltis, J. A.; Penn, R. L. Orientation Aggregation: Formation and Transformation of Mesocrystal Intermediates Revealed. *J. Am. Chem. Soc.* **2009**, *132*(7), 2163–2165.

Zhang, W.; Brombosz, S. M.; Mendoza, J. L.; Moore, J. S. A High-Yield, One-Step Synthesis of *o*-Phenylene Ethynylene Cyclic Trimer via Precipitation-Driven Alkyne Metathesis. *J. Org. Chem.* **2005**, *70*(24), 10198–10201.

Zhang, Y. Y.; Pei, Q. X.; Wang, C. M. Mechanical properties of graphynes under tension: A molecular dynamics study. *Appl. Phys. Lett.* **2012**, *101*, 081909.

Zhao, X.; Pachfule, P.; Li, S.; Langenhahn, T.; Ye, M.; Tian, G.; Schmidt, J.; Thomas, A. Silica-Templated Covalent Organic Framework-Derived Fe-N-Doped Mesoporous Carbon as Oxygen Reduction Electrocatalyst. *Chem. Mater.* **2019**, *31*(9), 3274–3280.

Zhou, Y.; Park, M.; Hong, S.; Lah, M. S. A designed metal-organic framework based on a metal-organic polyhedron. *Chem. Commun.* **2008**, 2340–2342.

Zwaneveld, N. A. A.; Pawlak, R.; Abel, M.; Catalin, D.; Gigmes, D.; Bertin, D.; Porte, L. Organized Formation of 2D Extended Covalent Organic Frameworks at Surfaces. *J. Am. Chem. Soc.* **2008**, *130*(21), 6678–6679.